Aeroradiometric Measurements in the Framework of the Swiss Exercise ARM19

Gernot Butterweck, Benno Bucher, Ladislaus Rybach, Cristina Poretti,
Stéphane Maillard, Mauro Schindler, Bénédicte Hofstetter-Boillat,
Sabine Mayer, Gerald Scharding

Aeroradiometric Measurements in the Framework of the Swiss Exercise ARM19

Gernot Butterweck[1], Benno Bucher[2], Ladislaus Rybach[3], Cristina Poretti[4],
Stéphane Maillard[5], Mauro Schindler[5], Bénédicte Hofstetter-Boillat[1],
Sabine Mayer[1], Gerald Scharding[4]

1   Department of Radiation Safety and Security, Logistics Division, Paul Scherrer Institute (PSI),
5232 Villigen PSI, Switzerland
2   Swiss Federal Nuclear Safety Inspectorate (ENSI), Industriestrasse 19,
5200 Brugg, Switzerland
3   Institute of Geophysics, Swiss Federal Institute of Technology Zürich (ETHZ),
8092 Zürich, Switzerland
4   Swiss National Emergency Operations Center (NEOC),
3003 Bern, Switzerland
5   Nuclear Biological Chemical - Explosive Ordnance Disposal (NBC-EOD) Centre of Competence,
3700 Spiez, Switzerland

Abstract

The flights of the civil part ARM19z of the exercise were performed between June 2nd and June 6th, 2019, covering the recurrent measuring areas around the nuclear power plants Gösgen and Mühleberg, a transversal from Chur to Torre (TI) and an altitude profile over lake Neuchâtel. A short report of the measurement results of ARM19z was placed on the NEOC website `https://www.naz.ch/` on June 7th, 2019. The flights of the military part of the exercise ARM19m were performed from September 2nd to September 5th. ARM19m contained source search exercises over the Spiez military training area, measurements over a prospective reference area at the Thun military training area and measurements in the vicinity of the towns Bulle, Köniz and Vevey.

The survey of the environs of the Swiss nuclear power plants Gösgen (KKG) and Mühleberg (KKM) showed no artificial radionuclides outside of the plant premises.

The measurements over the towns of Bulle, Köniz and Vevey expanded the database of radiation background over Swiss cities. No unusual values of the radiological quantities were observed.

An altitude profile over lake Neuchâtel lead to a revision of a model planned to be used for compensating the influence of airborne radon progeny on the measurement.

The deterioration of the energy resolution of several NaI(Tl) crystals used in the RLL detectors continues to downgrade system performance.

The analysis of cosmic dose rate data measured over the boiling water reactor of KKM indicates a misinterpretation of high energy photons emitted by the radionuclide ^{16}N using the evaluation software developed by the manufacturer of the RLL system (Mirion).

Results of training flights over radionuclide sources demonstrated the advantage of the online identification of radionuclides by the Mirion software and the subsequent alert to the operators. Nevertheless, in cases with several sources of different radionuclides, a visual inspection of the associated photon spectra by operators well acquainted with gammaspectrometry is advisable.

First estimates of correction factors for ^{232}Th and ^{40}K activity concentrations were determined from results of current and past measurements to align data evaluations with ARM and Mirion software.

Contents

List of Figures

List of Tables

1 Introduction

Swiss airborne gamma spectrometry measurements started in 1986. Methodology and software for calibration, data acquisition and mapping were developed at the Institute of Geophysics of the Swiss Federal Institute of Technology Zurich (ETHZ). Between 1989 and 1993 the environs of Swiss nuclear installations were measured annually on behalf of the Swiss Federal Nuclear Safety Inspectorate (ENSI) during exercises performed annually as system check and drill for the operators. This schedule was changed to biannual inspections in 1994, together with an organizational inclusion of the airborne gamma-spectrometric system (ARM) into the Emergency Organization Radioactivity (EOR) of the Federal Office for Civil Protection (FOCP). The deployment of the airborne gamma-spectrometric system is organized by the National Emergency Operations Centre (NEOC). NEOC is also responsible for the recruitment and instruction of the measurement team and the operational readiness of the system. Aerial operations are coordinated and performed by the Swiss Air Force with Super Puma helicopters. The gamma-spectrometric equipment is stationed at the military airfields of Dübendorf and Payerne. The gamma-spectrometry system can be airborne within four hours. Responsibility for scientific support, development and maintenance of the aeroradiometric measurement equipment passed from ETHZ to the Radiation Metrology Section of the Paul Scherrer Institute (PSI) in 2003 in cooperation with ENSI. General scientific coordination and planning of the annual measuring flights is provided by the Expert Group for Aeroradiometrics (FAR). FAR was a working group of the Swiss Federal Commission for NBC protection (ComNBC) and consists of experts from all Swiss institutions concerned with aeroradiometry. FAR was re-organized as an expert group of the NEOC in 2008. Additional information can be found at `http://far.ensi.ch/`. In 2018 the ARM measuring system used by the NEOC in the past exercises was replaced with the RLL (Radiometrie Land-Luft) system owned by the Swiss armed force. Of the four systems available, under normal circumstances two systems are operated by staff of the NBC-EOD Centre of Competence (Komp Zen ABC-KAMIR) for measurement tasks with military character and two systems are assigned to NEOC for the deployment in case of civil emergencies with a radiological component. As identical measuring systems are used, the results of measuring flights performed by NBC-EOD Centre of Competence are included into the scientific report. Since 2018 the scientific report includes as before measuring flights of the NEOC (ARM19z) together with measuring flights performed by the NBC-EOD Centre of Competence (ARM19m).

This report focuses on methodological aspects and thus complements the short report of NEOC about the annual flight surveys (available from the NEOC website `https://www.naz.ch`).

1.1 Measuring System RLL

The measuring system RLL (Radiometrie Land-Luft) used both for civil and military measurements consists of a radiation detector with four NaI(Tl) scintillation crystals with a total volume 16.8 litres, associated photo-multipliers and multichannel analysers for low level measurements and one Geiger-Müller tube and associated electronics for high-level dose rate measurement. Detectors, Geiger-Müller tube and associated electronics are installed in an aluminium case with thermal insulation foam. The detection container is mounted in the cargo bay below the centre of the helicopter. The RLL system uses position, air pressure, air temperature and radar altitude provided by the helicopter via the internal ARINC bus. Figure 1 shows the complete system packaged for storage. The equipment control, data acquisition and storage are performed with a rugged computer working as a data server. Two further rugged redundant client computers are used as operator interface for real-time evaluation, data mapping and communication. All computers are installed in an equipment rack including a battery backed-up power supply. Both operators can operate the system with their associated client computer, display, keyboard and trackball. The additional third central display of the operator's console is mirrored on a screen in the cockpit located between both pilots and is used for information exchange with the pilots and general radiological situation awareness (figure 2). The measuring system RLL is mounted in an Aerospatiale AS 332 Super Puma helicopter (TH 06) of the Swiss Air Forces (figure 3). This helicopter has excellent navigation properties and allows emergency operation during bad weather conditions and night time.

Figure 1: Components of the RLL system. 1. Lifting platform for the installation of the detection container. 2. Floor plates and accessories case. 3. Monitors and operator console. 4. Detection container. 5. Operator seats and equipment rack.

Figure 2: Operator console of the RLL system. 1. Displays of the client computers. 2. Common display (mirrored in the cockpit). 3. Control panel with switches for power, lighting and communication and USB ports for file exchange.
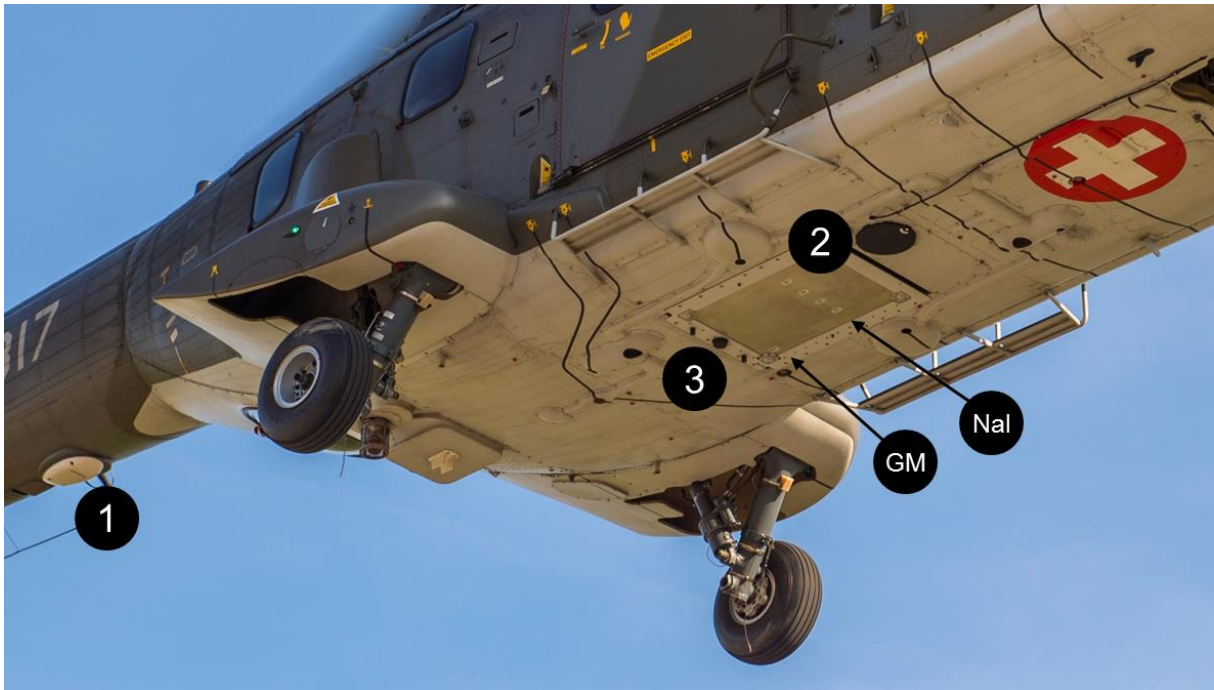
Figure 3: RLL detector mounted in the cargo bay of a Super Puma helicopter. 1. Radar altimeter. 2. Detection container marked with detector reference points. 3. UMTS antenna for data upload.

1.1.1 Quality issues

After the RLL measuring system was put into operation, quality issues with the spectrometric performance of the detectors were observed. The unsatisfactory energy resolution of single NaI(Tl) crystals were reported to the manufacturer who started to investigate the causes of the deterioration of detector performance. Unfortunately, this effect could also be observed with RLL detector number 002, which was used during the measuring flights of ARM19z. The analysis of the individual spectra of the four crystals during the exercise indicated a poor energy resolution of crystal 2 of RLL detector 002 used during the exercise. Measurements of the energy resolution in the calibration laboratory of PSI after the exercise confirmed the issue (figure 4). The energy resolution (full width at half maximum (FWHM) divided by peak energy) of the four crystals with associated photo-multiplier, amplifier and multi-channel analyser are listed in Table 1. Whereas the energy resolutions of crystals 1, 3 and 4 are acceptable, the energy resolution of crystal 2 with 11% is insufficient. Thus, it was decided to reject the data measured with crystal 2 for the data evaluation used in this report. Analogous to the procedure applied to the faulty crystal in 2017 (Butterweck et al., 2018) the spectra of crystal 2 are replaced with the spectra of crystal 3.

Figure 4: ^{137}Cs spectra measured with detector RLL002 in the calibration laboratory.

Crystal	Energy resolution [%]
1	8.4
2	11.0
3	8.0
4	8.6

Table 1: Energy resolution of Detector RLL002 for the ^{137}Cs peak at 661 keV.

1.2 Measuring flights

The advantage of aeroradiometric measurements lies in the high velocity of measurements in a large area, even over rough terrain. Uniform radiological information o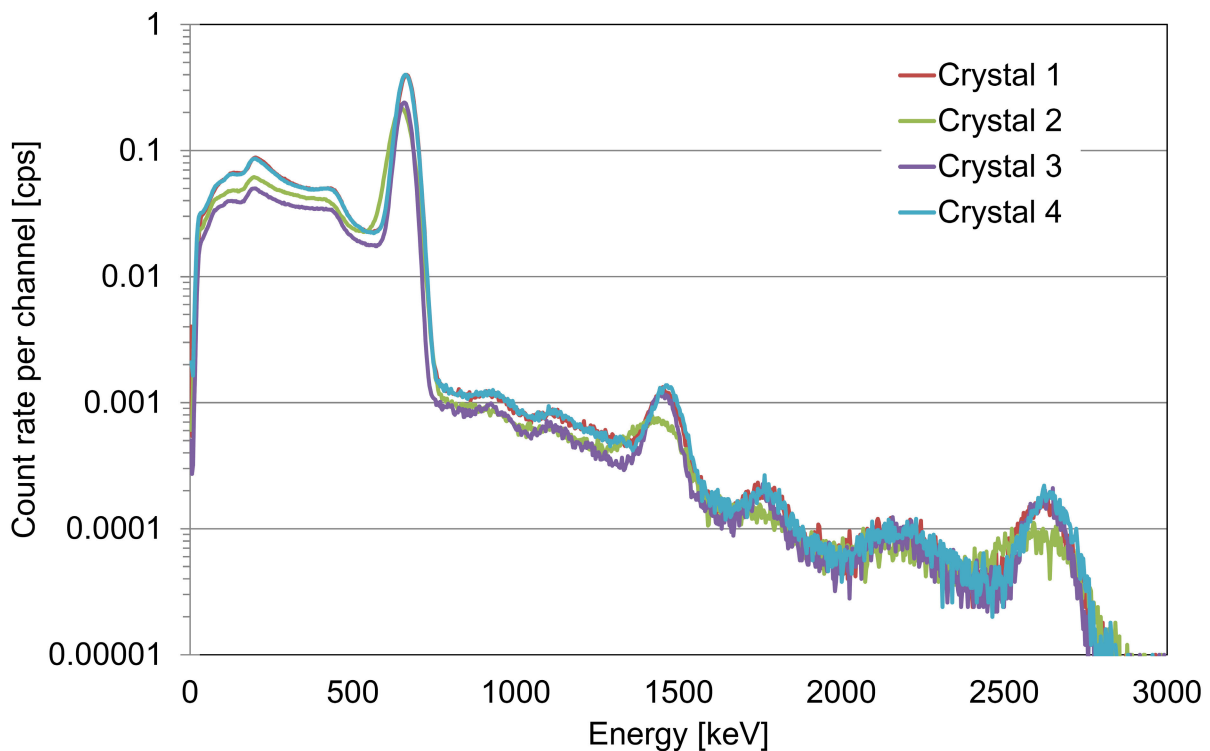f an area is obtained from a regular grid of measuring points. This grid is composed from parallel flight lines which are 100 m to 500 m apart, depending on the scope of the measurement. The flight altitude above ground is aspired to be constant during the measuring flight. Typical values lie between 50 m and 100 m above ground. The spectra are recorded in regular time intervals of typical one second, yielding integration over 28 meters of the flight line at a velocity of 100 km/h.

1.3 Data evaluation

1.3.1 ARM software

The data evaluation follows the methodology described in Schwarz (1991). Since 2000, the software developed by the Research Group for Geothermics and Radiometry of the Institute of Geophysics of the Swiss Federal Institute of Technology Zurich (ETHZ) (Bucher, 2001) is used. This evaluation method is used througout the report, unless an different method is indicated.

1.3.2 Mirion software

The proprietary software delivered together with the RLL system was developed by Mirion Technologies, France. An outline of the algorithms used can be found in Butterweck et al., 2018.

1.4 Data presentation

A first brief report (Kurzbericht) of the measurement results is compiled by the measurement team and published immediately after the end of the exercise on the homepage of NEOC. These reports are archived at `http://far.ensi.ch`.

Results of a further data evaluation are published in the form of a PSI-report, within the responsibility of the FAR. These reports are also archived at `http://far.ensi.ch`.

For all measuring areas, a map of the total dose rate (measuring quantity H*(10) extrapolated to 1 m above ground) and the flight lines is presented together with a map of the Man-Made-Gross-Count (MMGC) ratio. A map of the ^{232}Th activity concentration (measuring quantity activity per dry mass) yields quality information as it can be expected that this quantity is constant over time. As an additional quality measure, an appendix with the basic parameters of the data evaluation is added to simplify a re-evaluation of the data in the future. If the MMGC-ratio indicates elevated values, maps of individual radionuclides are added based on the average photon spectrum over the affected area. In the case of large changes of topography in the measured area, a map of the terrestrial dose rate consisting of the total dose rate reduced of the altitude dependent cosmic component is included. In the case of measuring flights with the main purpose of mapping natural radionuclide concentrations, a supplementary map of the ^{40}K activity concentration (measuring quantity activity per dry mass) is also presented. All maps use a gradual colour scale from blue for low values to red for high values. The maximum and minimum values are specified in the legend

together with the measurement unit of the depicted quantity. The colours for 10 percent steps between minimum and maximum values of the scale are given in Table 2. Values below the minimum or above the maximum get assigned the colours of the minimum or maximum, respectively. Minimum and maximum of the colour scale for the measured quantity are generally set to standard values to facilitate easier comparison of maps. Maps with different value ranges are added if considered helpful to the reader.
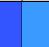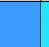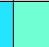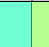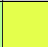
Percentage	0	10	20	30	40	50	60	70	80	90	100
Colour											

Table 2: Quantification of the color scale.

2 Results of the measuring flights during the exercise ARM19

The flights of the civil part ARM19z of the exercise were performed between June 2nd and June 6th, 2019, covering the recurrent measuring areas around the nuclear power plants Gösgen and Mühleberg, a transversal from Chur to Torre (TI) and an altitude profile over lake Neuchâtel. A short report of the measurement results of ARM19z was placed on the NEOC website `https://www.naz.ch/` on June 7th, 2019.

The flights of the military part of the exercise ARM19m were performed from September 2nd to September 5th. ARM19m contained source search exercises over the Spiez military training area, measurements over a prospective reference area at the Thun military training area and measurements in the vicinity of the towns Bulle, Köniz and Vevey. Flight velocity of the Super Puma helicopters of the Swiss Air Force was around 30 m/s with a ground clearance of 90 m for all measuring flights. The counting interval of the spectra was one second.

Personnel of the military units Stab BR NAZ and NBC-EOD Centre of Competence performed the measurements supported by experts from ENSI, PSI, ETHZ, ABC Abwehr Einsatzkompanie and NEOC.

Flight parameters of the measuring flights are listed in Table 3.

Location	Flight number	Measuring time [s]	Length of run [km]	Area [km^2]
		ARM19z		
KKM	Heli 2_20190603 0915	8817	404	102
KKG	Heli 2_20190604 0850	6818	337	81
KKG extended area	Heli 2_20190604 1050	25008	1138	999
	Heli 2_20190604 1345			
	Heli 2_20190605 0850			
	Heli 2_20190605 0930			
	Heli 2_20190605 1050			
	Heli 2_20190605 1340			
Lake Neuchâtel	Heli 2_20190603 1330	2423	-	-
Transversal	Heli 2_20190606 0915	2904	100	-
		ARM19m		
Bulle	Heli 3_20190905 0920	7247	274	71
Köniz	Heli 3_20190902 1415	13340	534	131
	Heli 3_20190902 1450			
	Heli 3_20190903 0930			
	Heli 3_20190903 1025			
	Heli 3_20190903 1335			
Spiez exercise 1	Heli 3_20190904 1335	1671	64	10
Spiez exercise 2	Heli 3_20190904 1410	644	24	5
Spiez exercise 3	Heli 3_20190904 1430	631	25	5
Thun reference 1	Heli 3_20190904 0945	1519	60	9
Thun reference 2	Heli 3_20190904 1040	1711	67	10
Vevey	Heli 3_20190905 1345	5124	194	50

Table 3: Flight data of ARM19.

2.1 ARM19z

2.1.1 Recurrent measurement area KKM

According to a biannual rotation of routine measurements, the environs of the nuclear power plant Mühleberg (KKM) were inspected in 2019. The data evaluation during the exercise was based completely on the software provided by the manufacturer of the RLL system (Mirion). These results were published at the end of the Exercise by the NEOC. Figure 5 shows the dose rate in the vicinity of KKM derived from the Mirion evaluation. For this report, an additional data evaluation was performed using the software developed for the previous ARM system to provide continuity of results. The derived dose rate map from the ARM software shows very similar results to the results of the Mirion software (Figure 6).

A direct comparison between both data evaluations (Figure 7) indicates an unexpected (see section 3) large deviation for elevated dose rates. These elevated dose rates were measured over the premises of KKM. Figure 8 shows the spectrum over the premises of KKM in comparison to a background spectrum. Whereas the background spectrum is dominated by photon emissions of natural radionuclides like ^{40}K and decay products of the uranium- and thorium decay series (^{214}Bi and ^{208}Tl, respectively), the spectrum over KKM shows the annihilation peak at 511 keV and peaks at 1173 keV and 1333 keV from the man-made radionuclide ^{60}Co. The ^{60}Co-signal over the premises of KKM originated from the interim storage facility for radioactive waste of the power plant. The lid of this storage facility was opened during the measuring flight. Additional to the visible peaks, a general elevation of the count rate can be observed throughout the spectrum. The general elevation of count rates over the premises of KKM is caused by high energy photon radiation of the activation product ^{16}N, a typical result for operating boiling water reactors. This effect was already observed in previous years and described in detail in the respective reports Bucher et al., 2007, Bucher et al., 2009 and Bucher et al., 2011. The high energy radiation of ^{16}N is interpreted by the Mirion algorithms as contribution of cosmic radiation. As the dose rate calibration factor for high energy counts originating from cosmic radiation is much higher compared to the calibration factor for counts produced by terrestrial radiation, the cosmic contribution of the dose rate is overestimated. Figure 9 illustrates the effect. Whereas the cosmic dose rate derived with the ARM software ranges between 43 nSv/h and 51 nSv/h, the Mirion software derives values up to 14000 nSv/h due to the misinterpretation of the ^{16}N-signal. The terrestrial dose rate is the difference between total dose rate (Figure 7) and the cosmic dose rate (Figure 9). The scatter diagram of the terrestrial dose rate (Figure 10) shows better agreement between the two evaluation methods compared to the total and cosmic dose rates.

The man-made gross-count (MMGC) ratio, an indicator for the presence of man-made radionuclides, shows outside of the premises of KKM no significantly elevated readings (Figure 11). The activity concentration of the natural radionuclide ^{232}Th (Figure 12) shows elevated values over the premises of KKM due to a misinterpretation of scattered high energy photon radiation of ^{16}N. Outside of the power plant, the variation of ^{232}Th is governed by the attenuation of terrestrial photons by water and the normal variation of the thorium content in soil and rock.
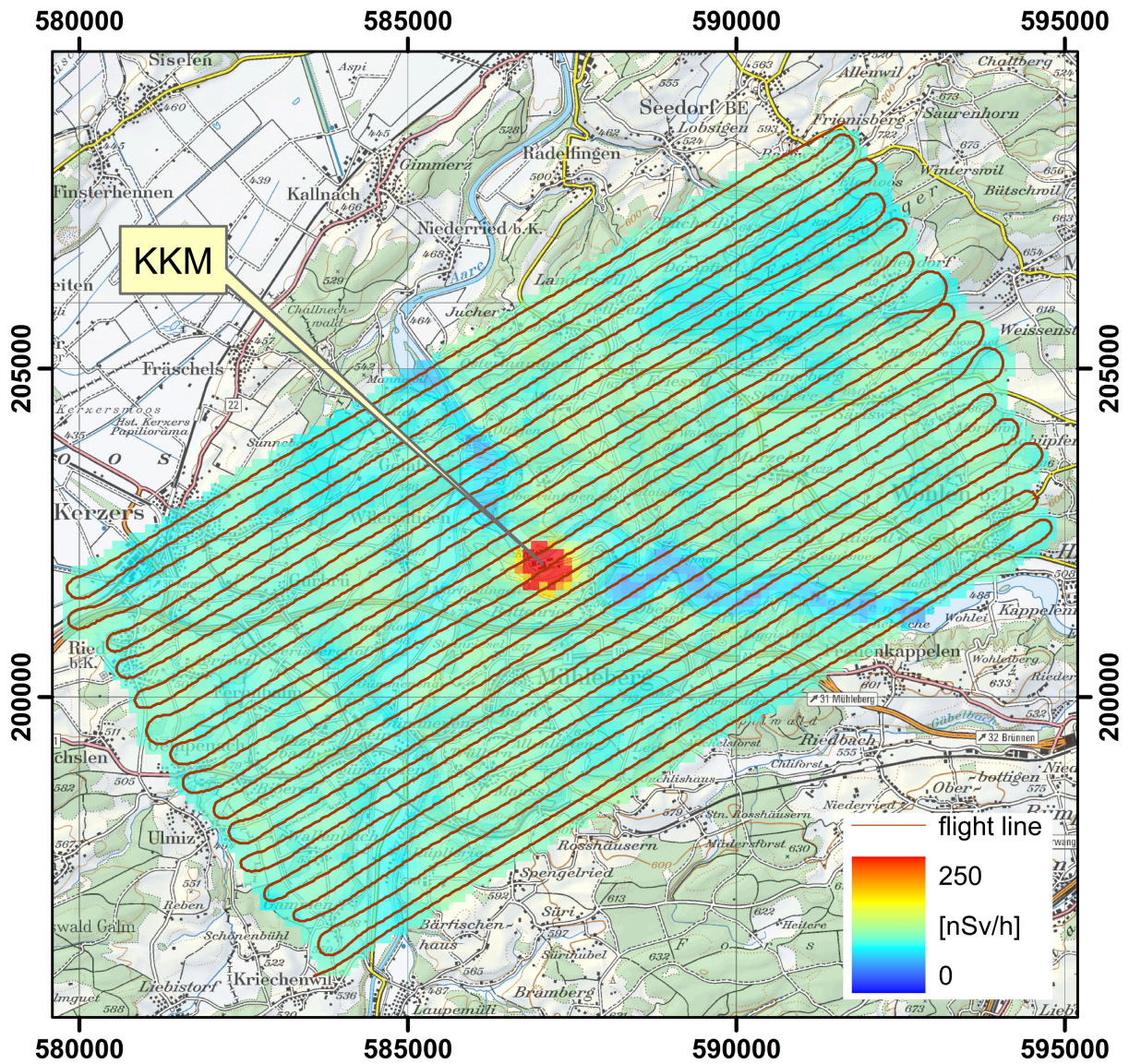
Figure 5: Dose rate in the vicinity of KKM evaluated with the Mirion software. PK100 ©2019 swisstopo (JD100042).
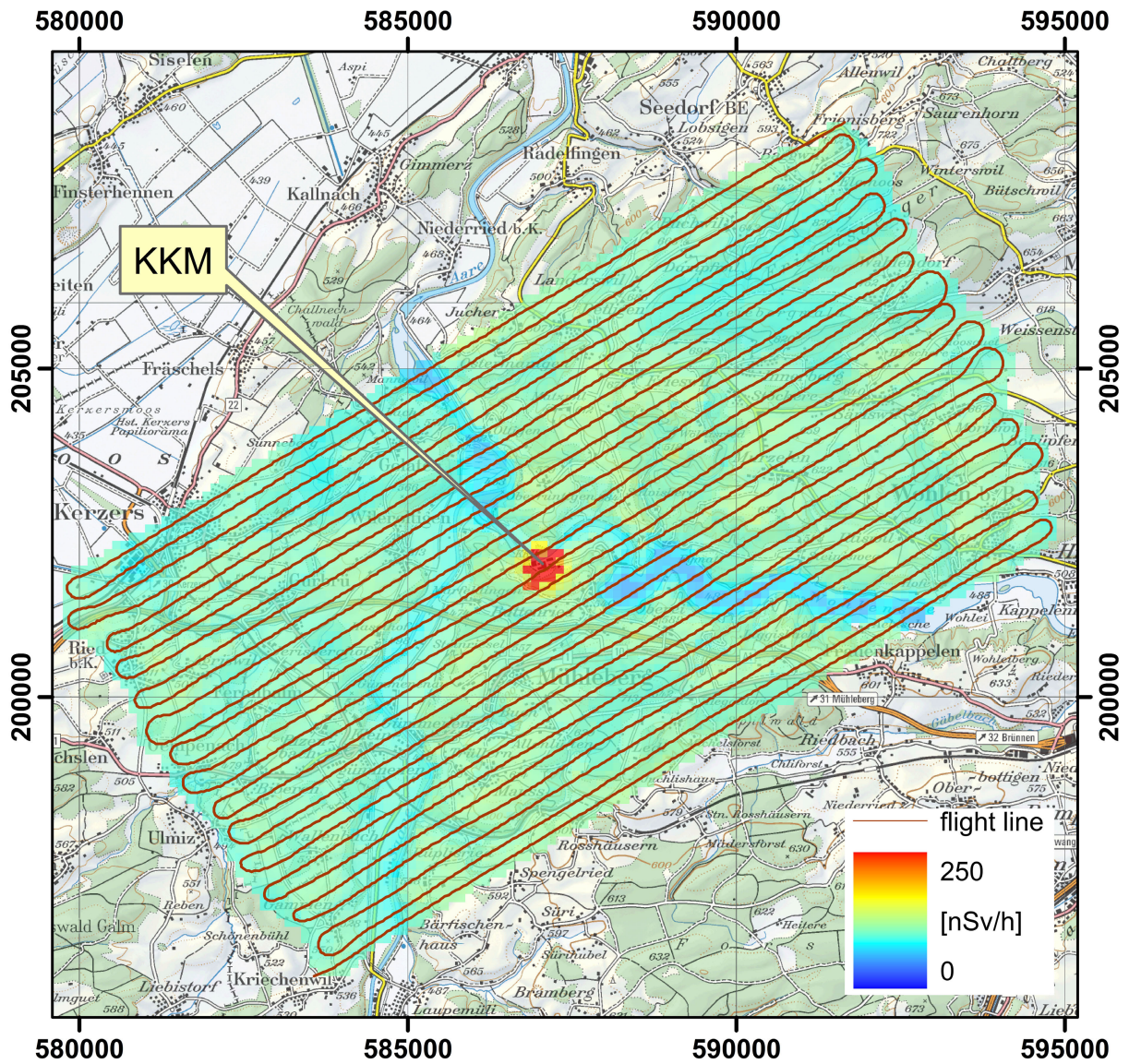
Figure 6: Dose rate in the vicinity of KKM evaluated with the ARM software.
PK100 ©2019 swisstopo (JD100042).
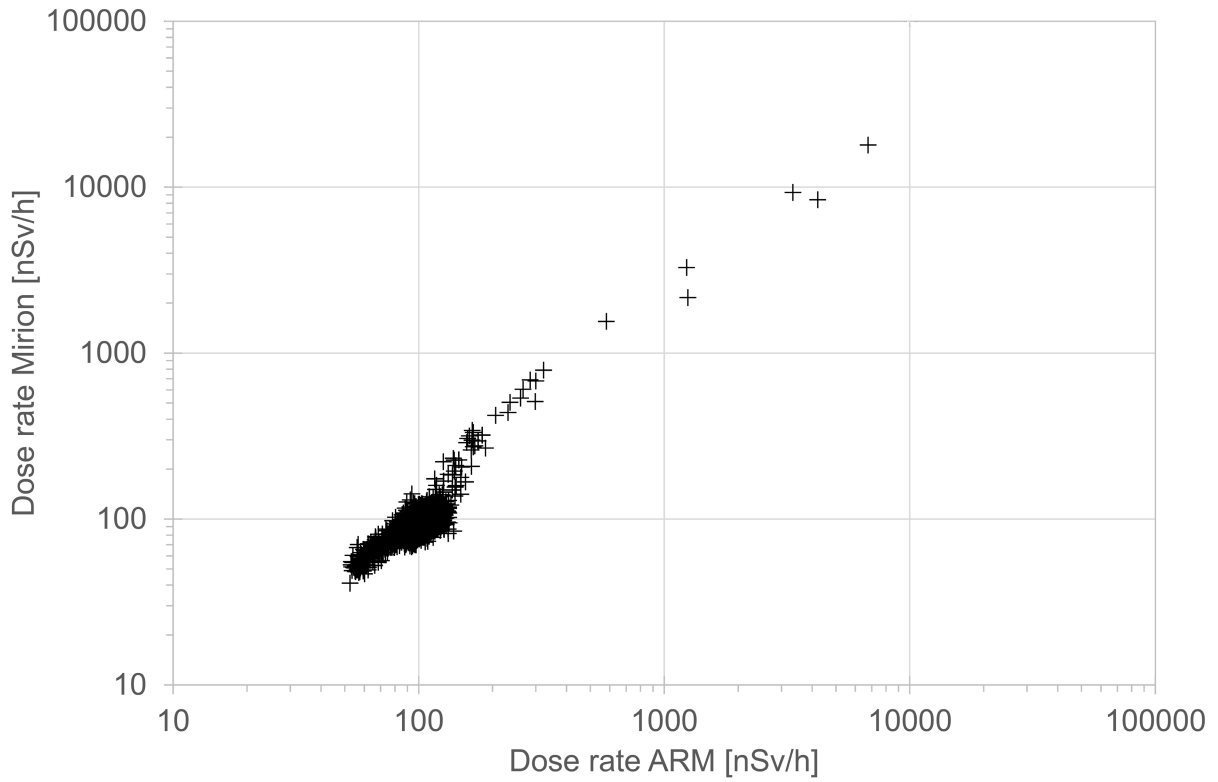
Figure 7: Scatter plot of the dose rates determined with Mirion and ARM software.
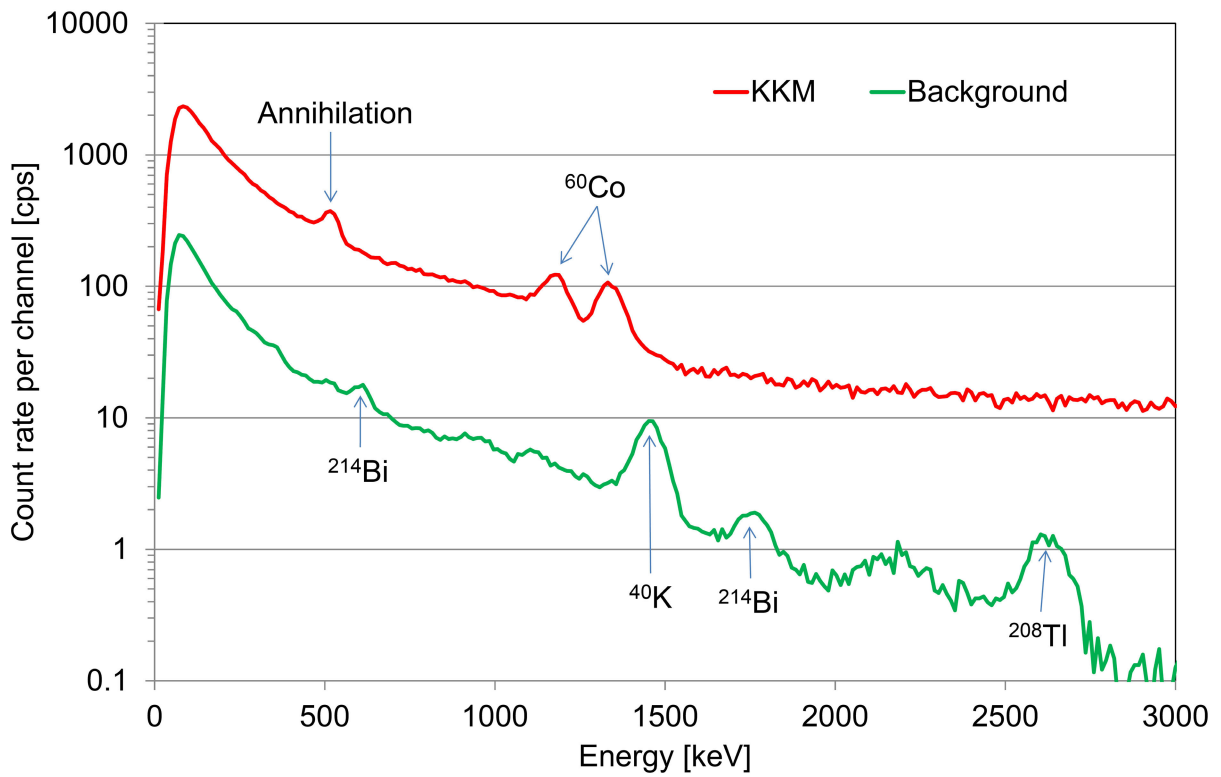
Figure 8: Photon spectrum over the premises of KKM compared to a background spectrum.
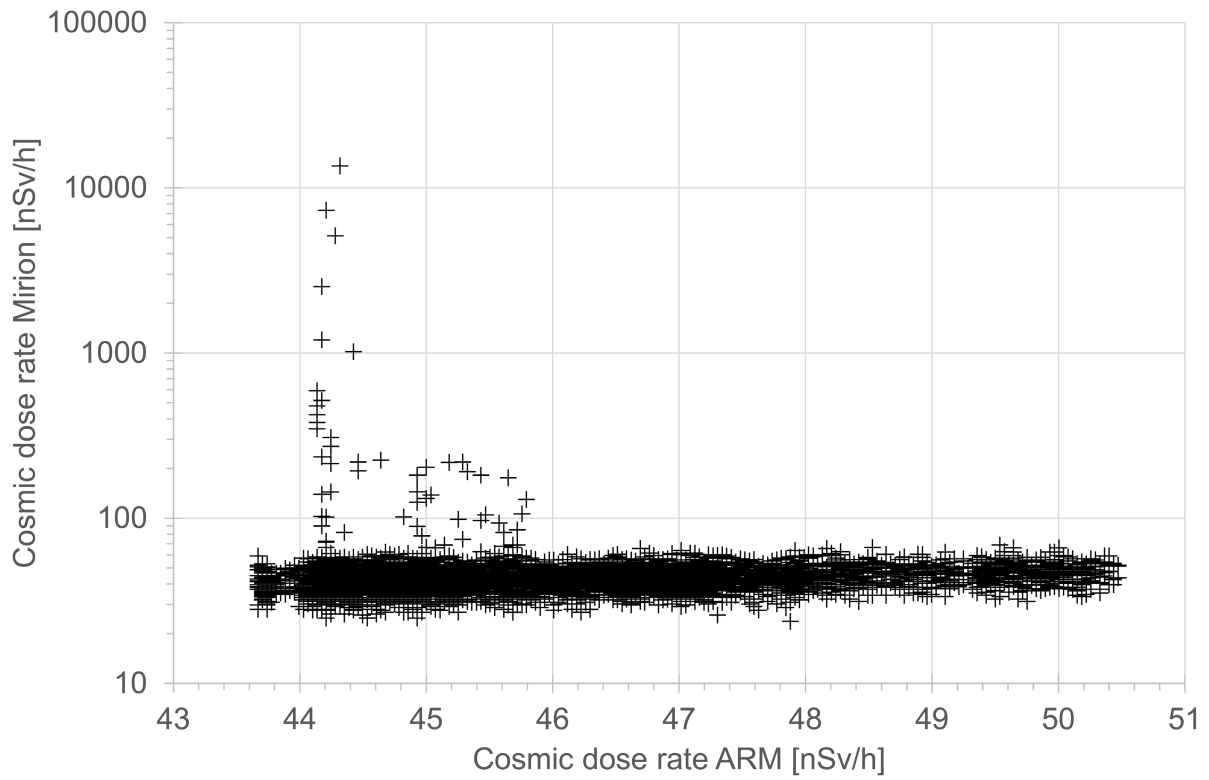
Figure 9: Scatter plot of the cosmic dose rates determined with Mirion and ARM software.
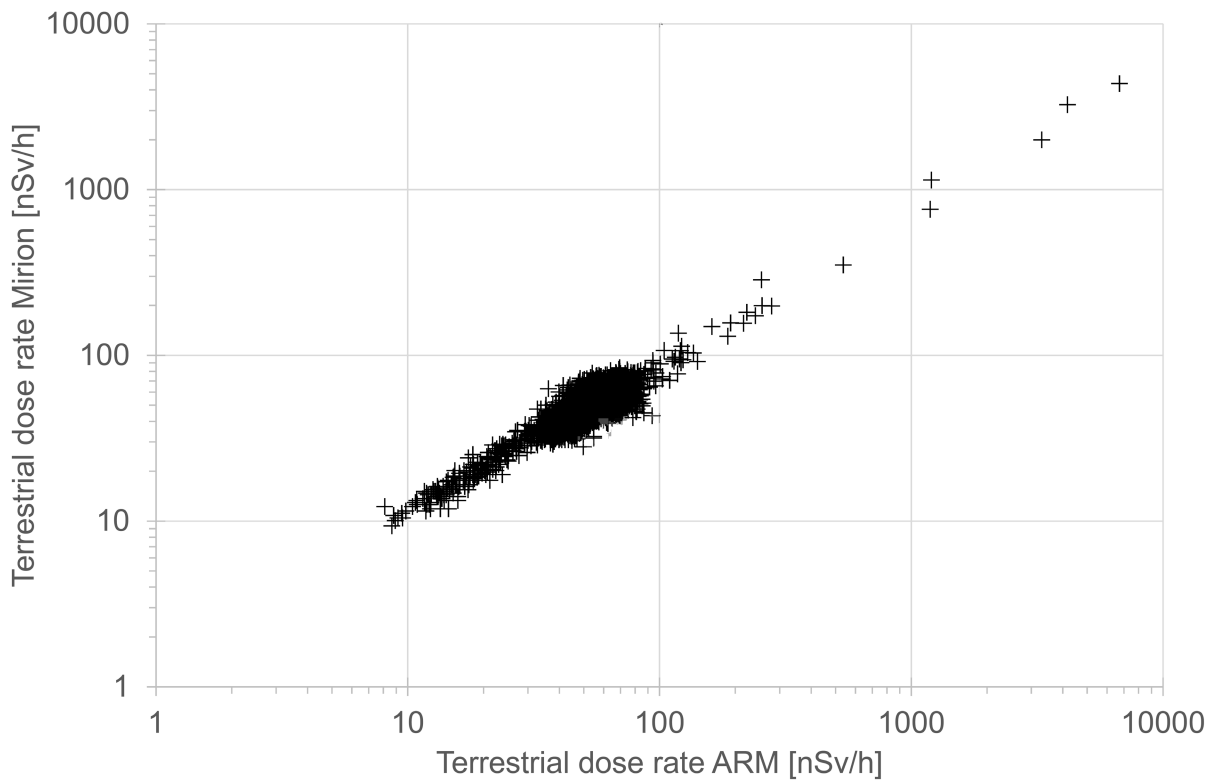
Figure 10: Scatter plot of the terrestrial dose rates determined with Mirion and ARM software.
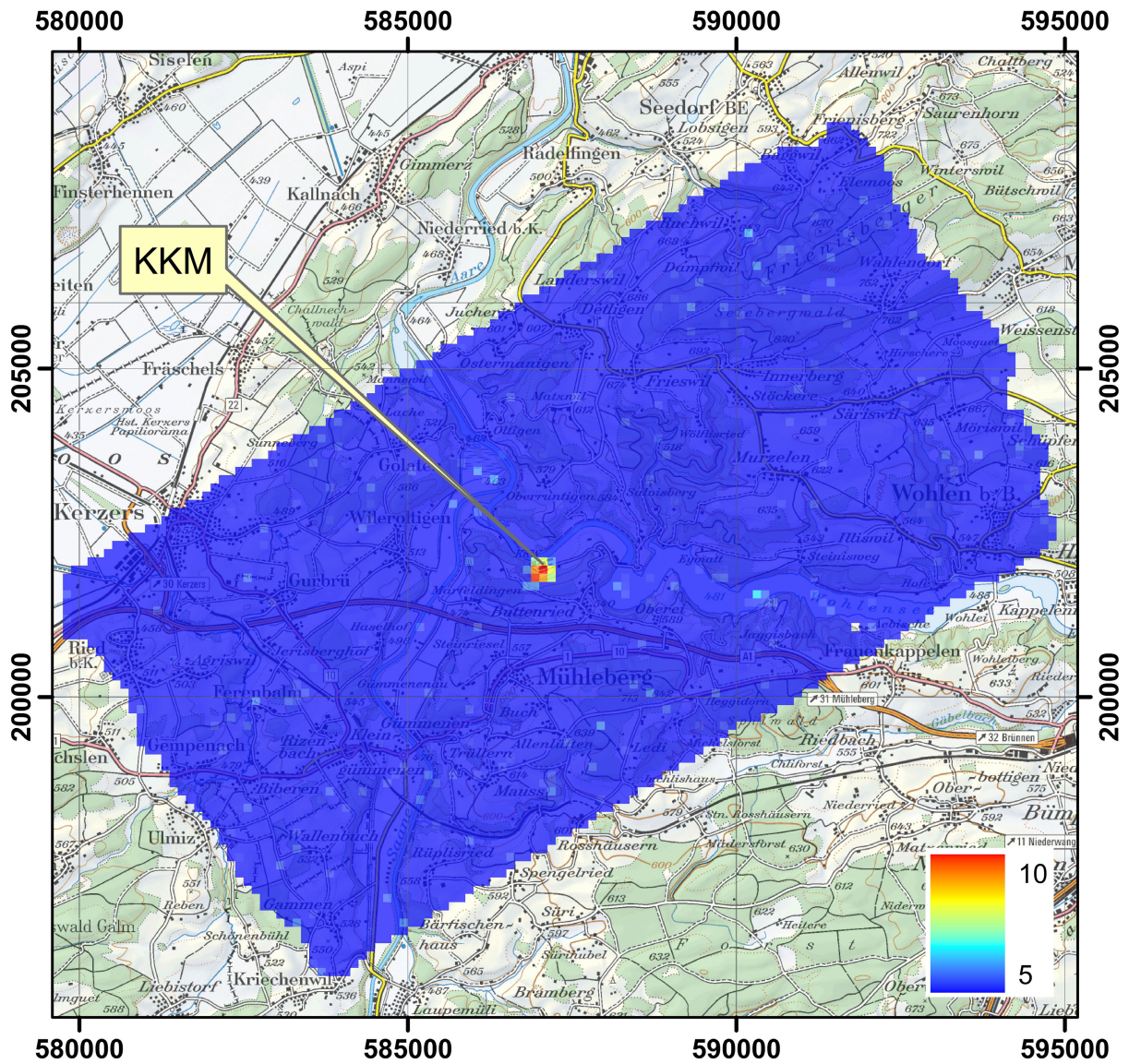
Figure 11: Man-made Gross-count (MMGC) ratio in the vicinity of KKM evaluated with the ARM software. PK100 ©2019 swisstopo (JD100042).
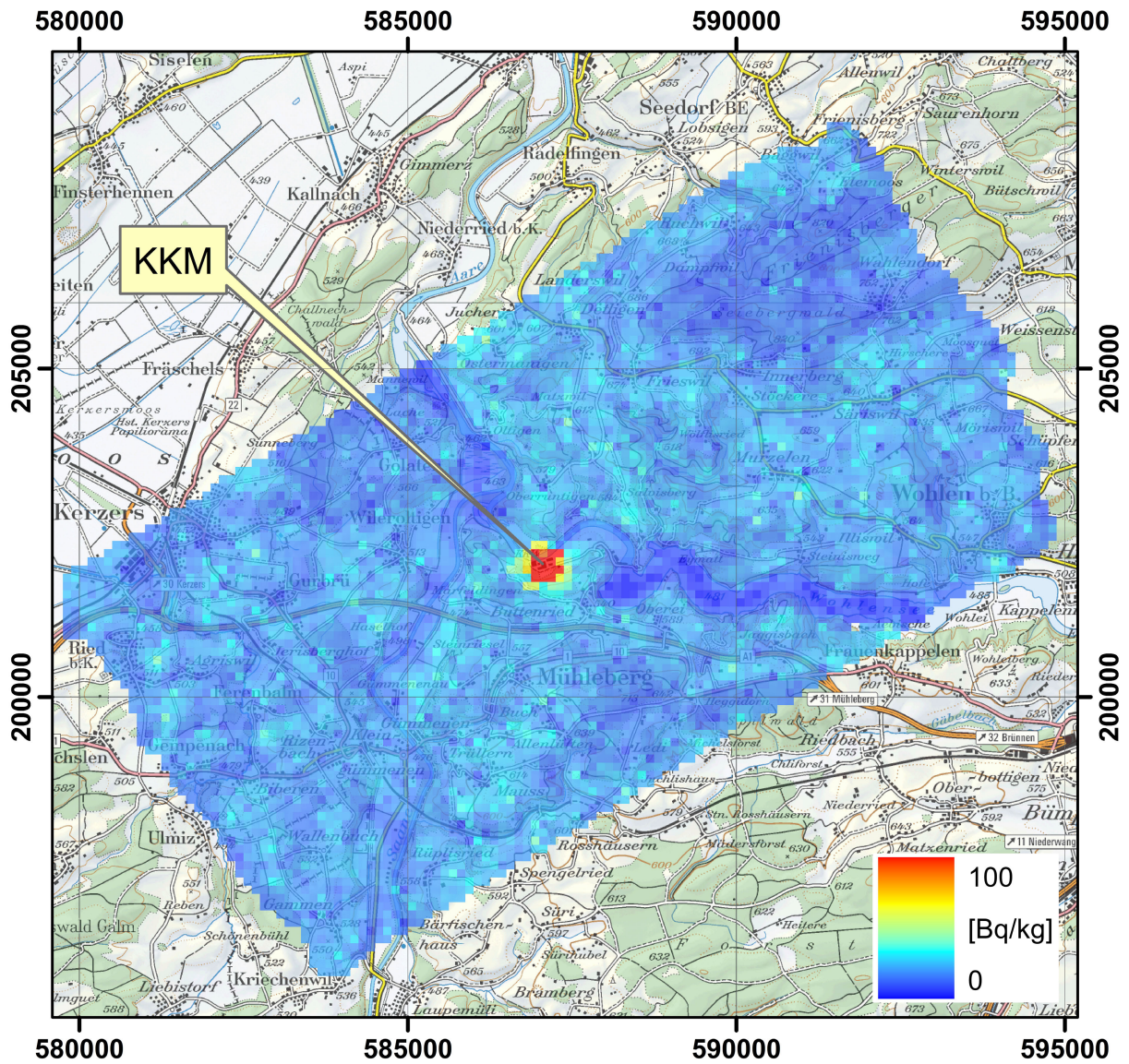
Figure 12: ^{232}Th activity concentration in the vicinity of KKM evaluated with the ARM software. PK100 ©2019 swisstopo (JD100042).

2.1.2   Extended recurrent measurement area KKG

In the pressurised reactor of the nuclear power plant Gösgen (KKG), the radioactive steam of the primary circuit stays completely in the heavily shielded containment. The power plant was inoperative during the measuring flights due to the annual revision. Thus, neither the dose rate map (Figure 13) nor the map of the MMGC-ratio (Figure 14) as indicator for the presence of artificial radionuclides show increased signals at the site of the plant. The map of the natural radionuclide ^{232}Th (Figure 15) is added for quality assurance purposes. The measurement around KKG was extended in the 2019 exercise with areas to the north-west, north and east of the recurrent measuring area. The respective maps (Figures 16, 17 and 18) of the extended measuring area show typical values for northern Switzerland.
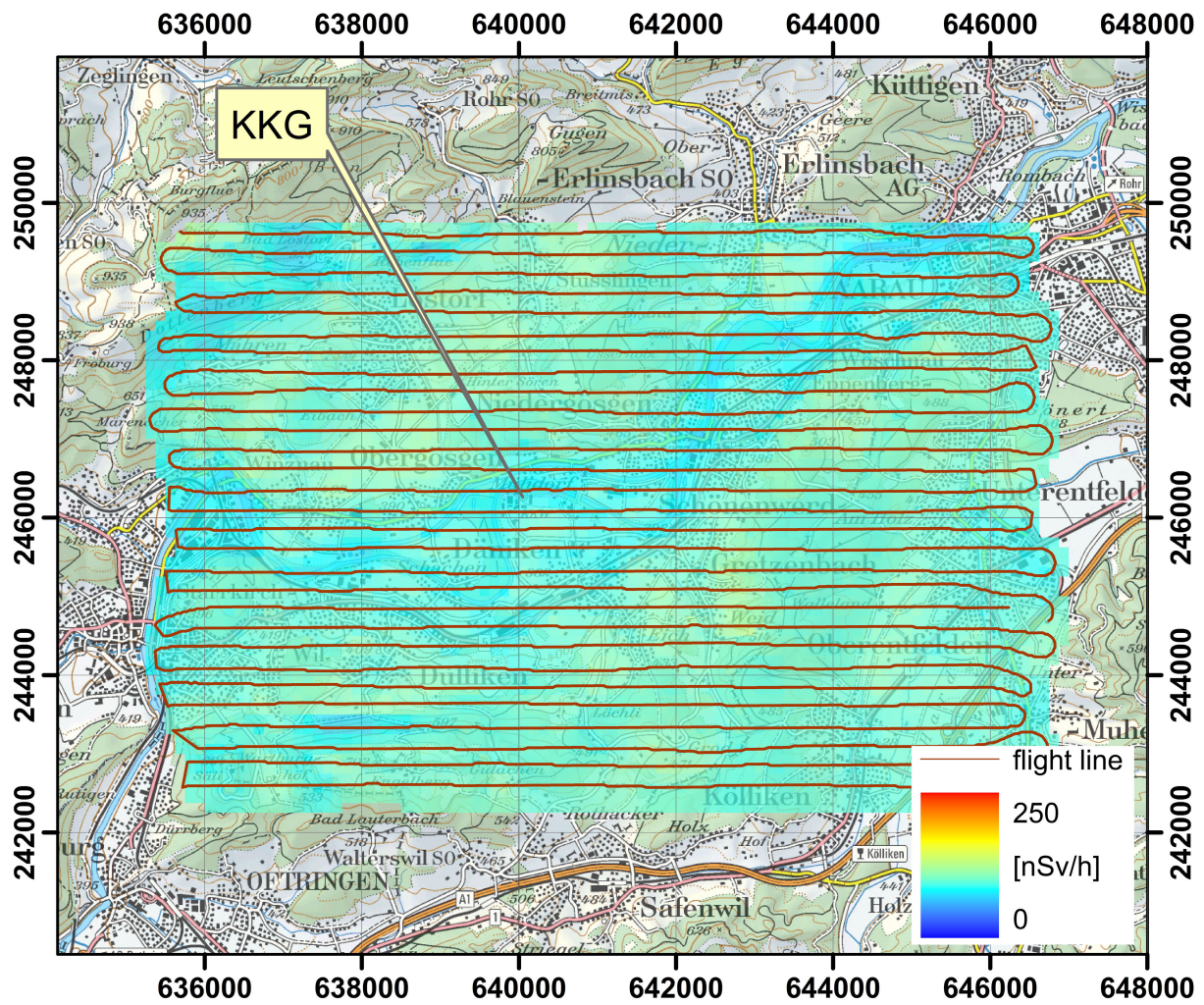
Figure 13: Dose rate in the vicinity of KKG.
PK100 ©2019 swisstopo (JD100042).
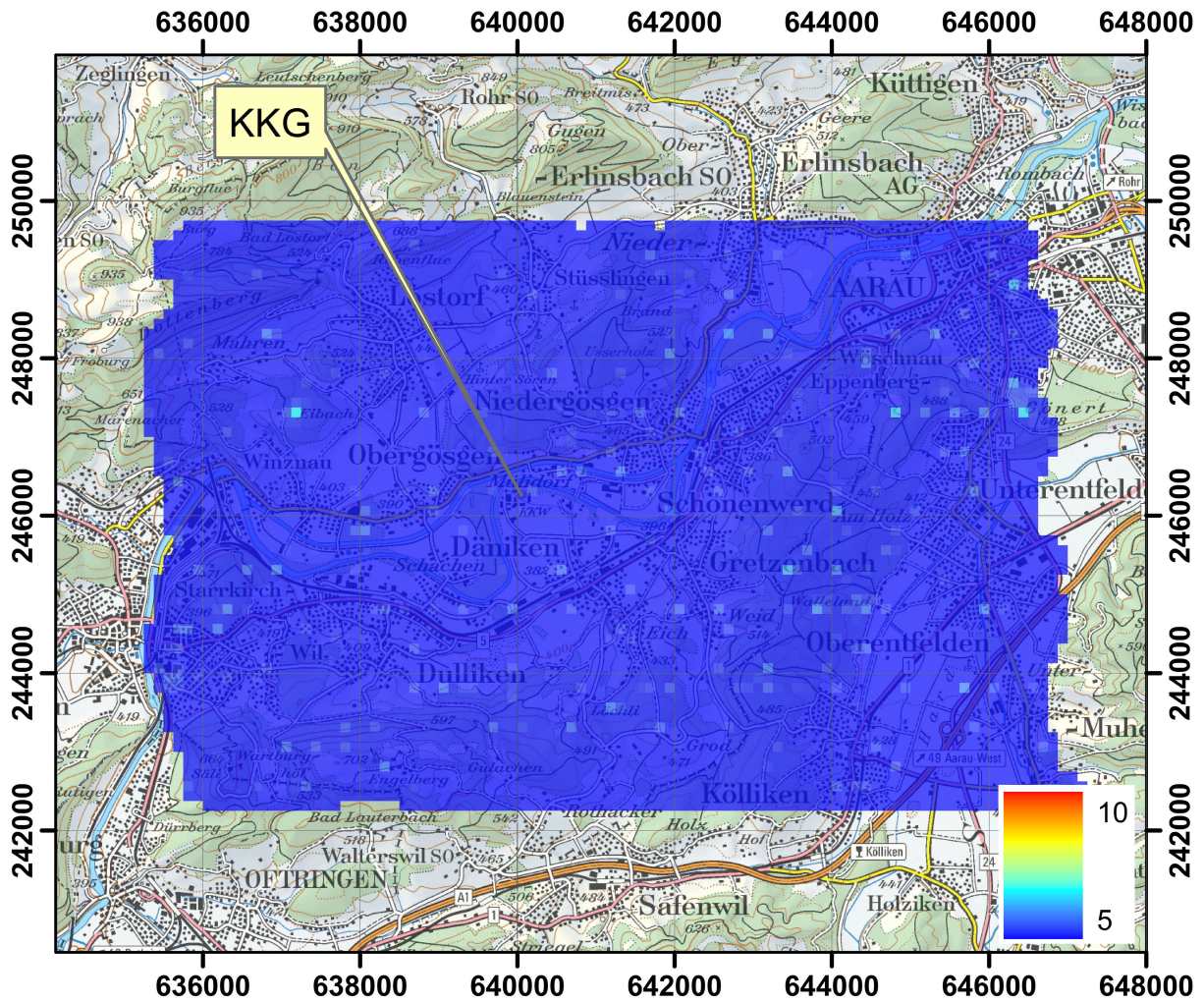
Figure 14: Man-made Gross-count (MMGC) ratio in the vicinity of KKG. PK100 ©2019 swisstopo (JD100042).
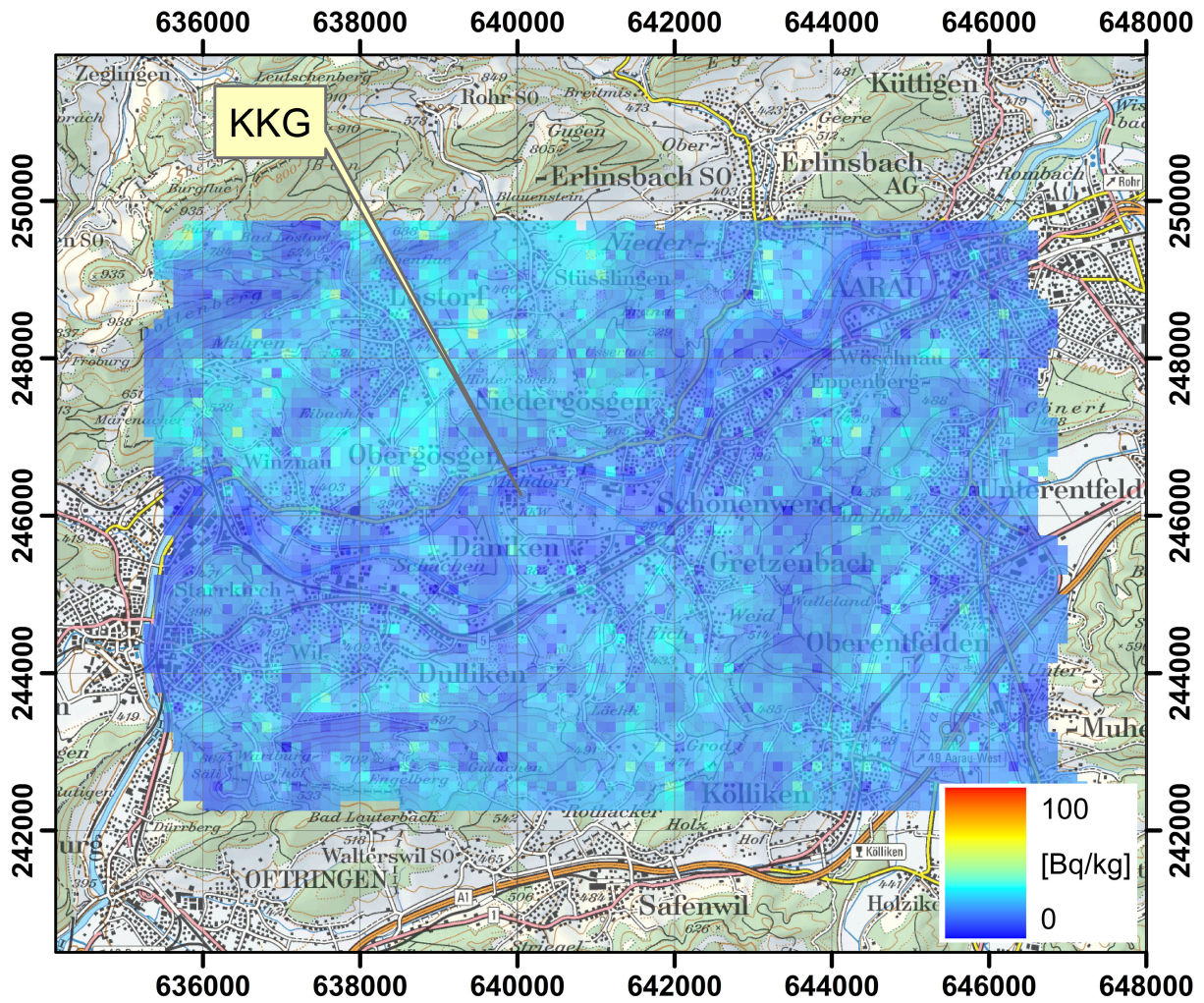
Figure 15: ^{232}Th activity concentration in the vicinity of KKG. PK100 ©2019 swisstopo (JD100042).
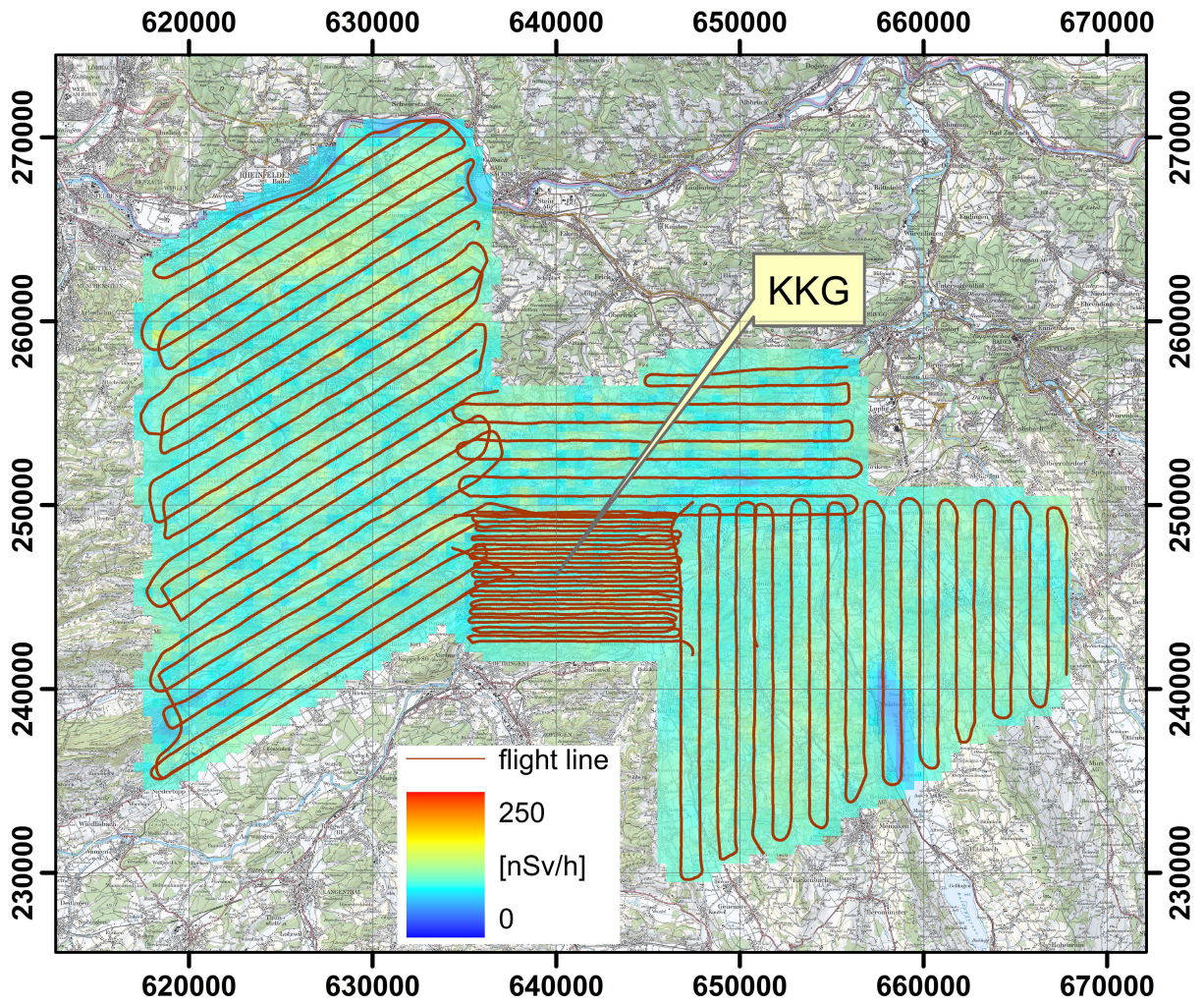
Figure 16: Dose rate in the extended vicinity of KKG.
PK100 ©2019 swisstopo (JD100042).
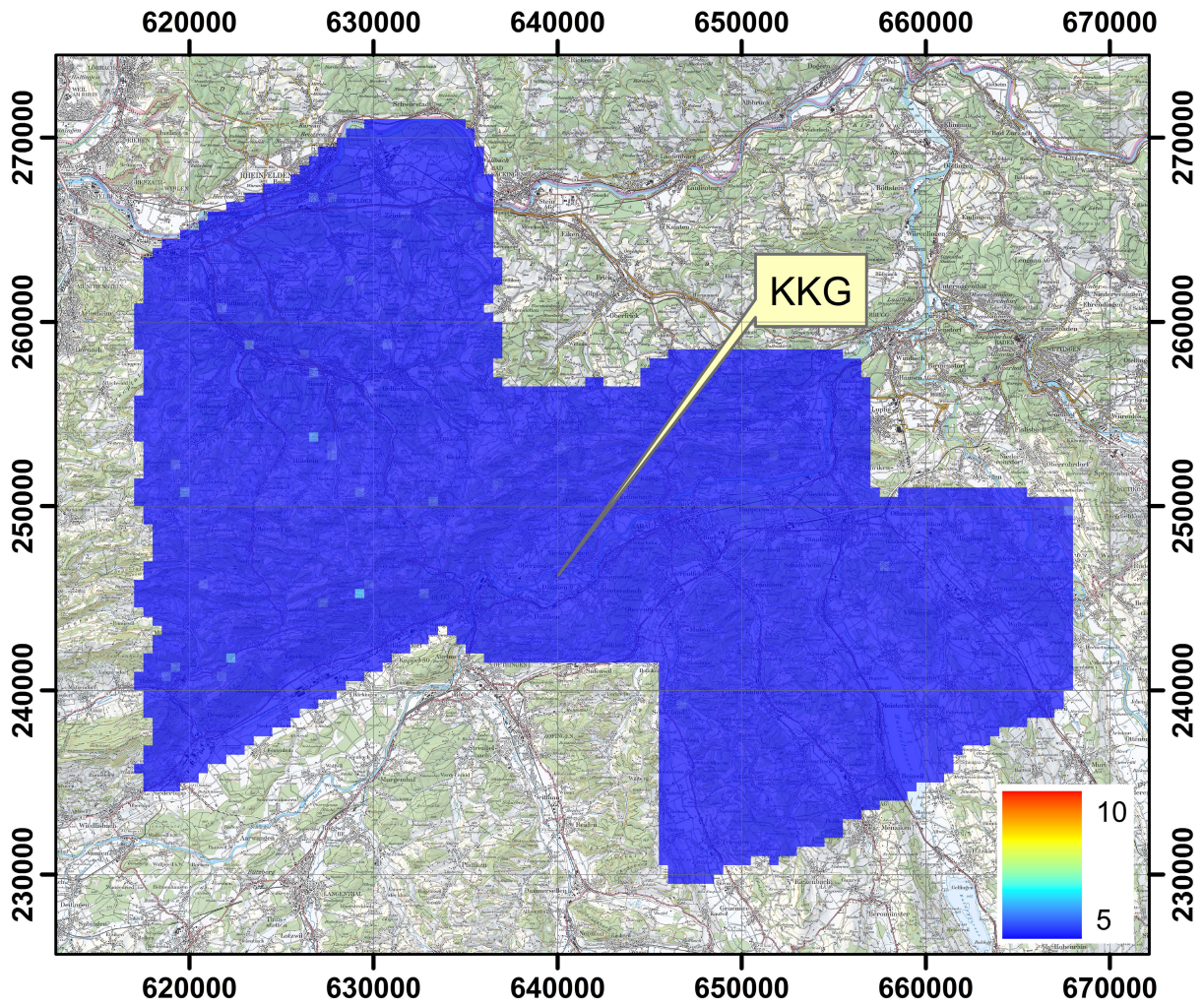
Figure 17: Man-made Gross-count (MMGC) ratio in the extended vicinity of KKG. PK100 ©2019 swisstopo (JD100042).
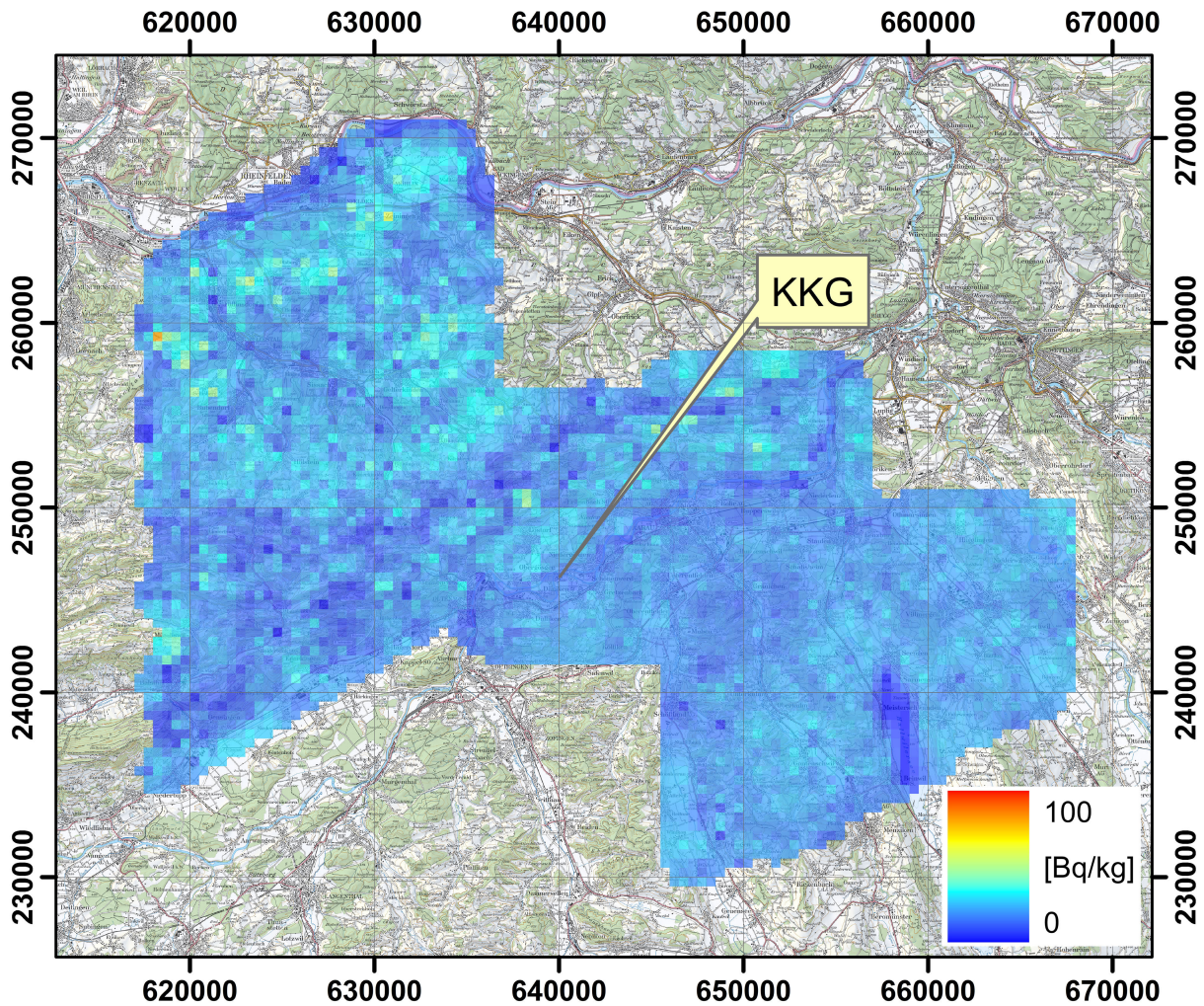
Figure 18: ^{232}Th activity concentration in the extended vicinity of KKG. PK100 ©2019 swisstopo (JD100042).

2.1.3 Transversal from Torre (TI) via Lukmanier and Disentis to Chur (GR)

During ARM19z, a transversal was measured ranging from Torre in the southern canton Ticino (TI) to Chur (canton Grisons (GR)) in the north. Figure 19 shows the flightline of the transversal. The altitude profile along the transversal, starting in the south, rises from 600 m to 2100 m above sea level (Figure 20). The total dose rate along the transversal (Figure 21) combines the effects of flight altitude due an elevated contribution of cosmic radiation and the variable contribution of natural radionuclides. Removing the dose rate contribution of cosmic radiation from the total dose rate yields the terrestrial component of dose rate (Figure 26). The terrestrial dose rate is correlated to the activity concentration of natural radionuclides in soil and rock (Figure 26), like for example ^{40}K (Figure 24) ^{232}Th (Figure 25). Thus, the dose rate attributed to natural radionuclides (Figure 23) is nearly identical to the terrestrial component.

The photons emitted from the natural radionuclides are attenuated if they have to pass through layers of water. Thus, lower values of dose rates and activity concentrations are observed when the flight line crosses rivers and lakes.
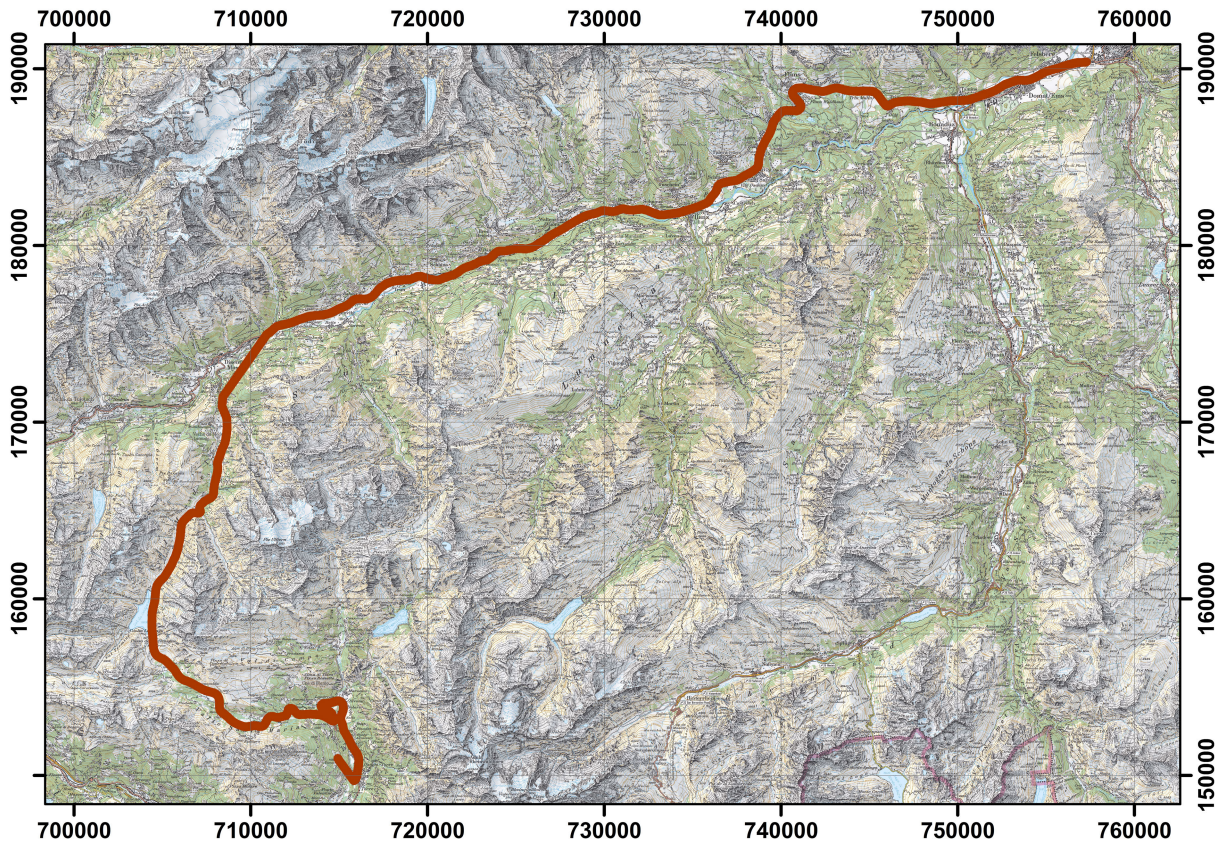
Figure 19: Flight line of the transversal from Torre (TI) to Chur (GR).
PK100 ©2019 swisstopo (JD100042).
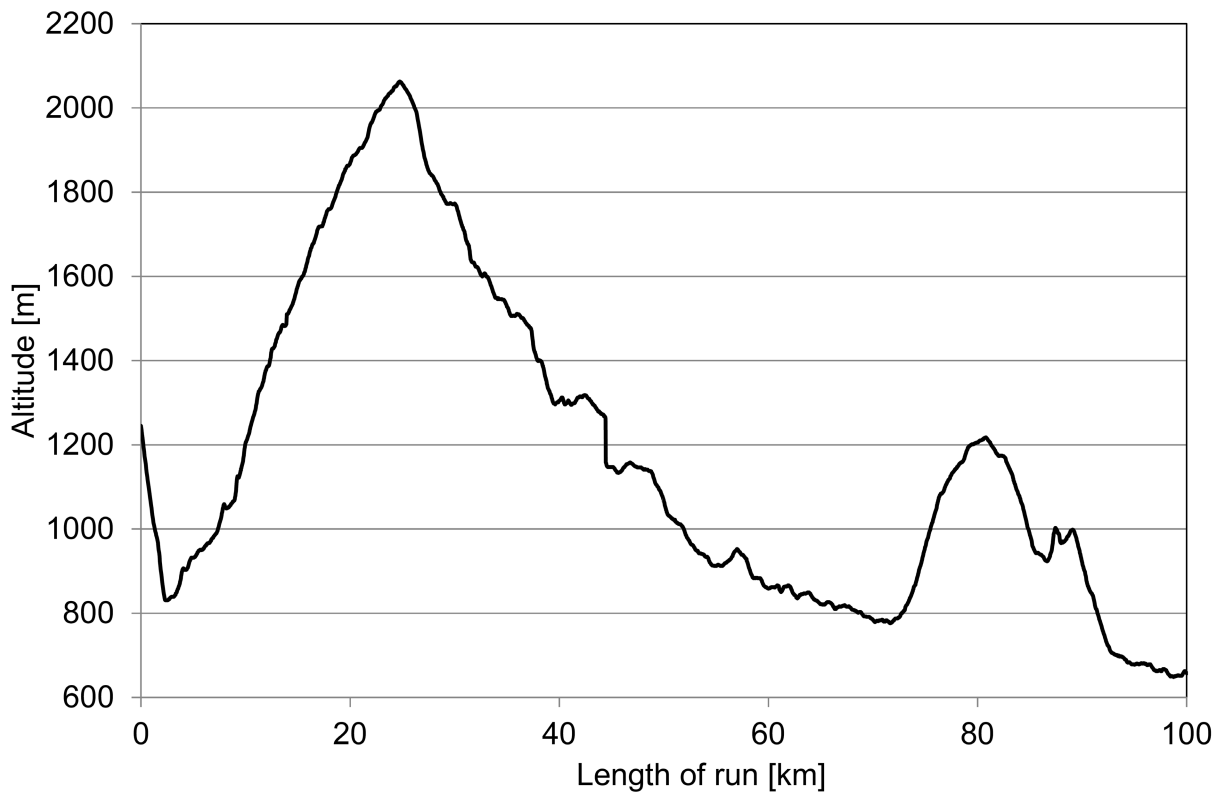
Figure 20: Altitude profile of the transversal from Torre (TI) to Chur (GR).
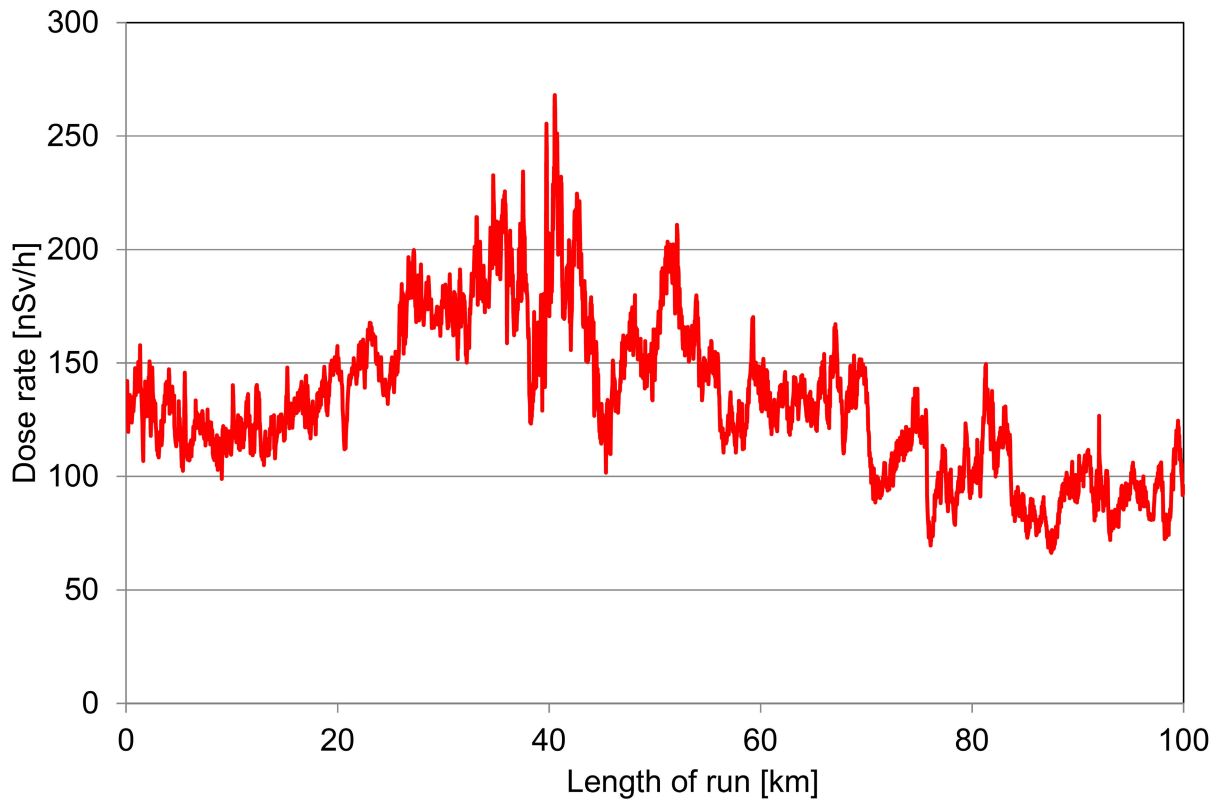
Figure 21: Dose rate along the transversal from Torre (TI) to Chur (GR).
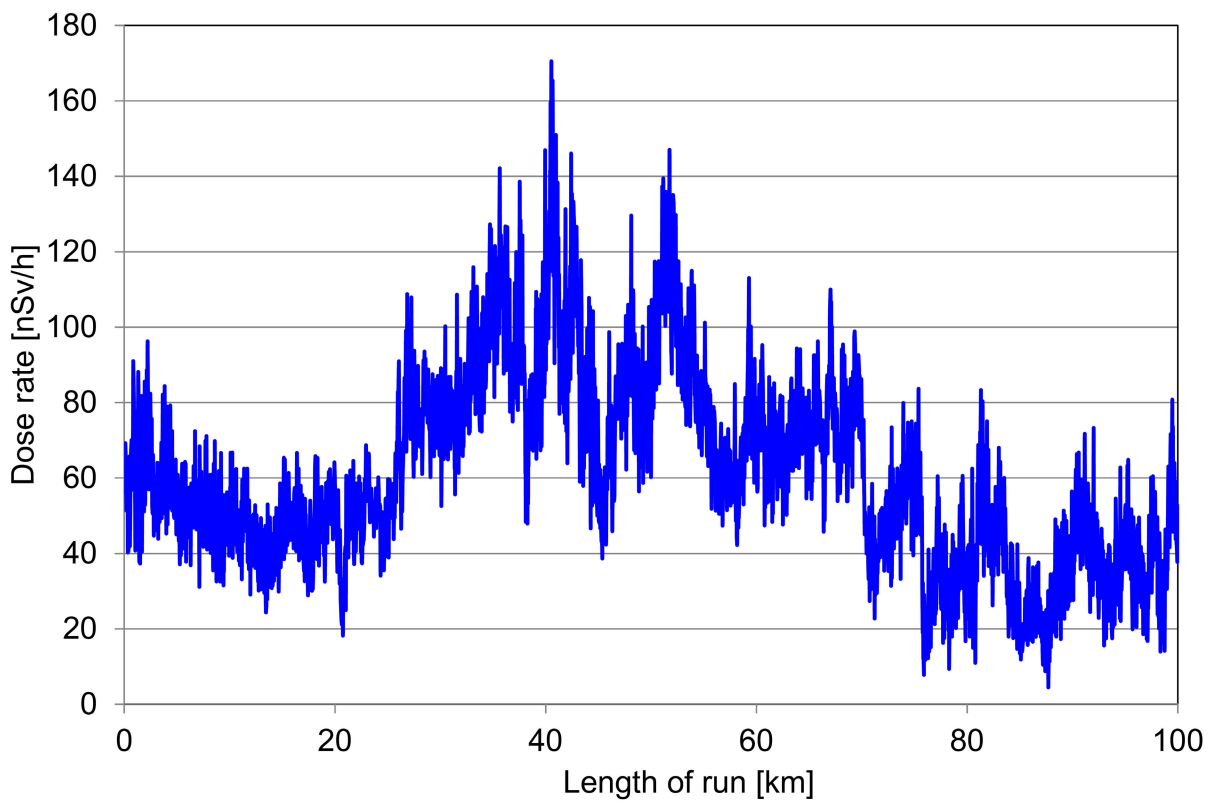
Figure 22: Terrestrial component of the dose rate along the transversal from Torre (TI) to Chur (GR).
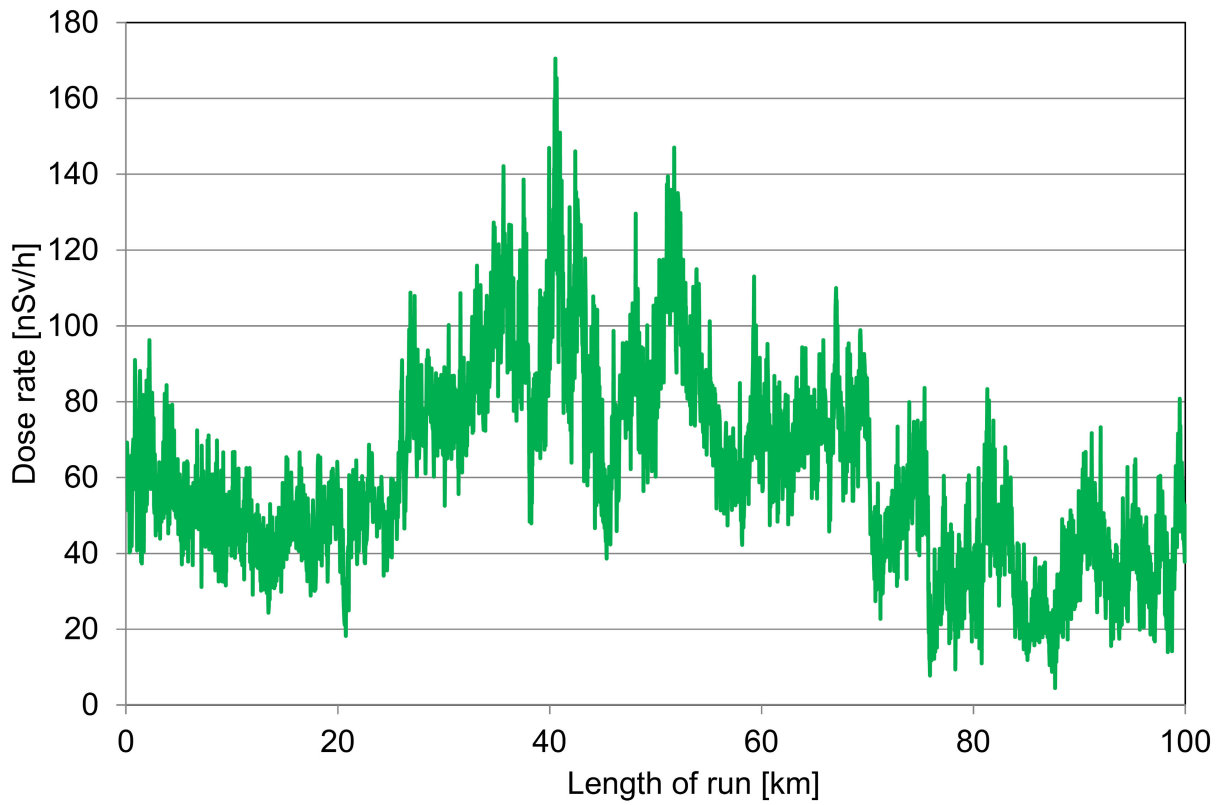
Figure 23: Dose rate caused by natural radionuclides along the transversal from Torre (TI) to Chur (GR).
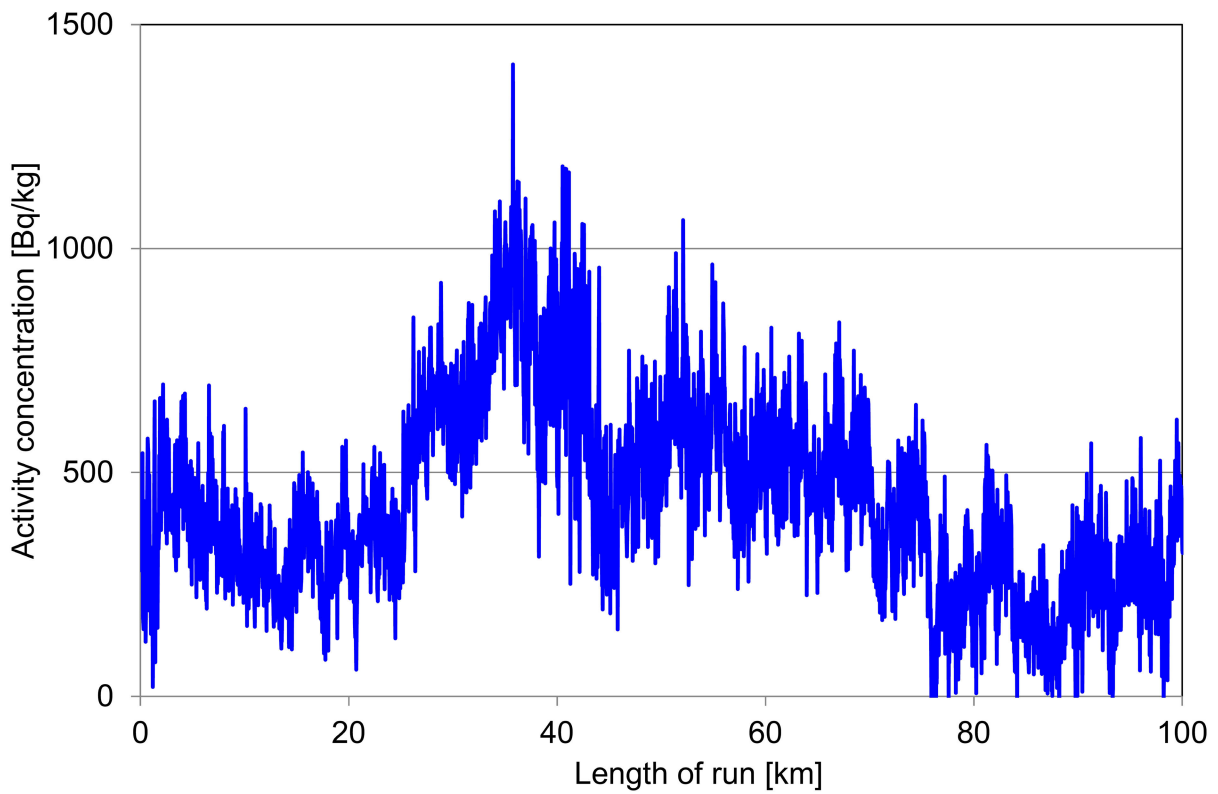
Figure 24: ^{40}K activity concentration along the transversal from Torre (TI) to Chur (GR).
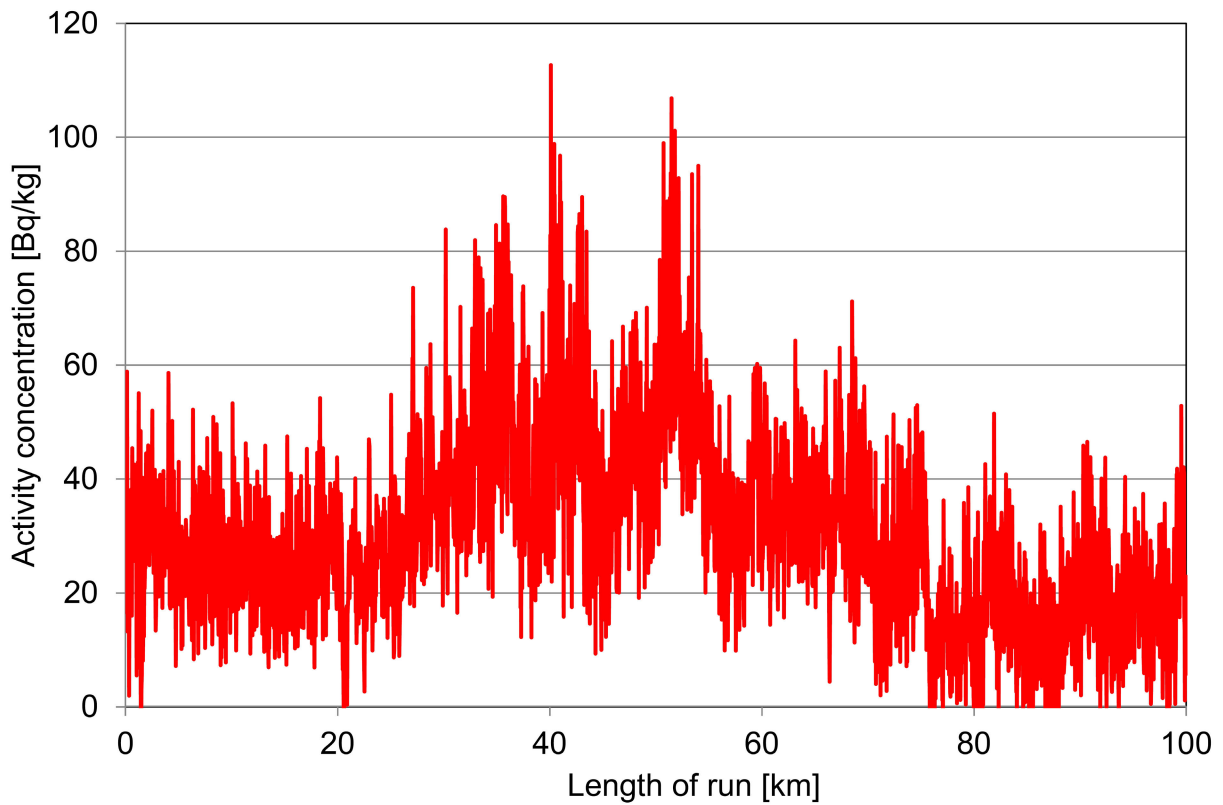
Figure 25: ^{232}Th activity concentration along the transversal from Torre (TI) to Chur (GR).
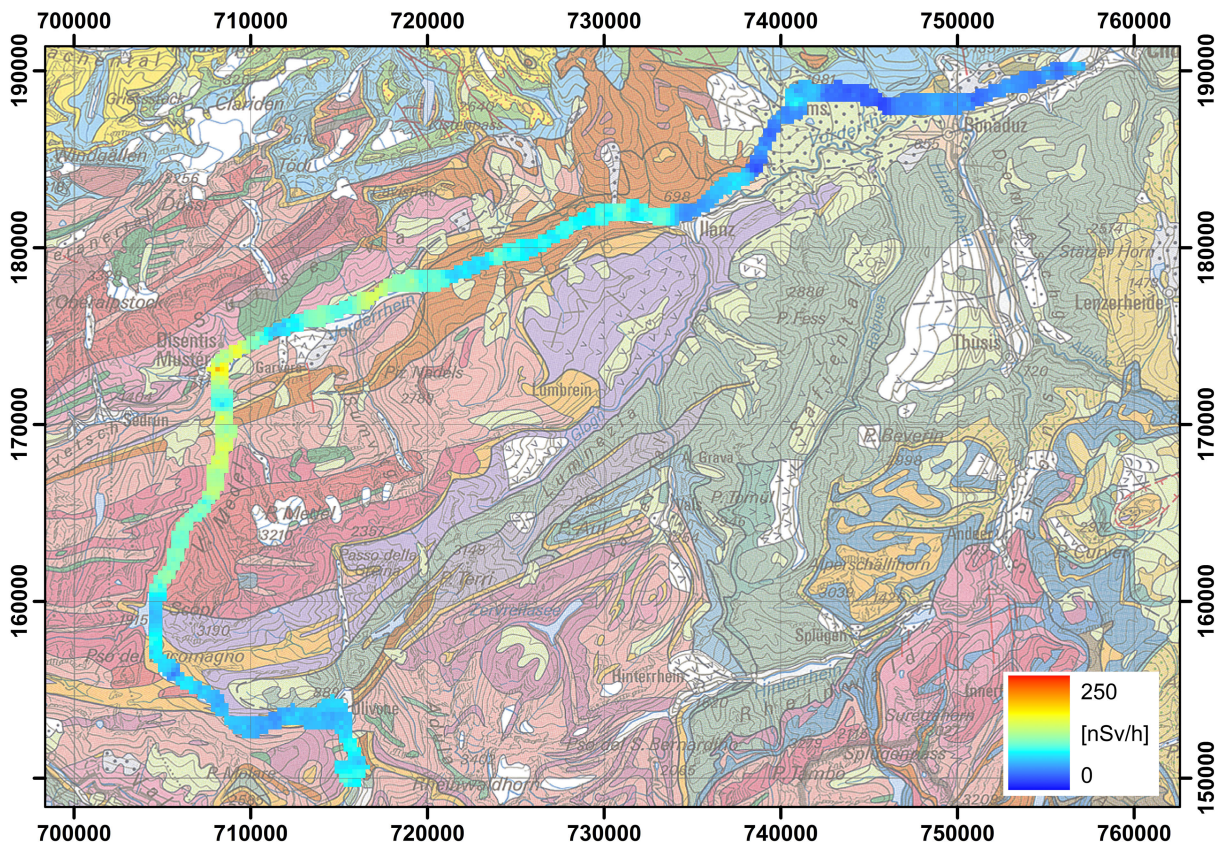
Figure 26: Terrestrial dose rate of the transversal from Torre (TI) to Chur (GR) plotted over a geological overview map. GK500 ©2019 swisstopo (JD100042).

2.1.4 Altitude profile over Lake Neuchâtel

The background of the measurement systems and the influence of cosmic radiation on the measured signal can be determined by measurements in different altitudes over a body of water which attenuates direct radiation of terrestrial radionuclides. The comparison of an altitude profile over the North Sea measured in 2018 (Butterweck et al., 2019) to altitude profiles over two Swiss lakes measured with the same detector indicated an influence of airborne radon progeny on altitude profiles over inland lakes. These measurements were used to derive a mathematical model for the influence of airborne radon progeny on the measured count rate in the different energy windows based on the ratio of counts in the energy range between 100 keV and 400 keV to the counts in the energy range between 1400 keV to 2997 keV, called further radon ratio. A square root dependence was found to be an optimal fit to the three data points in each energy window (Figure 27). The addition of data points from an altitude profile over lake Neuchâtel measured during the civil exercise ARM19z necessitated a revision of the model. The postulated square root dependence was abandoned in favour of a simpler linear model. In a first step, the baseline radon ratio was determined (Figure 28). The x- and y-axes from Figure 28 were exchanged in comparison to Figure 27, as the y-axis intercept thus yields the radon ratio with no additional influence of airborne radon progeny. The revised model of additional counts originating from airborne radon progeny can be formulated as

$CR_{Rn} = F_{Rn} * (R_{Rn} - R_{Rn,0})$

with:

CR_{Rn}:   Additional count rate due to airborne radon progeny [cps]
F_{Rn}:   Factor correlating the Rn-ratio to the additional count rate [cps]
R_{Rn}:   Rn-ratio [ ]
$R_{Rn,0}$:   Baseline Rn-ratio without airborne radon progeny [ ]

The baseline radon ratio $R_{Rn,0}$ agrees well for all energy windows with a relative standard deviation of 0.4% and an average value of 6.78 and can be considered constant for all energy windows. The correlation factor F_{Rn} can thus be determined with a linear regression of the data as depicted in Figure 29 with this constant baseline radon ratio subtracted. The values derived from the current set of four data points are listed in table 4. The SDI window is a special case, as the count rate in each channel is weighed with the energy of the channel to render the SDI index. The additional count rate in the SDI window given in table 4 is the additional SDI index divided by the midpoint energy of the SDI window.

The model for a potential correction for counts generated by airborne radon progeny is still under development. Data from additional altitude profiles over inland lakes and open seas are needed before an according correction can be integrated into the data evaluation.
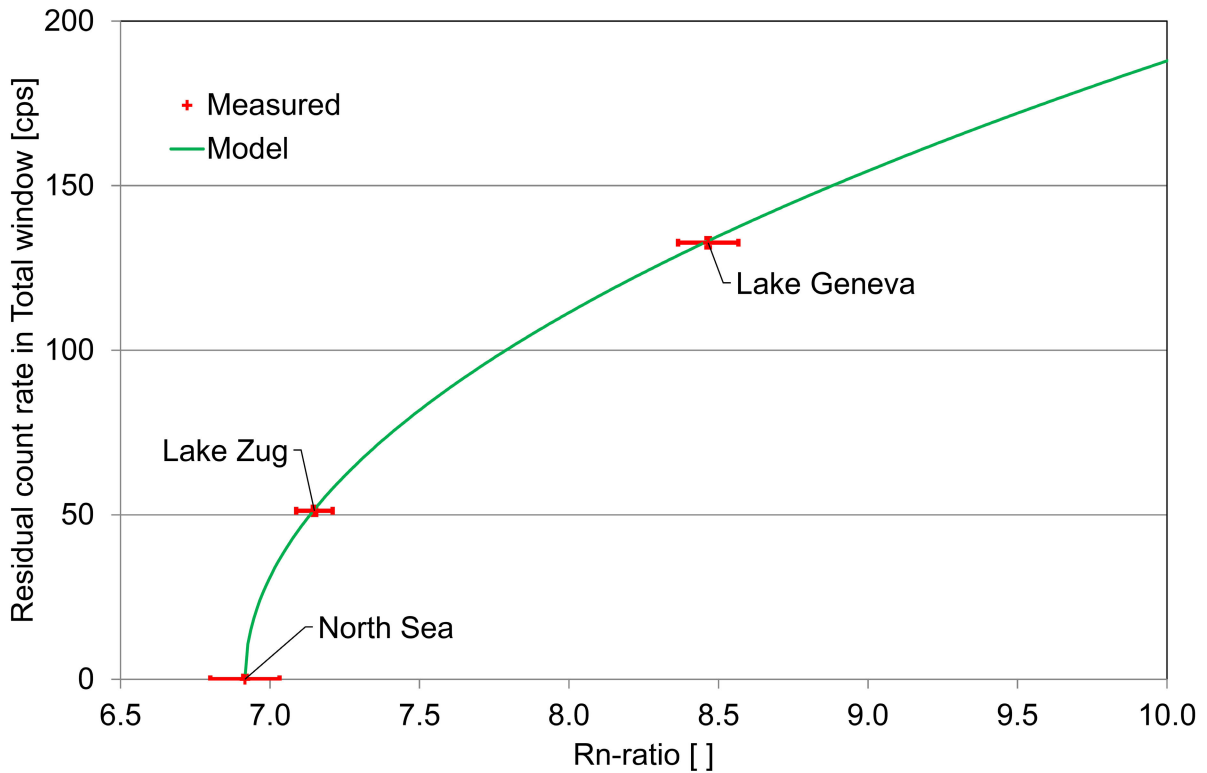
Figure 27: Residual count rate in the total window in dependence on the Rn-ratio. Square root model (see PSI-report 19-01).
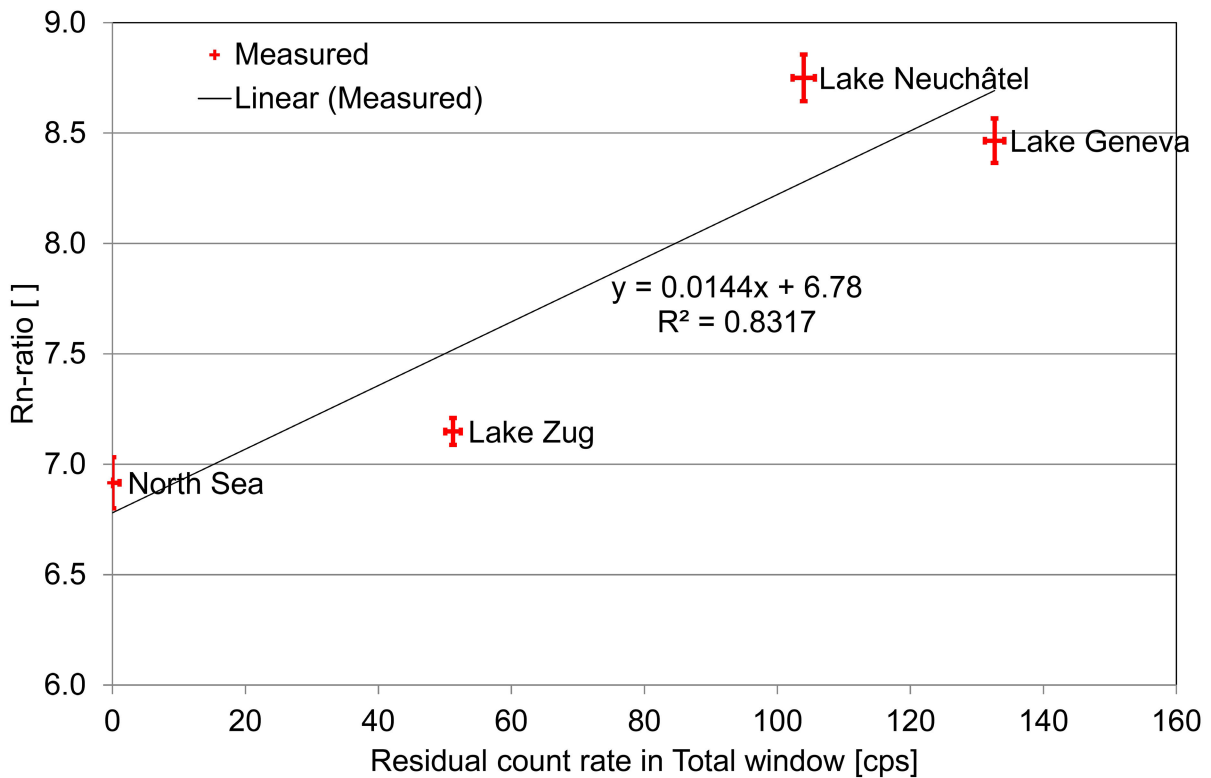
Figure 28: Rn-ratio in dependence on the residual count rate in the total window. Linear model.
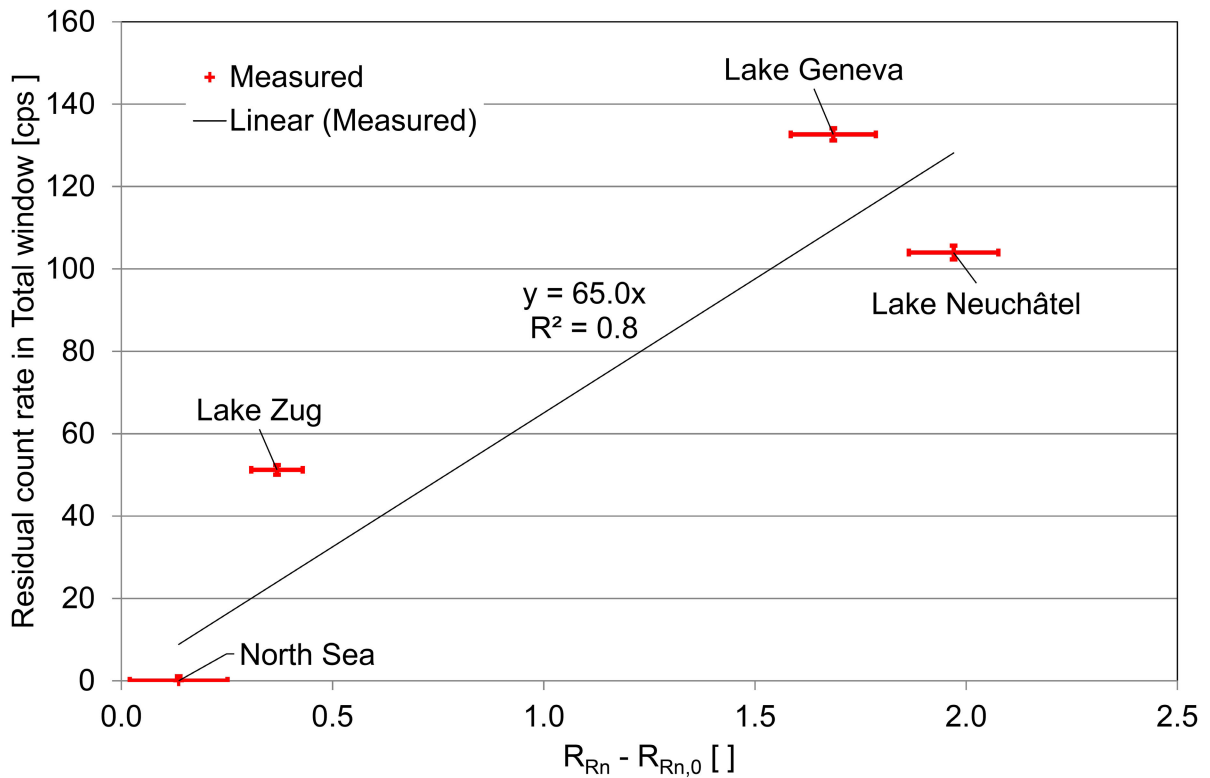
Figure 29: Residual count rate in the total window in dependence on the Rn-ratio minus the baseline Rn-ratio. Linear model.

Energy window	Energy range [keV]	F_{Rn} [cps]
Caesium	600 - 720	10.2 ± 1.4
Cobalt	1100 - 1400	8.6 ± 1.2
Uranium	1664 - 1853	3.6 ± 0.5
Total	401 - 2997	65 ± 10
Potassium	1369 - 1558	4.1 ± 0.5
MMGC1	400 - 1400	54 ± 8
MMGC2	1400 - 2997	11.2 ± 2.0
SDI	240 - 2997	45 ± 7
Thorium	2407 - 2797	2.0 ± 0.6

Table 4: Radon correlation factor derived from four altitude profiles.

2.2 ARM19m

2.2.1 Bulle, Köniz and Vevey

For the extension of the series of radiological background maps over Swiss cities, the vicinity of Bulle, Köniz and Vevey was measured during ARM19m. The maps of the ambient dose rate (Figures 30, 33 and 36) show reduced values over lakes and rivers. The dose rate reduction is caused by the attenuation of photon radiation originating from natural radionuclides in rock and soil in the overlaying water layer. The maps of the MMGC-ratio

(Figures 31, 34 and 37), an indicator for the presence of man-made radionuclides, do not show any elevated values in the measured areas. The maps of the ^{232}Th activity concentration (Figures 32, 35 and 38) depict typical values over land and reduced readings over the rivers due to the attenuation of the water layer. In the measuring area around Köniz, a flight line was repeated after an automatic nuclide identification warning of the RLL system. The warning could not be reproduced in the repetition of the flight line.
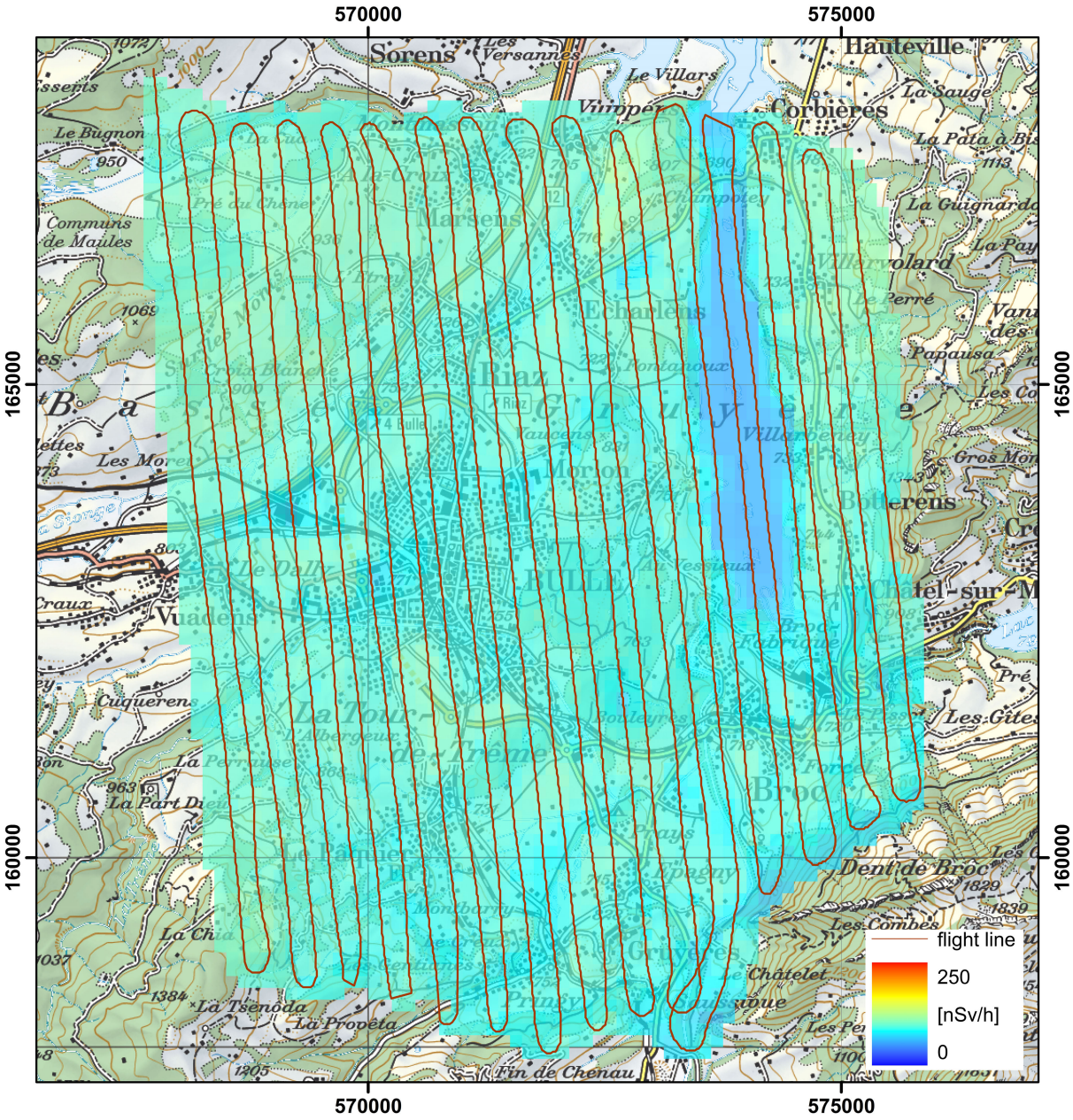
Figure 30: Dose rate in the vicinity of Bulle.
PK100 ©2019 swisstopo (JD100042).
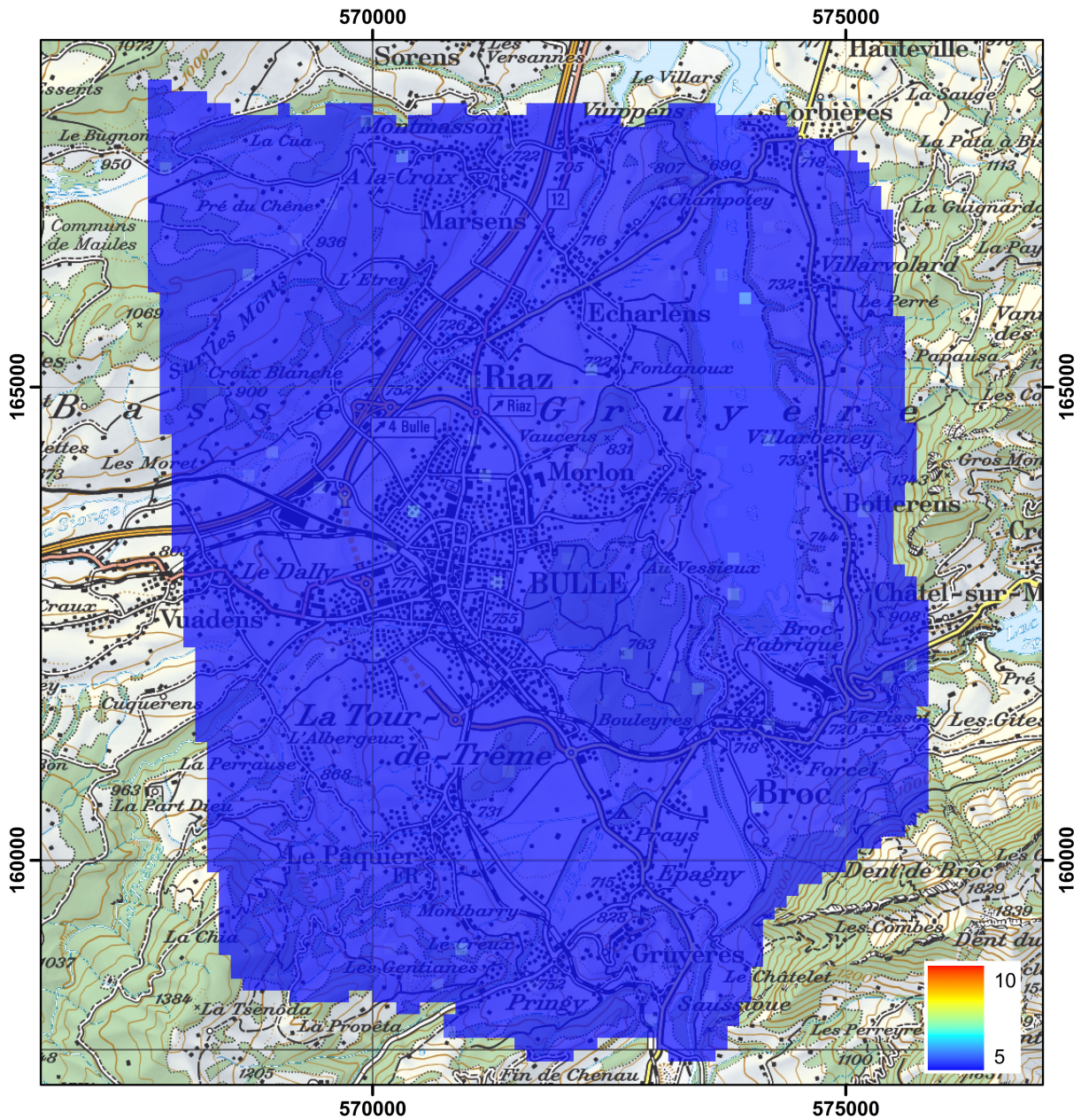
Figure 31: Man-made Gross-count (MMGC) ratio in the vicinity of Bulle. PK100 ©2019 swisstopo (JD100042).
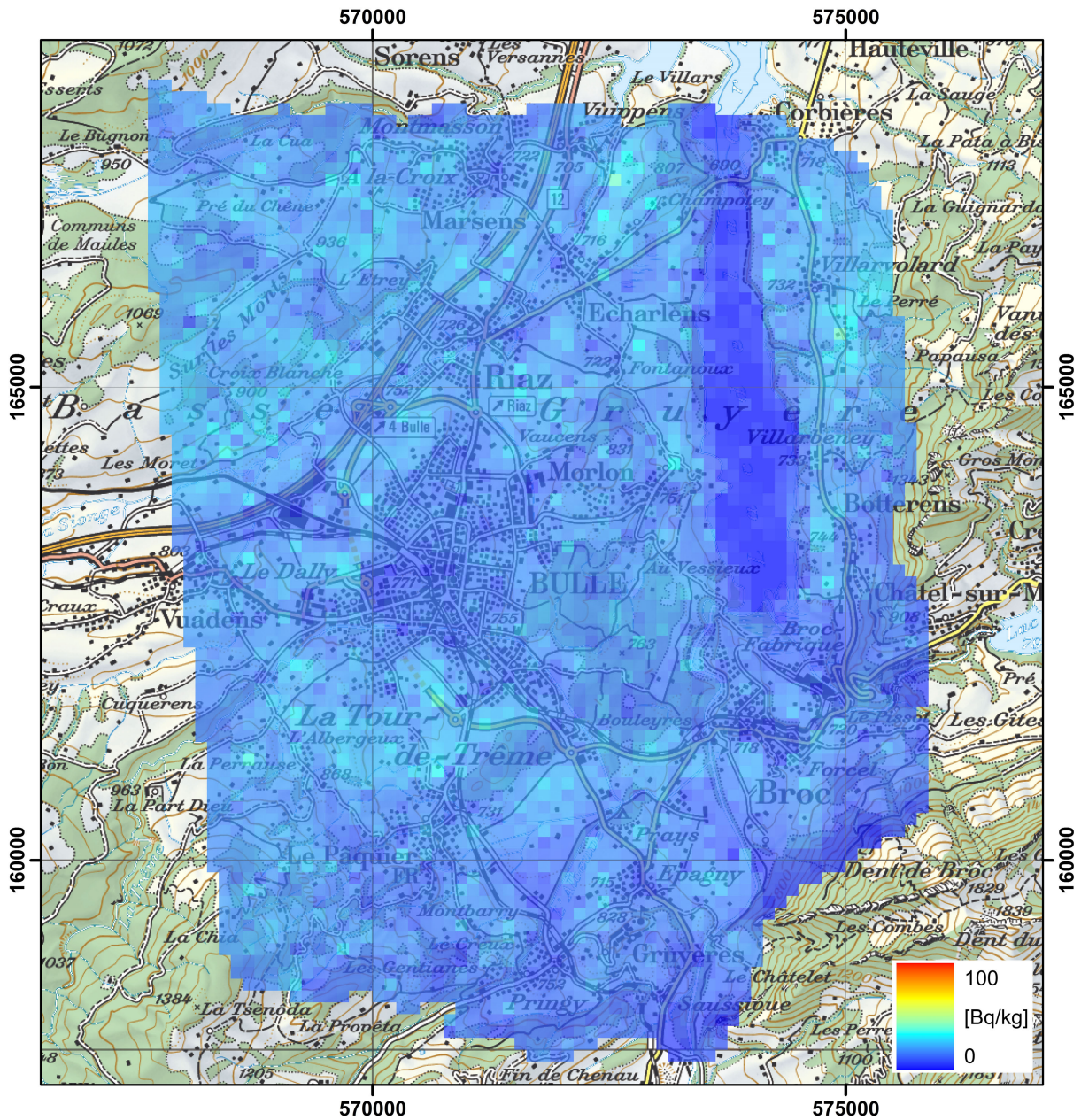
Figure 32: [232]Th activity concentration in the vicinity of Bulle. PK100 ©2019 swisstopo (JD100042).
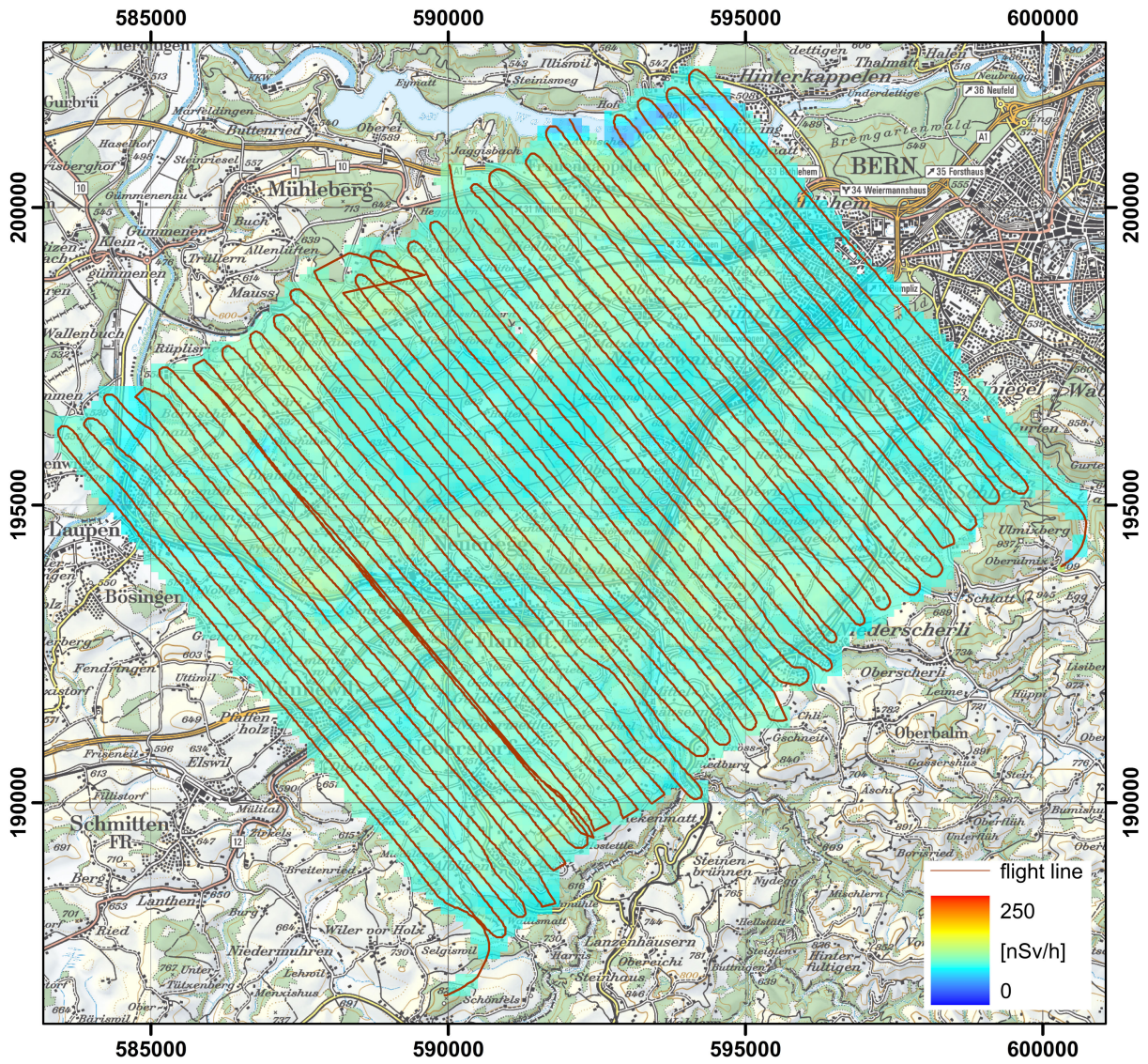
Figure 33: Dose rate in the vicinity of Köniz.
PK100 ©2019 swisstopo (JD100042).
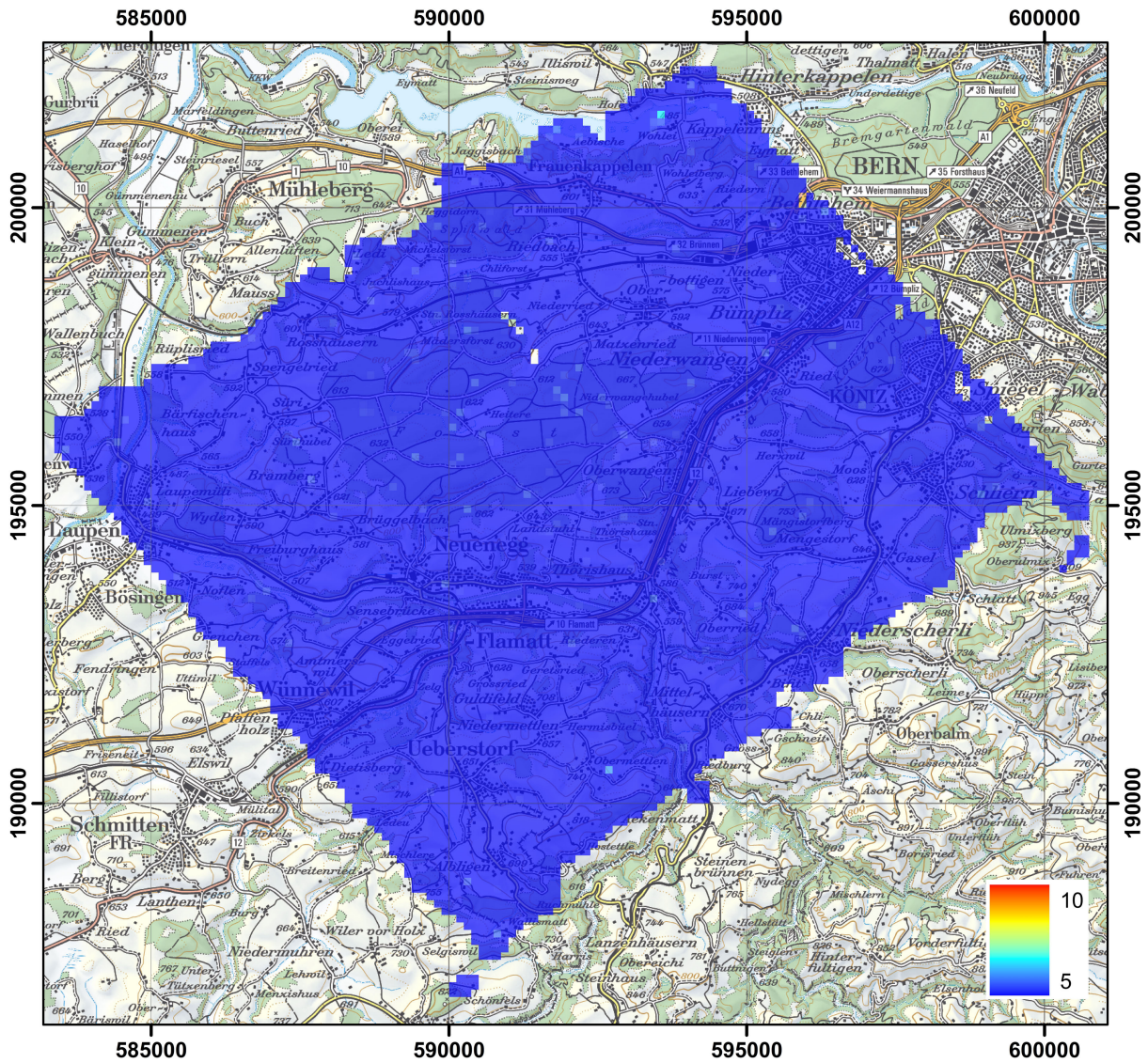
Figure 34: Man-made Gross-count (MMGC) ratio in the vicinity of Köniz. PK100 ©2019 swisstopo (JD100042).
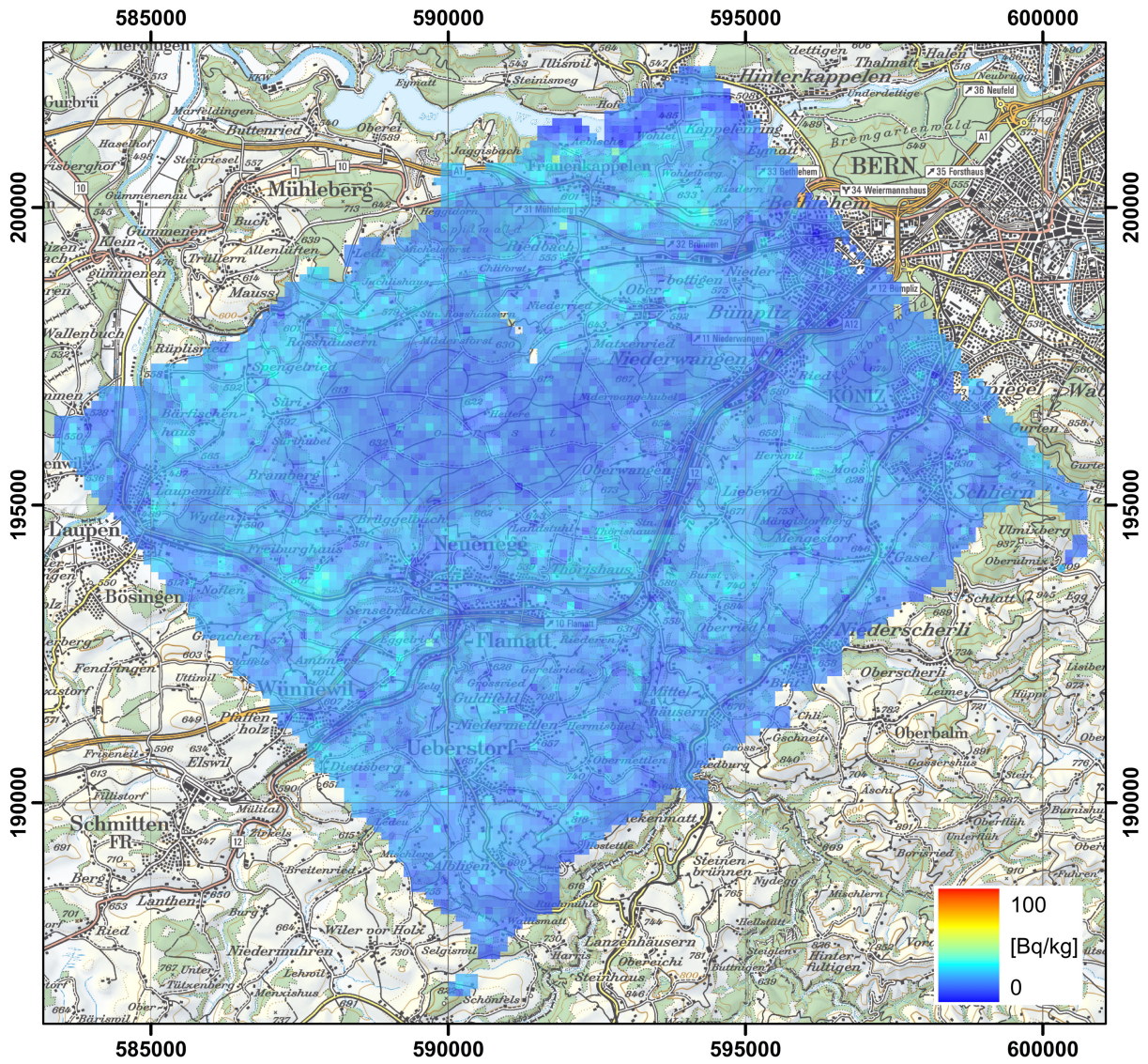
Figure 35: ^{232}Th activity concentration in the vicinity of Köniz. PK100 ©2019 swisstopo (JD100042).
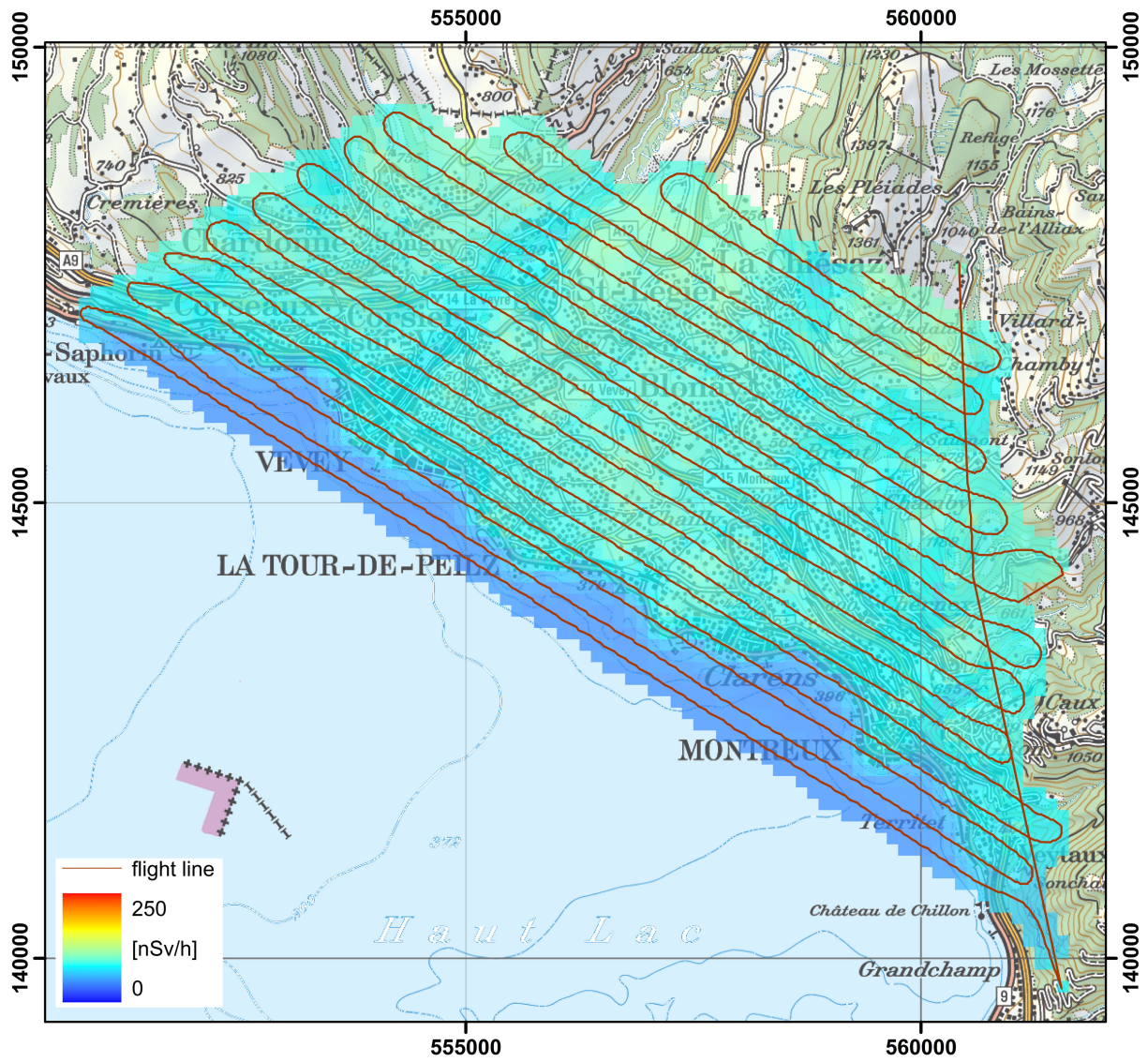
Figure 36: Dose rate in the vicinity of Vevey.
PK100 ©2019 swisstopo (JD100042).
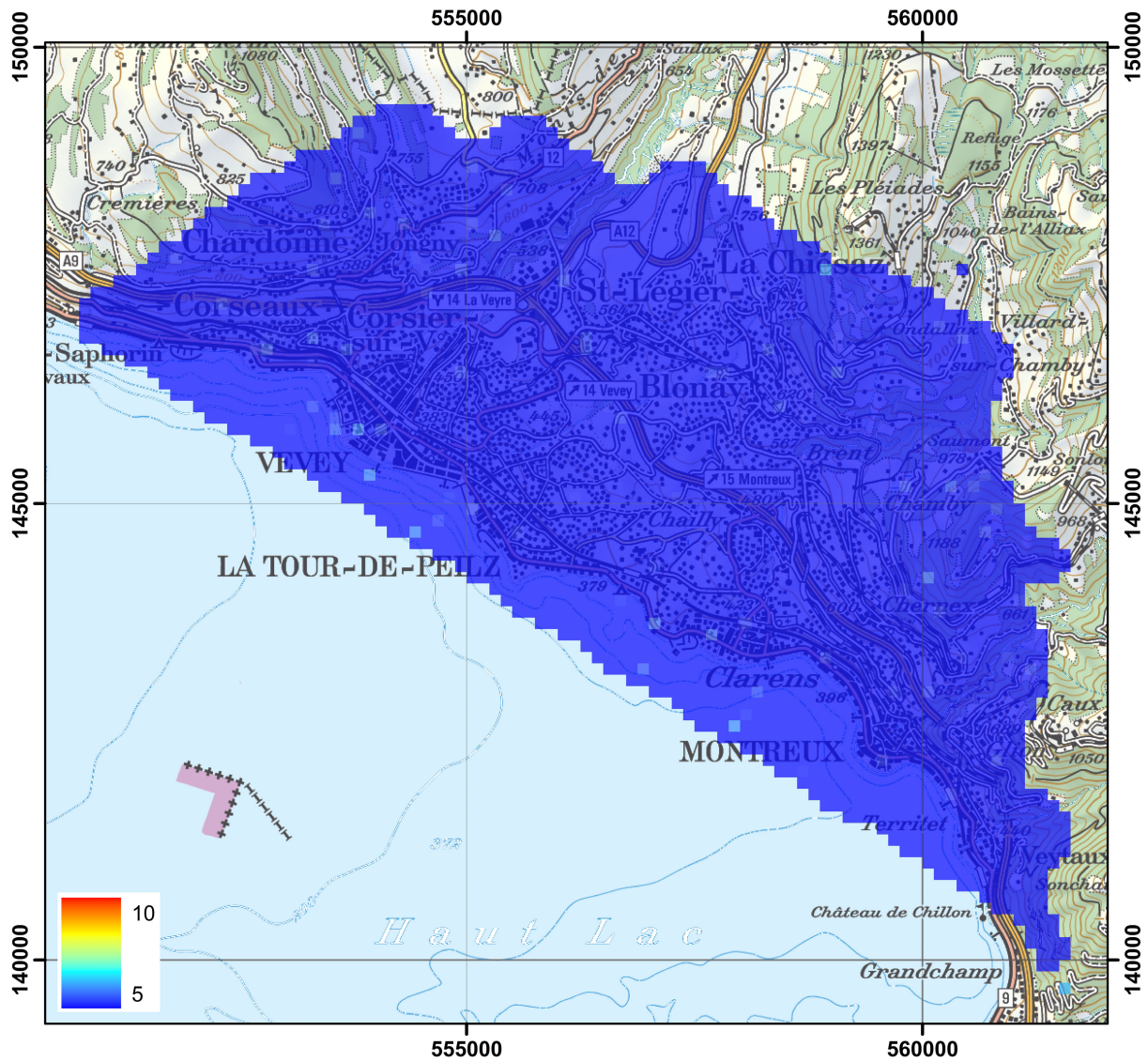
Figure 37: Man-made Gross-count (MMGC) ratio in the vicinity of Vevey. PK100 ©2019 swisstopo (JD100042).
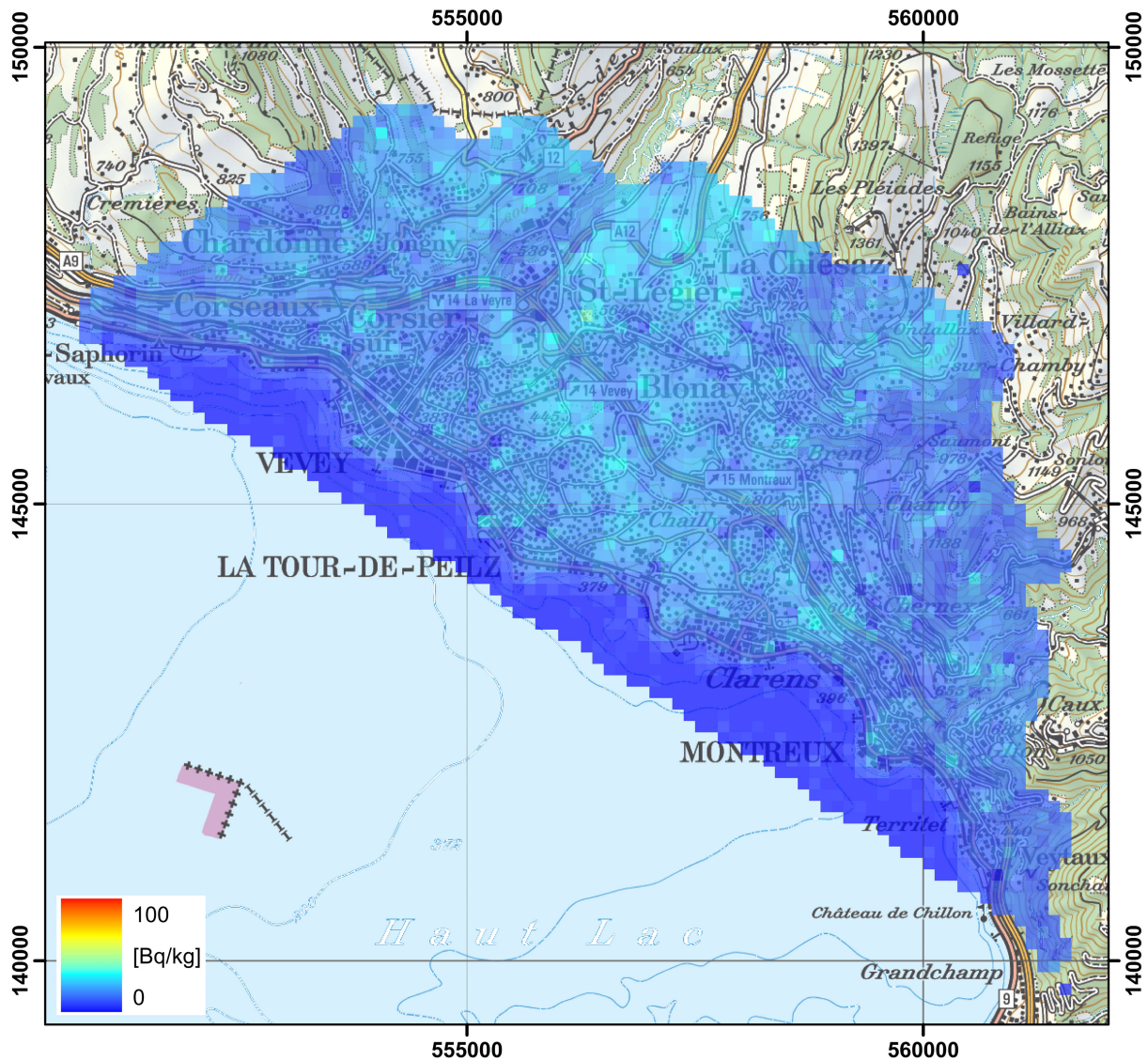
Figure 38: ^{232}Th activity concentration in the vicinity of Vevey. PK100 ©2019 swisstopo (JD100042).

2.2.2 Thun military training ground

During the international exercise in 2017 (Butterweck et al., 2017), the concept of a reference site for checks of system performance with natural radioactivity was tested. The area selected in the Linth plain did fulfil the criteria of flat terrain in reasonable distance to one of the airbases with RLL-equipment. Unfortunately, this reference area had to be discarded due to a high and variable water content in the ground. Alternative locations were discussed and in a next step of the selection process, measurements were performed over Thun military training ground. The maps of dose rate (Figure 39, average 91±7 nSv/h), ^{232}Th activity concentration (Figure 40, average 17±8 Bq/kg) and ^{40}K activity concentration (Figure 41, average 215±77 Bq/kg) show rather low values, which render the usefulness of this site as reference area questionable. The map of the MMGC-ratio (Figure 42) yields no indication of significant ^{137}Cs deposition due to the Chernobyl accident.

36
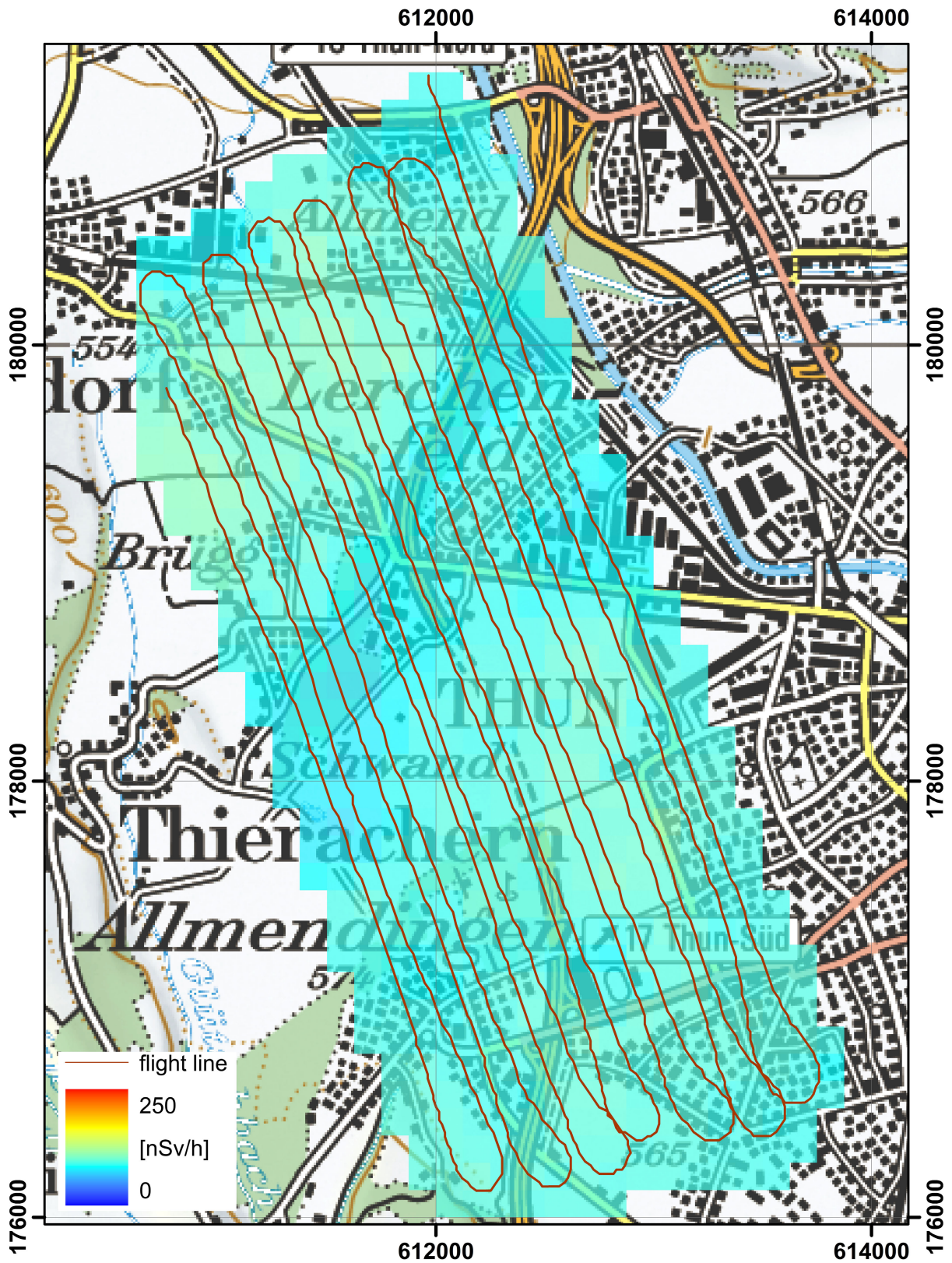
Figure 39: Dose rate over Thun military training ground.
PK100 ©2019 swisstopo (JD100042).
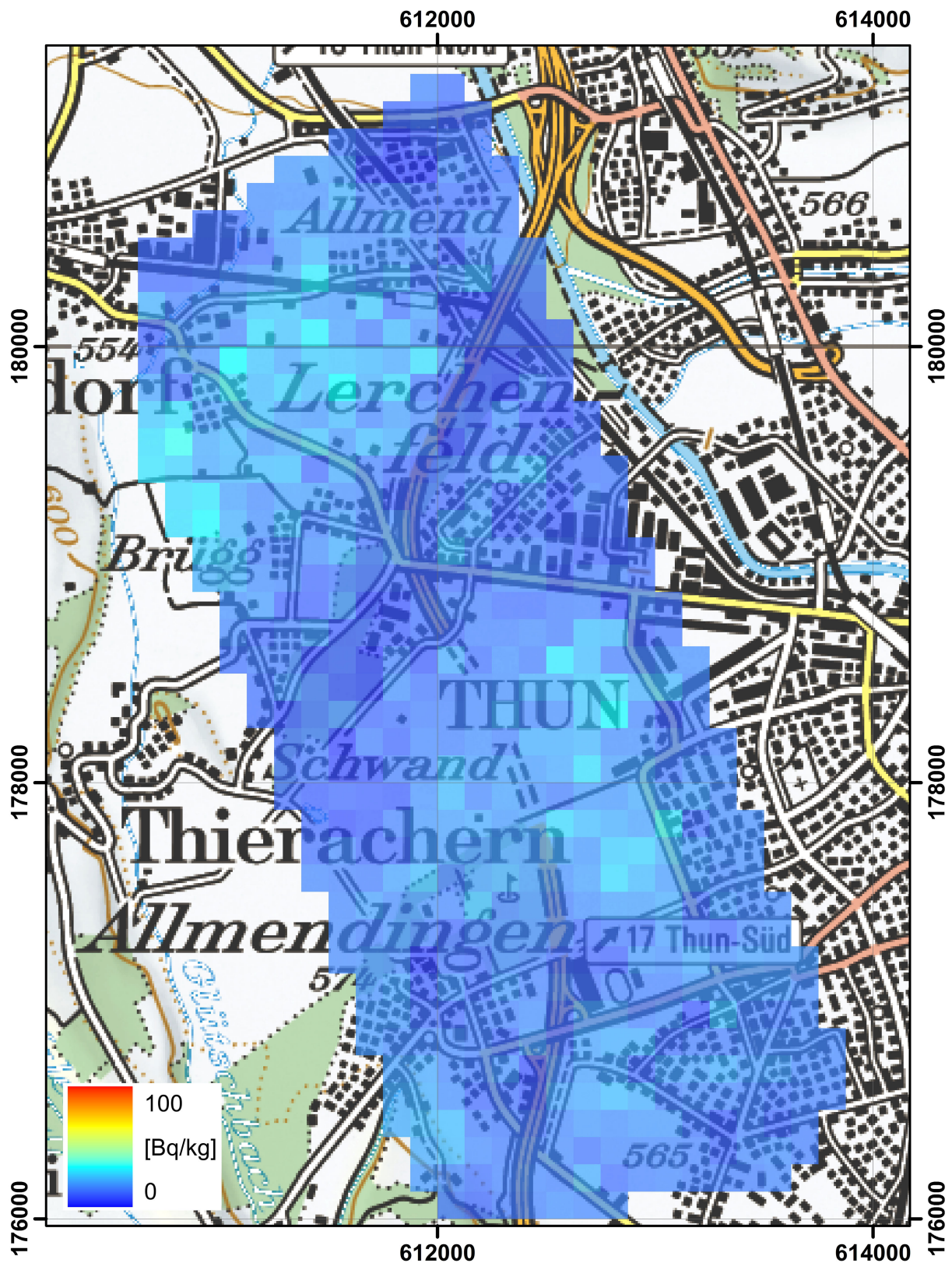
Figure 40: ^{232}Th activity concentration over Thun military training ground. PK100 ©2019 swisstopo (JD100042).
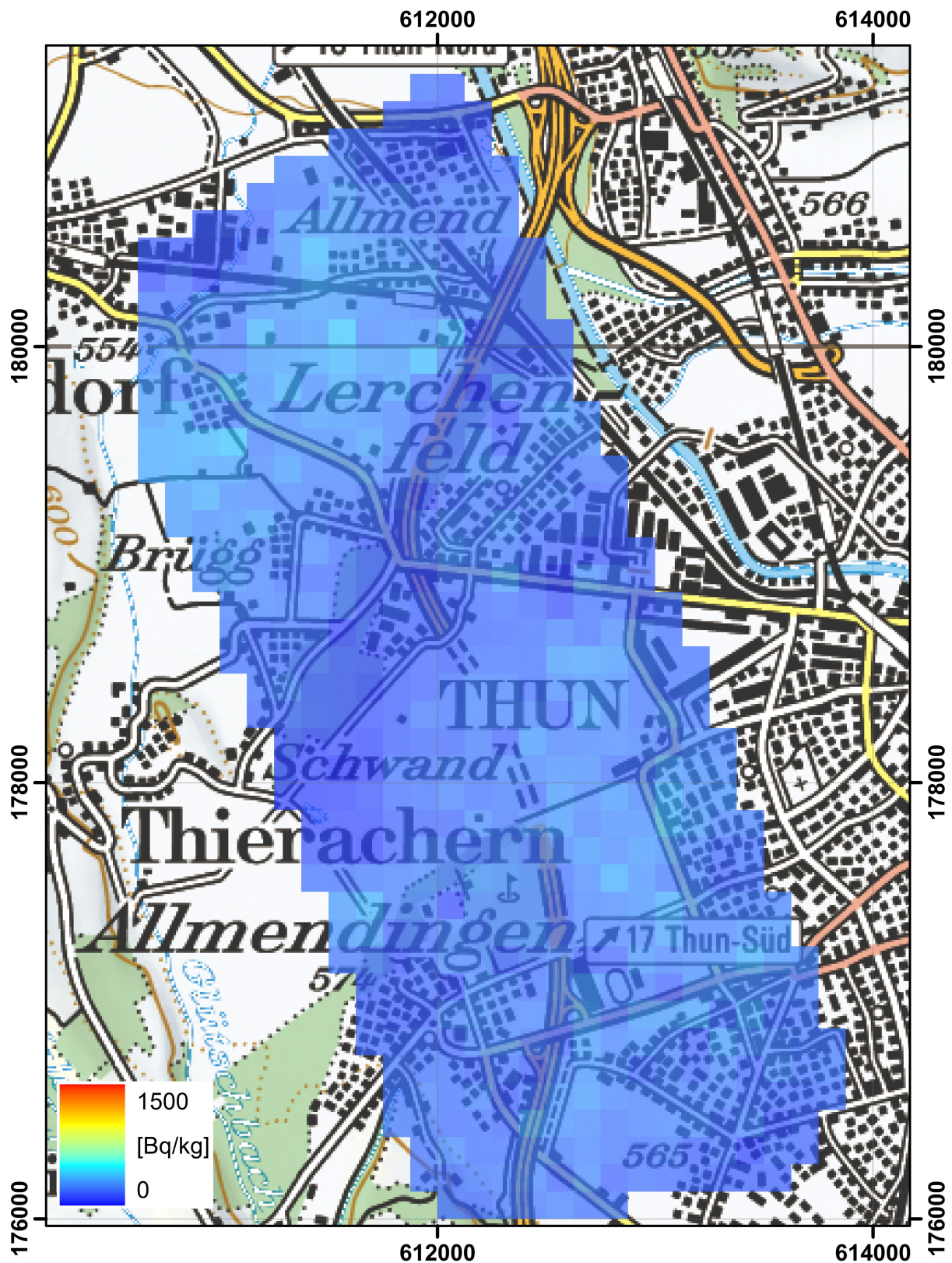
Figure 41: ^{40}K activity concentration over Thun military training ground. PK100 ©2019 swisstopo (JD100042).
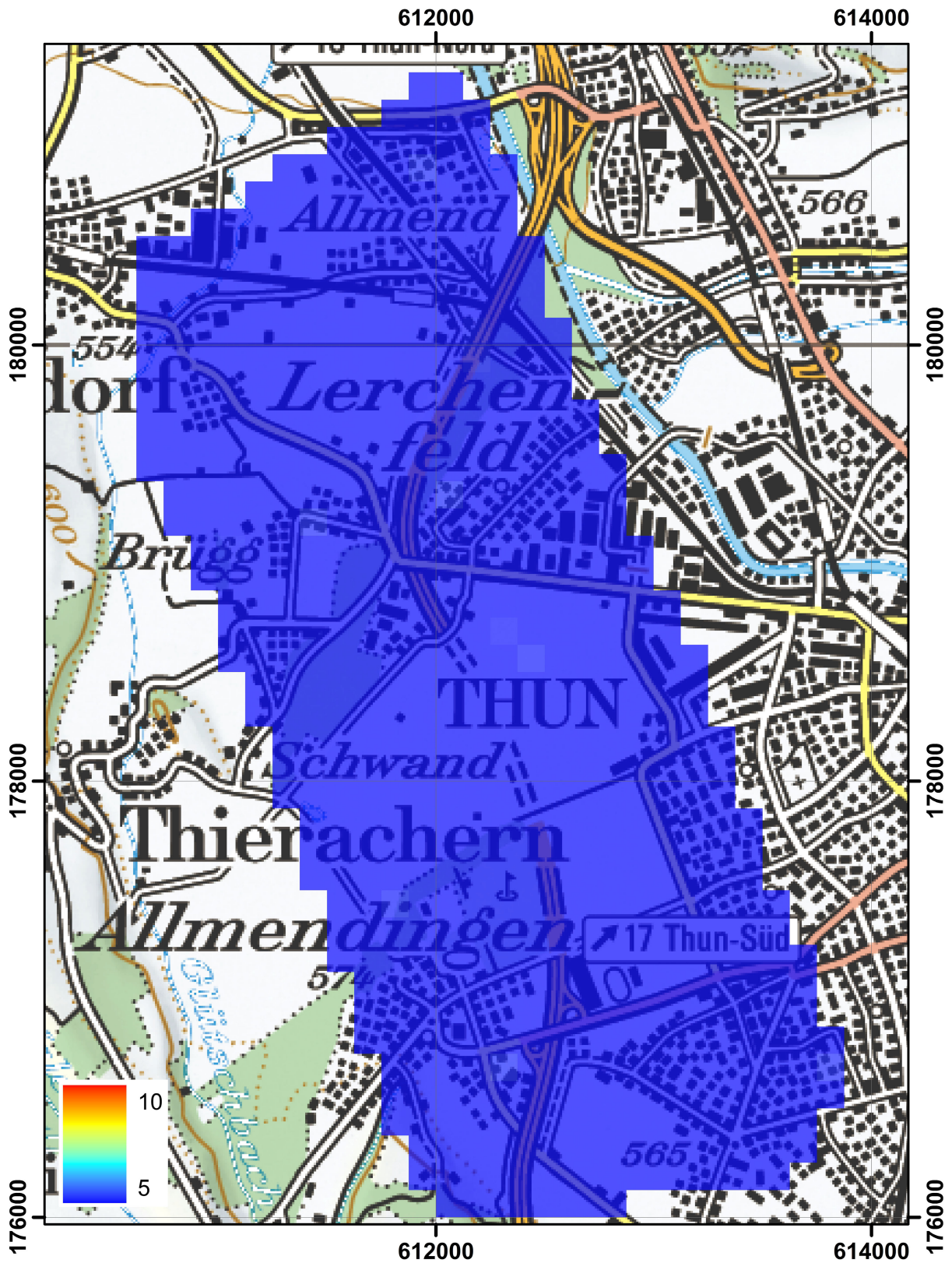
Figure 42: Man-made Gross-count (MMGC) ratio over Thun military training ground. PK100 ©2019 swisstopo (JD100042).

2.2.3 Spiez military training ground

For the training of military RLL operators, radioactive source search exercises were performed during ARM19m over Spiez military training ground. The first exercise shows a clear signal of the source on the maps of dose rate (Figure 43) and MMGC-ratio (Figure 44). The on-line evaluation software detected artificial radioactivity and created according event notifications during the flight marked with symbols in Figure 45, identifying the radionuclide ^{137}Cs. A closer look on the average spectrum over the dose rate anomaly (Figure 46) shows an additional signal which can be attributed to the radionuclide ^{60}Co, which was not identified by the automated algorithms. The flight of the second exercise was performed after the strong ^{137}Cs source was removed. The maps of the dose rate (Figure 47) and MMGC-ratio (Figure 48) show only slightly increased values over the remaining source. The average spectrum over the area with elevated values identifies the radionuclide ^{60}Co. The Mirion on-line software announced the presence of an artificial radioactive source during the flight (Figure 49). This time, the source nuclide was correctly identified as ^{60}Co by the automated algorithms. The third exercise was a short flight to confirm that all radioactive sources were removed from the training area. The maps of dose rate (Figure 51) and MMGC-ratio (Figure 52) show no remaining anomalies and no detection alert was given by the Mirion on-line evaluation (Figure 53).

The results show the advantage of the on-line identification of radionuclides by the Mirion software and the subsequent alert to the operators. Nevertheless, in cases with several sources of different radionuclides, a visual inspection of the associated photon spectra by operators well acquainted with gammaspectrometry is advisable.
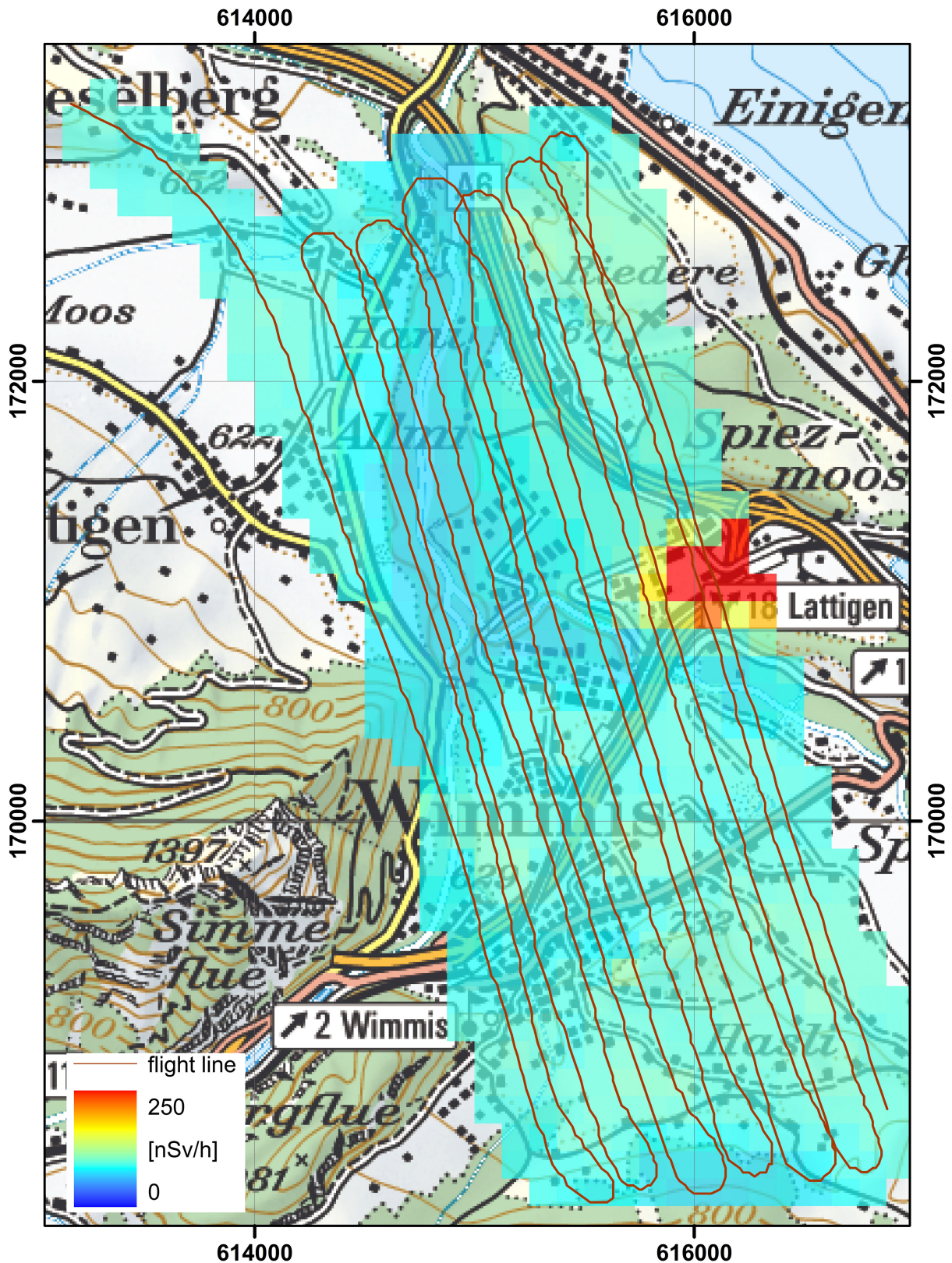
Figure 43: Dose rate of the first exercise over Spiez military training ground. Data evaluation with the ARM software. PK100 ©2019 swisstopo (JD100042).
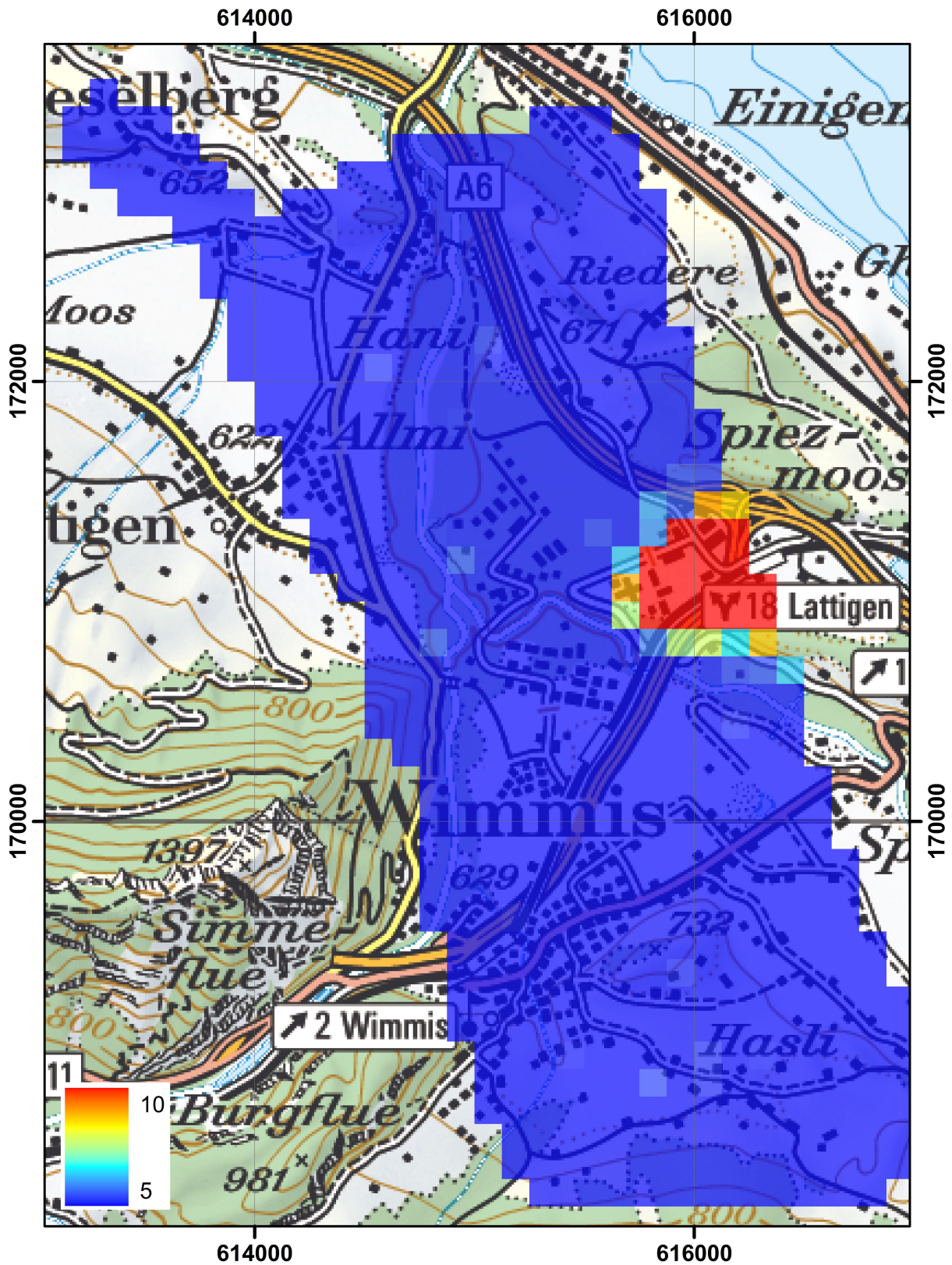
Figure 44: Man-made Gross-count (MMGC) ratio of the first exercise over Thun military training ground. PK100 ©2019 swisstopo (JD100042).

Kompetenzzentrum ABC-KAMIR

Radiometrie System

Mapping		**Edition Date :**	09.09.2019 13:34:34
Measurement :	Ground dose rate (G)	**Grid size :**	50m
Type :	Average		
Extrapolation :	5		
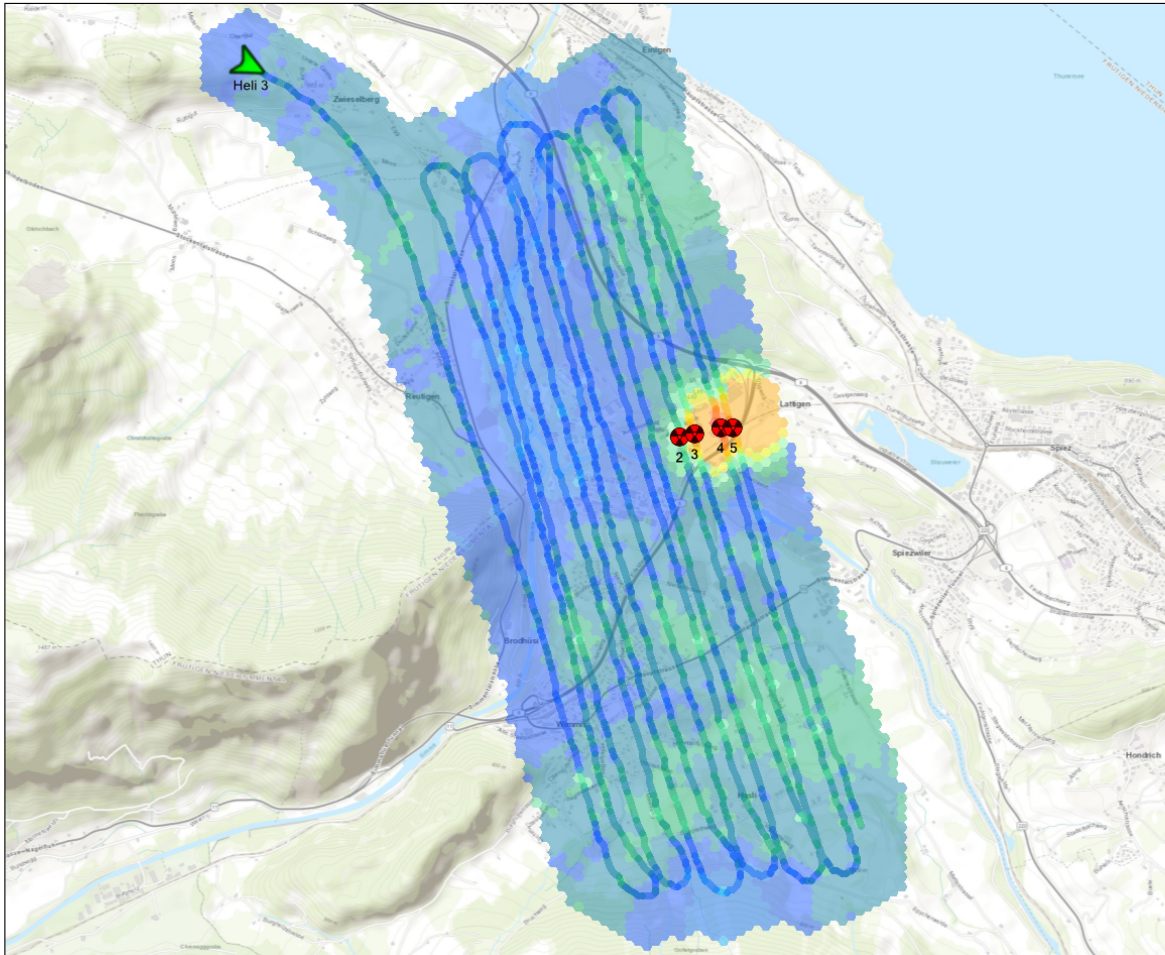
Ground dose rate (G)(μSv/h)

Invalid	0.050	0.060	0.070	0.080	0.090	0.100	0.120	0.140	0.160	0.180	0.200	0.500	1.000	2.000	5.000	10.000	50.000

Figure 45: Dose rate of the first exercise over Spiez military training ground. Output of the on-line Mirion data evaluation software.
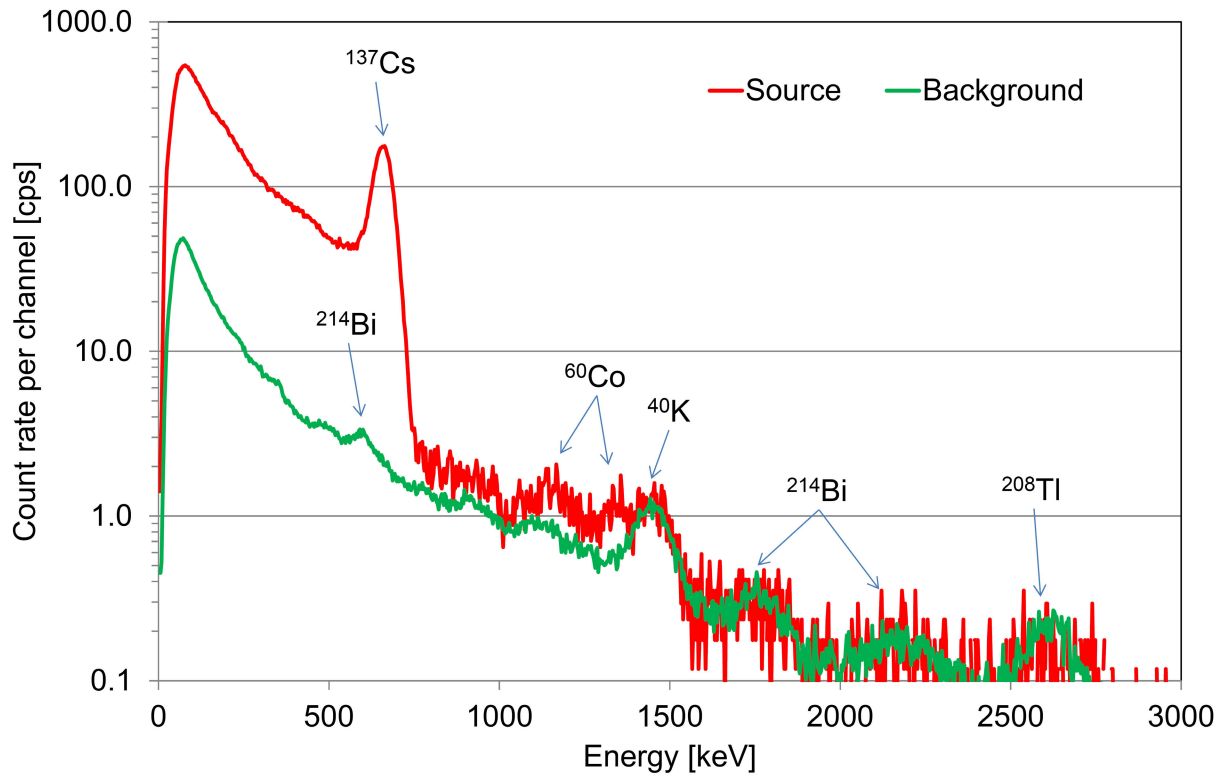
Figure 46: Photon spectrum of the first exercise over the source at Spiez military training ground compared to a background spectrum.
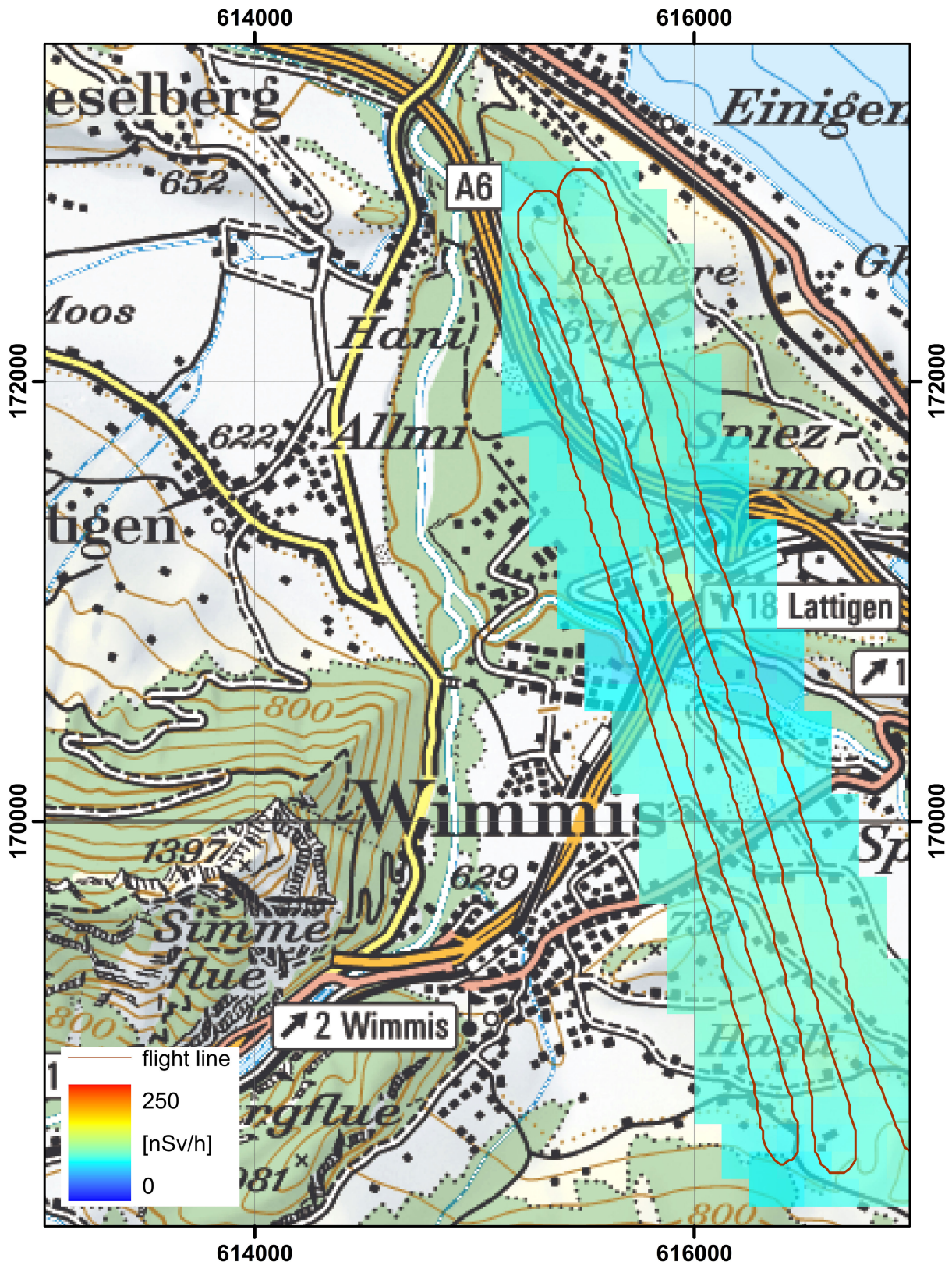
Figure 47: Dose rate of the second exercise over Spiez military training ground. Data evaluation with the ARM software.
PK100 ©2019 swisstopo (JD100042).
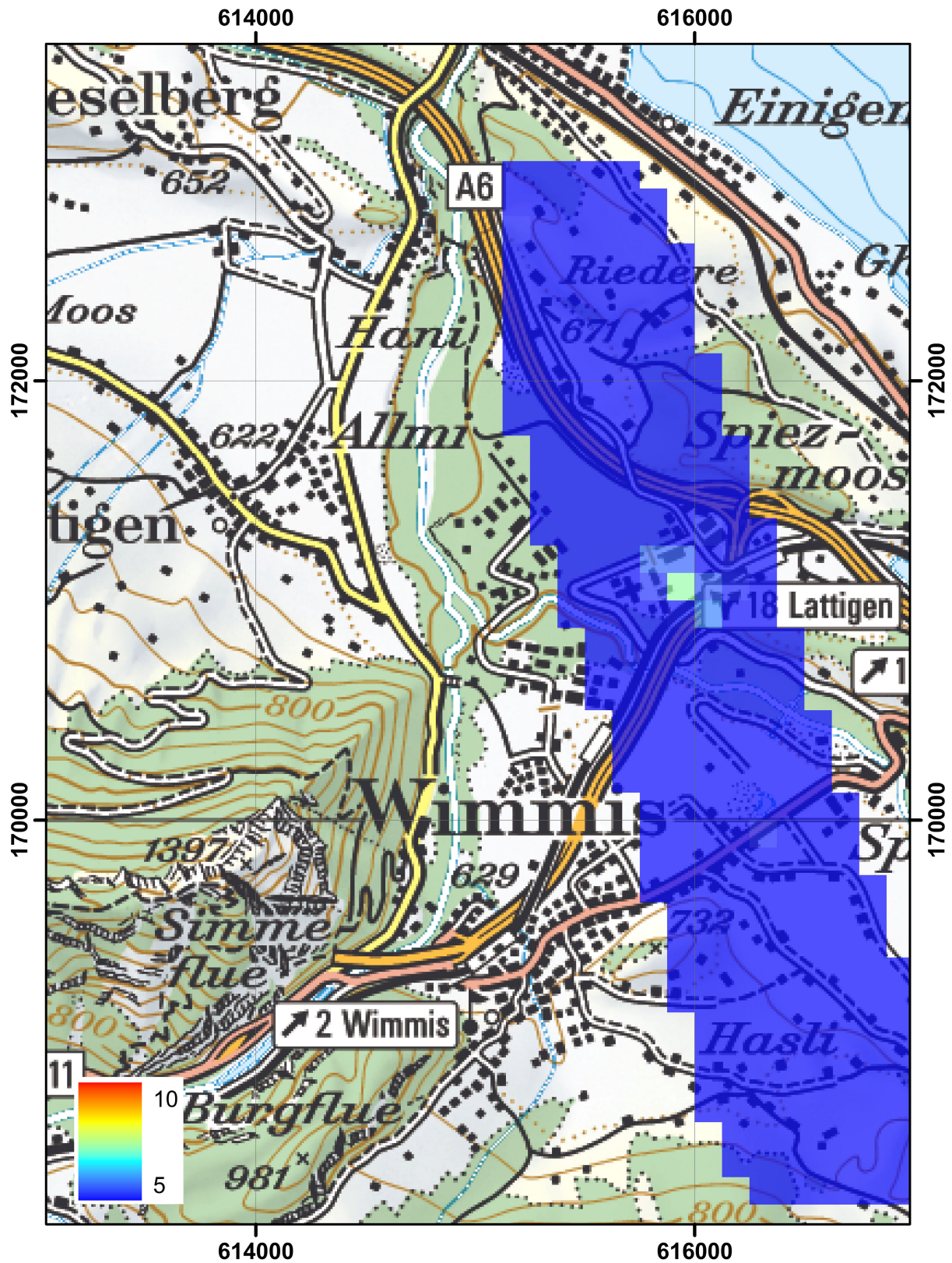
Figure 48: Man-made Gross-count (MMGC) ratio of the second exercise over Thun military training ground. PK100 ©2019 swisstopo (JD100042).

Mapping		Edition Date :	09.09.2019 13:35:30
Measurement : Ground dose rate (G)		**Grid size :**	50m
Type : Average			
Extrapolation : 5			
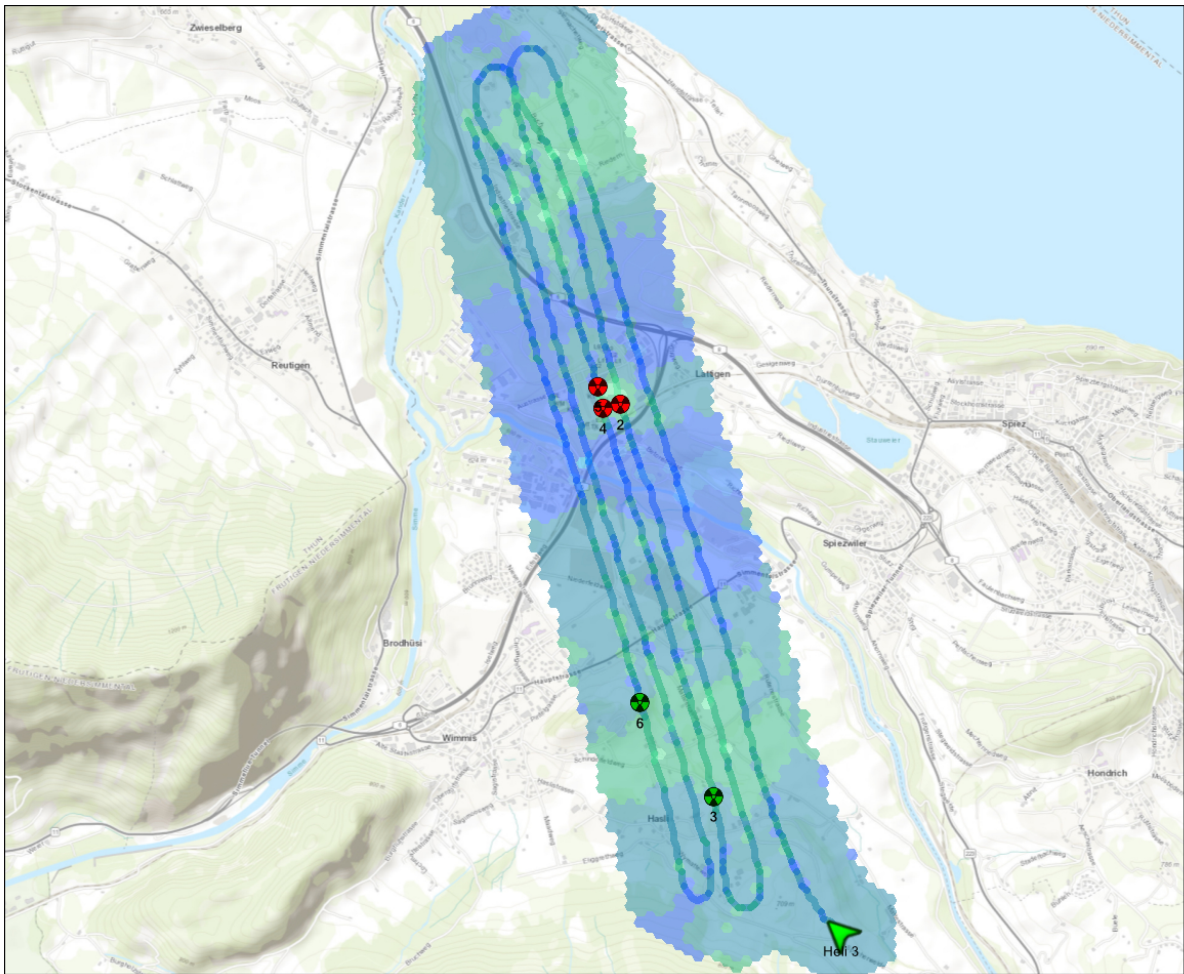
Ground dose rate (G)(µSv/h)

Invalid	0.050	0.060	0.070	0.080	0.090	0.100	0.120	0.140	0.160	0.180	0.200	0.500	1.000	2.000	5.000	10.000	50.000

Figure 49: Dose rate of the second exercise over Spiez military training ground. Output of the on-line Mirion data evaluation software.
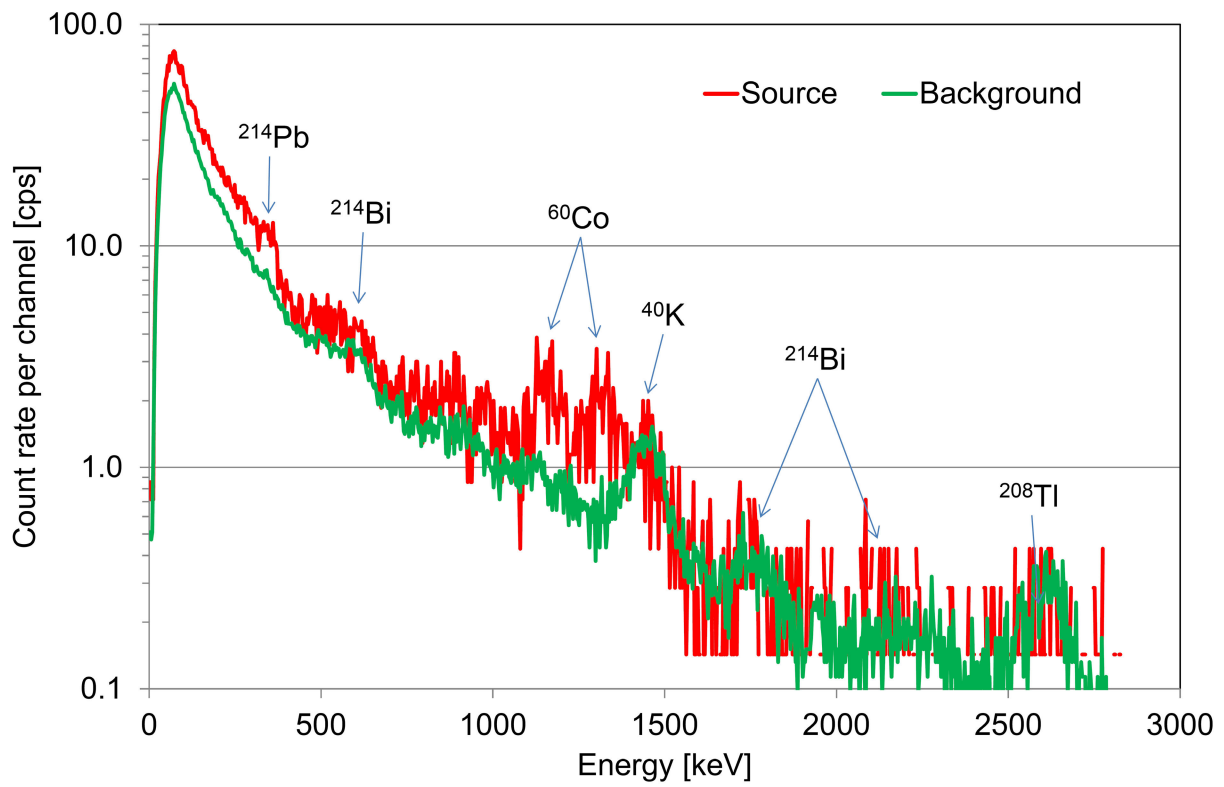
Figure 50: Photon spectrum of the second exercise over the source at Spiez military training ground compared to a background spectrum.
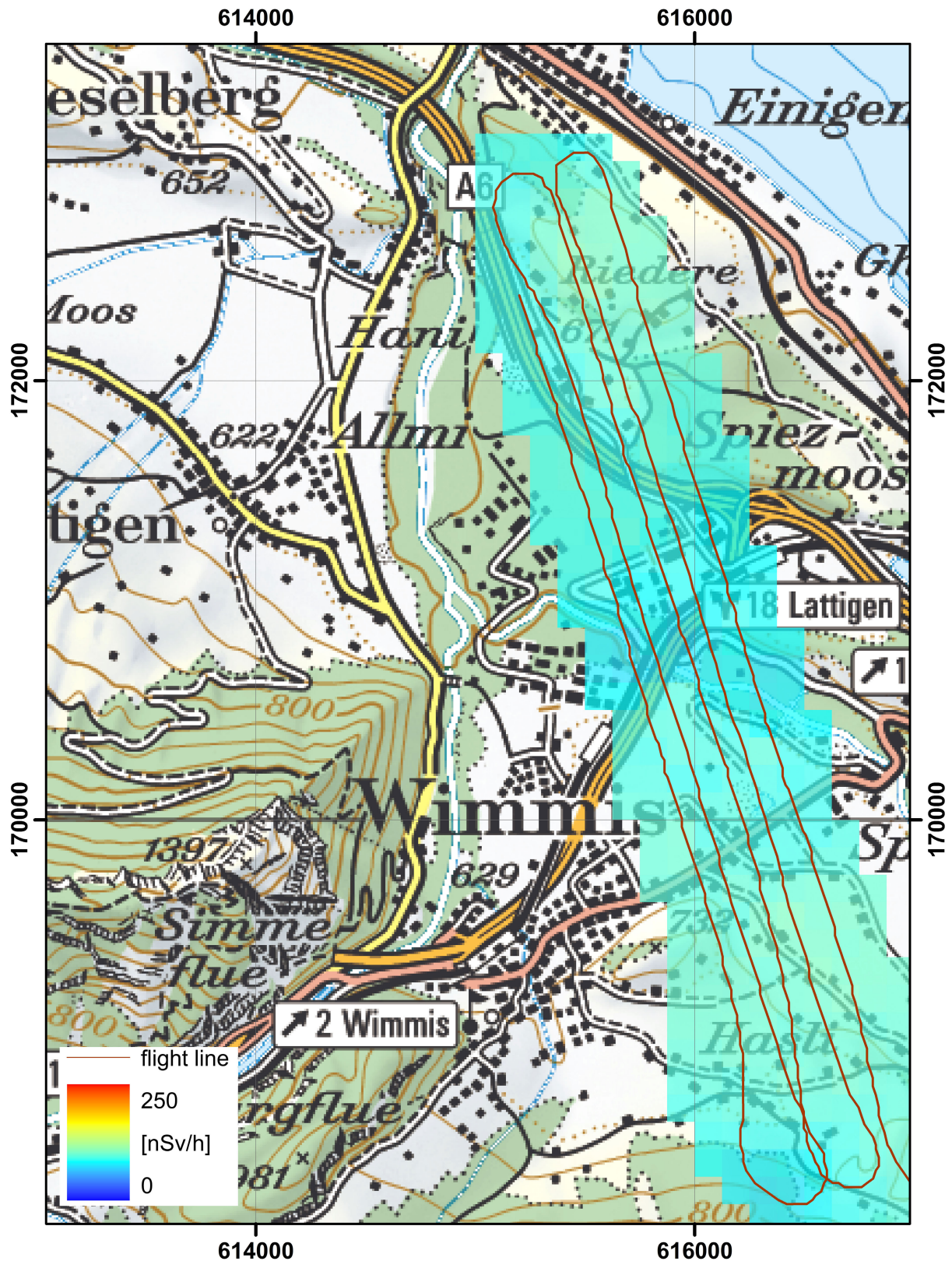
Figure 51: Dose rate of the third exercise over Spiez military training ground. Data evaluation with the ARM software.
PK100 ©2019 swisstopo (JD100042).
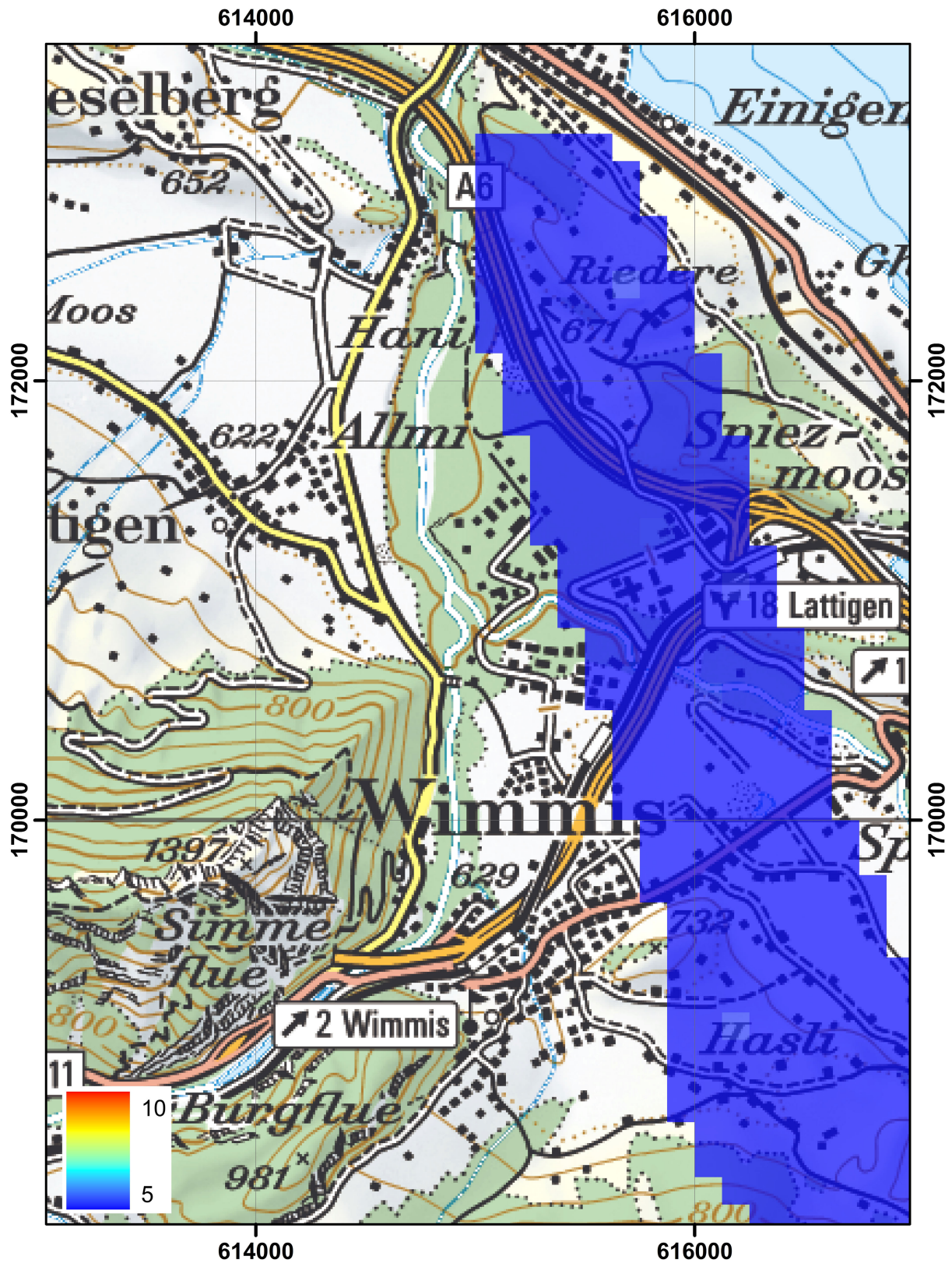
Figure 52: Man-made Gross-count (MMGC) ratio of the third exercise over Thun military training ground. PK100 ©2019 swisstopo (JD100042).

Mapping		Edition Date :	09.09.2019 13:36:06
Measurement :	Ground dose rate (G)	**Grid size :**	50m
Type :	Average		
Extrapolation :	5		
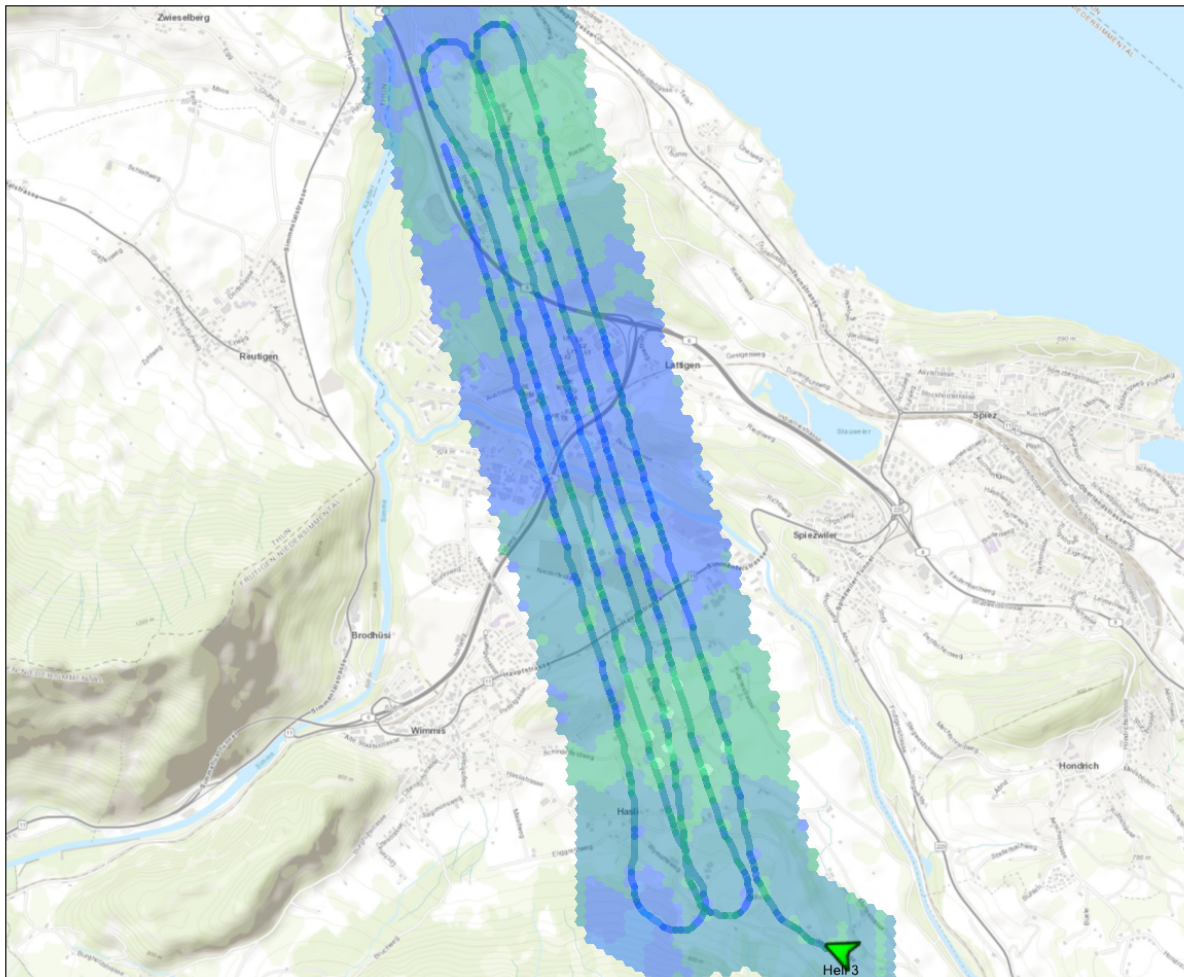
Ground dose rate (G)(µSv/h)																	
Invalid	0.050	0.060	0.070	0.080	0.090	0.100	0.120	0.140	0.160	0.180	0.200	0.500	1.000	2.000	5.000	10.000	50.000

Figure 53: Dose rate of the third exercise over Spiez military training ground. Output of the on-line Mirion data evaluation software.

3 Alignment of evaluation parameters

The raw data measured with the RLL system are evaluated during the measuring flight using software provided by the manufacturer of the system (Mirion). To compare these results with the ARM evaluation software, several measuring flights were analysed using both evaluation programs. Table 5 shows the ratio of the averages determined over the different measuring areas with the Mirion and ARM evaluation software for dose rate (DHSR) and ^{232}Th and ^{40}K activity concentrations (AD_Th-232 and AD_K-40, respectively). The averages over the ratios determined in the different measuring areas is given in the last row of table 5 together with the according standard deviation as indication of the variation between the different areas and detectors. The variation of the ratio of total dose rates does not yield a consistent picture yet, partly caused by changes in the dose rate evaluation used in the ARM-software in 2017 (Butterweck et al., 2018). Nevertheless, first estimates of correction factors for ^{232}Th and ^{40}K activity concentrations can be used to align both evaluation procedures.

Area	Year	RLL-Detector	Ratio ARM/Mirion		
			DHSR	AD_Th-232	AD_K-40
Vicosoprano	2016	004	1.00	1.19	1.37
Cham	2016	004	1.01	1.17	1.48
PSI, KKB,KKL, Zwilag	2016	004	1.01	1.18	1.45
Murg valley	2017	001	1.24	1.19	1.47
Linth plain	2017	001	1.11	1.13	1.37
Yverdon	2018	003	1.12	1.12	1.36
Bulle	2019	003	1.08	1.16	1.48
Köniz	2019	003	1.08	1.18	1.42
Vevey	2019	003	1.07	1.12	1.48
Training ground Thun	2019	003	1.08	1.18	1.43
KKG extended	2019	002	1.06	1.06	1.32
Average			1.10 ± 0.09	1.15 ± 0.04	1.42 ± 0.06

Table 5: Ratio of average values determined with ARM and RLL evaluation software.

4 Conclusions

The survey of the environs of the Swiss nuclear power plants Gösgen (KKG) and Mühleberg (KKM) showed no artificial radionuclides outside of the plant premises.

The measurements over the towns of Bulle, Köniz and Vevey expanded the database of radiation background over Swiss cities. No unusual values of the radiological quantities were observed.

An altitude profile over lake Neuchâtel lead to a revision of a model planned to be used for compensating the influence of airborne radon progeny on the measurement.

The deterioration of the energy resolution of several NaI(Tl) crystals used in the RLL detectors continues to downgrade system performance.

The analysis of cosmic dose rate data measured over the boiling water reactor of KKM indicates a misinterpretation of high energy photons emitted by the radionuclide ^{16}N using the evaluation software developed by the manufacturer.

Results of training flights over radionuclide sources demonstrated the advantage of the online identification of radionuclides by the Mirion software and the subsequent alert to the operators. Nevertheless, in cases with several sources of different radionuclides, a visual inspection of the associated photon spectra by operators well acquainted with gammaspectrometry is advisable.

First estimates of correction factors for ^{232}Th and ^{40}K activity concentrations were determined from results of current and past measurements to align data evaluations with ARM and Mirion software.

5 Literature

Bucher, B.: Methodische Weiterentwicklungen in der Aeroradiometrie. Dissertation Nr. 13973, ETH Zürich, 2001.

Schwarz, G. F.: Methodische Entwicklungen zur Aerogammaspektrometrie. Beiträge zur Geologie der Schweiz, Geophysik Nr. 23, Schweizerische Geophysikalische Kommission, 1991.

Bucher, B., Butterweck, G., Rybach, L., Schwarz, G.: Aeroradiometrische Messungen im Rahmen der Übung ARM06. PSI-Bericht 07-02, ISSN 1019-0643, Paul Scherrer Institut, Villigen, Schweiz, 2007.

Bucher, B., Guillot, L., Strobl, C., Butterweck, G., Gutierrez, S., Thomas, M., Hohmann, C., Krol, I., Rybach, L., Schwarz, G.: International Intercomparison Exercise of Airborne Gammaspectrometric Systems of Germany, France and Switzerland in the Framework of the Swiss Exercise ARM07. PSI-Bericht Nr. 09-07, ISSN 1019-0643, Paul Scherrer Institut, Villigen, Schweiz, 2009.

Bucher, B., Butterweck, G., Rybach, L., Schwarz, G., Mayer, S.: Aeroradiometrische Messungen im Rahmen der Übung ARM10. PSI-Bericht Nr. 11-02, ISSN 1019-0643, Paul Scherrer Institut, Villigen, Schweiz, 2011.

Butterweck, G., Bucher, B., Rybach, L., Poretti, C., Maillard, S., Schwarz, G., Hofstetter-Boillat, B., Hohmann, E., Mayer, S., Scharding, G.: Aeroradiometric Measurements in the Framework of the Swiss Exercises ARM16 and LAURA. PSI-Report No. 17-01, ISSN 1019-0643, Paul Scherrer Institut, Villigen, Switzerland, 2017.

Butterweck, G., Bucher, B., Gryc, L., Debayle, C., Strobl, C., Maillard, S., Thomas, M., Helbig, A., Krol, I., Chuzel, S., Couvez, C., Ohera, M., Rybach, L., Poretti, C., Hofstetter-Boillat, B., Mayer, S., Scharding, G.: International Intercomparison Exercise of Airborne Gamma-Spectrometric Systems of the Czech Republic, France, Germany and Switzerland in the Framework of the Swiss Exercise ARM17. PSI-Report No. 18-04, ISSN 1019-0643, Paul Scherrer Institut, Villigen, Switzerland, 2018.

Butterweck, G., Bucher, B., Rybach, L., Poretti, C., Maillard, S., Schindler, M., Hofstetter-Boillat, B., Mayer, S., Scharding, G.: Aeroradiometric Measurements in the Framework of the Swiss Exercises ARM18 and the International Exercise CONTEX 2018. PSI-Report No. 19-01, ISSN 1019-0643, Paul Scherrer Institut, Villigen, Switzerland, 2019.

6 Previous reports

Schwarz, G. F., Klingelé, E. E., Rybach, L.: Aeroradiometrische Messungen in der Umgebung der schweizerischen Kernanlagen. Bericht für das Jahr 1989 zuhanden der Hauptabteilung für die Sicherheit der Kernanlagen (HSK). Interner Bericht, Institut für Geophysik, ETH Zürich, 1990.

Schwarz, G. F., Klingelé, E. E., Rybach, L.: Aeroradiometrische Messungen in der Umgebung der schweizerischen Kernanlagen. Bericht für das Jahr 1990 zuhanden der Hauptabteilung für die Sicherheit der Kernanlagen (HSK). Interner Bericht, Institut für Geophysik, ETH Zürich, 1991.

Schwarz, G. F., Klingelé, E. E., Rybach, L.: Aeroradiometrische Messungen in der Umgebung der schweizerischen Kernanlagen. Bericht für das Jahr 1991 zuhanden der Hauptabteilung für die Sicherheit der Kernanlagen (HSK). Interner Bericht, Institut für Geophysik, ETH Zürich, 1992.

Schwarz, G. F., Klingelé, E. E., Rybach, L.: Aeroradiometrische Messungen in der Umgebung der schweizerischen Kernanlagen. Bericht für das Jahr 1992 zuhanden der Hauptabteilung für die Sicherheit der Kernanlagen (HSK). Interner Bericht, Institut für Geophysik, ETH Zürich, 1993.

Schwarz, G. F., Klingelé, E. E., Rybach, L.: Aeroradiometrische Messungen in der Umgebung der schweizerischen Kernanlagen. Bericht für das Jahr 1993 zuhanden der Hauptabteilung für die Sicherheit der Kernanlagen (HSK). Interner Bericht, Institut für Geophysik, ETH Zürich, 1994.

Schwarz, G. F., Rybach, L.: Aeroradiometrische Messungen im Rahmen der Übung ARM94. Bericht für das Jahr 1994 zuhanden der Fachgruppe Aeroradiometrie (FAR). Interner Bericht, Institut für Geophysik, ETH Zürich, 1995.

Schwarz, G. F., Rybach, L.: Aeroradiometrische Messungen im Rahmen der Übung ARM95. Bericht für das Jahr 1995 zuhanden der Fachgruppe Aeroradiometrie (FAR). Interner Bericht, Institut für Geophysik, ETH Zürich, 1996.

Schwarz, G. F., Rybach, L., Bärlocher, C.: Aeroradiometrische Messungen im Rahmen der Übung ARM96. Bericht für das Jahr 1996 zuhanden der Fachgruppe Aeroradiometrie (FAR). Interner Bericht, Institut für Geophysik, ETH Zürich, 1997.

Bucher, B., Rybach, L., Schwarz, G., Bärlocher, C.: Aeroradiometrische Messungen im Rahmen der Übung ARM97. Bericht für das Jahr 1997 zuhanden der Fachgruppe Aeroradiometrie (FAR). Interner Bericht, Institut für Geophysik, ETH Zürich, 1998.

Bucher, B., Rybach, L., Schwarz, G., Bärlocher, C.: Aeroradiometrische Messungen im Rahmen der Übung ARM98. Bericht für das Jahr 1998 zuhanden der Fachgruppe Aeroradiometrie (FAR). Interner Bericht, Institut für Geophysik, ETH Zürich, 1999.

Bucher, B., Rybach, L., Schwarz, G., Bärlocher, C.: Aeroradiometrische Messungen im Rahmen der Übung ARM99. Bericht für das Jahr 1999 zuhanden der Fachgruppe Aeroradiometrie (FAR). Interner Bericht, Institut für Geophysik, ETH Zürich, 2000.

Bucher, B., Rybach, L., Schwarz, G., Bärlocher, C.: Aeroradiometrische Messungen im Rahmen der Übung ARM00. Bericht für das Jahr 2000 zuhanden der Fachgruppe Aeroradiometrie (FAR). Interner Bericht, Institut für Geophysik, ETH Zürich, 2001.

Bucher, B., Rybach, L., Schwarz, G., Bärlocher, C.: Aeroradiometrische Messungen im Rahmen der Übung ARM01. Bericht für das Jahr 2001 zuhanden der Fachgruppe Aeroradiometrie (FAR). Interner Bericht, Paul Scherrer Institut, Villigen, Schweiz, 2002.

Bucher, B., Rybach, L., Schwarz, G., Bärlocher, C.: Aeroradiometrische Messungen im Rahmen der Übung ARM02. Bericht für das Jahr 2002 zuhanden der Fachgruppe Aeroradiometrie (FAR). Interner Bericht, Paul Scherrer Institut, Villigen, Schweiz, 2003.

Bucher, B., Rybach, L., Schwarz, G.: Aeroradiometrische Messungen im Rahmen der Übung ARM03. PSI-Bericht 04-14, ISSN 1019-0643, Paul Scherrer Institut, Villigen, Schweiz, 2004.

Bucher, B., Butterweck, G., Rybach, L., Schwarz, G.: Aeroradiometrische Messungen im Rahmen der Übung ARM04. PSI-Bericht 05-10, ISSN 1019-0643, Paul Scherrer Institut, Villigen, Schweiz, 2005.

Bucher, B., Butterweck, G., Rybach, L., Schwarz, G.: Aeroradiometrische Messungen im Rahmen der Übung ARM05. PSI-Bericht 06-06, ISSN 1019-0643, Paul Scherrer Institut, Villigen, Schweiz, 2006.

Bucher, B., Butterweck, G., Rybach, L., Schwarz, G.: Aeroradiometrische Messungen im Rahmen der Übung ARM06. PSI-Bericht 07-02, ISSN 1019-0643, Paul Scherrer Institut, Villigen, Schweiz, 2007.

Bucher, B., Guillot, L., Strobl, C., Butterweck, G., Gutierrez, S., Thomas, M., Hohmann, C., Krol, I., Rybach, L., Schwarz, G.: International Intercomparison Exercise of Airborne Gammaspectrometric Systems of Germany, France and Switzerland in the Framework of the Swiss Exercise ARM07. PSI-Bericht Nr. 09-07, ISSN 1019-0643, Paul Scherrer Institut, Villigen, Schweiz, 2009.

Bucher, B., Butterweck, G., Rybach, L., Schwarz, G.: Aeroradiometrische Messungen im Rahmen der Übung ARM08. PSI-Bericht Nr. 09-02, ISSN 1019-0643, Paul Scherrer Institut, Villigen, Schweiz, 2009.

Bucher, B., Butterweck, G., Rybach, L., Schwarz, G., Strobl, C.: Aeroradiometrische Messungen im Rahmen der Übung ARM09. PSI-Bericht Nr. 10-01, ISSN 1019-0643, Paul Scherrer Institut, Villigen, Schweiz, 2010.

Bucher, B., Butterweck, G., Rybach, L., Schwarz, G., Mayer, S.: Aeroradiometrische Messungen im Rahmen der Übung ARM10. PSI-Bericht Nr. 11-02, ISSN 1019-0643, Paul Scherrer Institut, Villigen, Schweiz, 2011.

Bucher, B., Butterweck, G., Rybach, L., Schwarz, G., Mayer, S.: Aeroradiometric Measurements in the Framework of the Swiss Exercise ARM11. PSI-Report No. 12-04, ISSN 1019-0643, Paul Scherrer Institut, Villigen, Switzerland, 2012.

Butterweck, G., Bucher, B., Rybach, L., Schwarz, G., Hödlmoser, H., Mayer, S., Danzi, C. Scharding, G.: Aeroradiometric Measurements in the Framework of the Swiss Exercise ARM12. PSI-Report No. 13-01, ISSN 1019-0643, Paul Scherrer Institut, Villigen, Switzerland, 2013.

Butterweck, G., Bucher, B., Rybach, L., Schwarz, G., Hohmann, E., Mayer, S., Danzi, C. Scharding, G.: Aeroradiometric Measurements in the Framework of the Swiss Exercise ARM13. PSI-Report No. 15-01, ISSN 1019-0643, Paul Scherrer Institut, Villigen, Switzerland, 2015.

Butterweck, G., Bucher, B., Rybach, L., Schwarz, G., Hohmann, E., Mayer, S., Danzi, C. Scharding, G.: Aeroradiometric Measurements in the Framework of the Swiss Exercises ARM14 and FTX14. PSI-Report No. 15-02, ISSN 1019-0643, Paul Scherrer Institut, Villigen, Switzerland, 2015.

Butterweck, G., Bucher, B., Rybach, L., Schwarz, G., Hofstetter-Boillat, B., Hohmann, E., Mayer, S., Danzi, C. Scharding, G.: Aeroradiometric Measurements in the Framework of the Swiss Exercises ARM15, GNU15 and the International Exercise AGC15. PSI-Report No. 15-04, ISSN 1019-0643, Paul Scherrer Institut, Villigen, Switzerland, 2015.

Butterweck, G., Bucher, B., Rybach, L., Poretti, C., Maillard, S., Schwarz, G., Hofstetter-Boillat, B., Hohmann, E., Mayer, S., Scharding, G.: Aeroradiometric Measurements in the Framework of the Swiss Exercises ARM16 and LAURA. PSI-Report No. 17-01, ISSN 1019-0643, Paul Scherrer Institut, Villigen, Switzerland, 2017.

Butterweck, G., Bucher, B., Gryc, L., Debayle, C., Strobl, C., Maillard, S., Thomas, M., Helbig, A., Krol, I., Chuzel, S., Couvez, C., Ohera, M., Rybach, L., Poretti, C., Hofstetter-Boillat, B., Mayer, S., Scharding, G.: International Intercomparison Exercise of Airborne Gamma-Spectrometric Systems of the Czech Republic, France, Germany and Switzerland in the Framework of the Swiss Exercise ARM17. PSI-Report No. 18-04, ISSN 1019-0643, Paul Scherrer Institut, Villigen, Switzerland, 2018.

Butterweck, G., Bucher, B., Rybach, L., Poretti, C., Maillard, S., Schindler, M., Hofstetter-Boillat, B., Mayer, S., Scharding, G.: Aeroradiometric Measurements in the Framework of the Swiss Exercises ARM18 and the International Exercise CONTEX 2018. PSI-Report No. 19-01, ISSN 1019-0643, Paul Scherrer Institut, Villigen, Switzerland, 2019.

The reports since 1994 can be found and downloaded from the FAR website `http://far.ensi.ch`.

7 Evaluation parameter files

The parameter files used for the evaluation of raw data in this report are listed below to improve the traceability of the presented results. The detector definition files have been re-evaluated for all detectors in 2014. A software modification was performed to take into account different formats of terrain model files used for topographic correction, leading to a change in the detector definition file.

7.1 DefinitionFile_Processing_ch.txt

This file defines the standard parameters used for the calculation and gridding of measured data used throughout this report.

```
Definition file Swiss MGS32
"Windows"
10
Total    401.    2997.      0.    0
K-40     1369.   1558.    1460.   1
U-238    1664.   1853.    1765.   1
Th-232   2407.   2797.    2615.   1
Cs-137    600.    720.     660.   2
Co-60    1100.   1400.       0.   2
MMGC1     400.   1400.       0.   0
MMGC2    1400.   2997.       0.   0
LOW        40.    720.       0.   0
MID       720.   2997.       0.   0
"Ratios"
3
MMGCVerhältnis    MMGC1   MMGC2   Ratio_MMGC
LOWHigh           LOW     MMGC2   RatioLowHigh
LowMid            LOW     MID     RatioLowMid
"Conversion factors Activity to Dose Rate"
8
Total       0        NoCalibration    "    "    0
AD_K-40       0.044    DHSR            "nSv/h"   1
AD_U-238      0.55     DHSR            "nSv/h"   1
AD_Th-232     0.77     DHSR            "nSv/h"   1
AD_Cs-137     0.2      DHSR            "nSv/h"   2
Co-60       0        NoCalibration    "    "    0
MMGC1       0        NoCalibration    "    "    0
MMGC2       0        NoCalibration    "    "    0
"Typ des Darstellungsgrenzwertes"
1
Nachweistyp  0
"counts of spectra to stack"
1
Counts 1
"Auszugebende Werte"
```

```
30
"DHSR TOT              ","DHSR_TOT","nSv/h         ",0.00,250.00
"AP_Co-60              ","AP_Co-60","MBq           ",0.00,150.00
"AP_Cs-137             ","AP_Cs-137","MBq          ",0.00,40.00
"Terr. DL              ","DHSR_TOT","nSv/h         ",0.00,250.00
"CR_Caesium            ","CR_Cs-137","cps          ",20.00,120.00
"CR_Cobalt             ","CR_Co-60","cps           ",0.00,100.00
"NR_Caesium            ","NR_Cs-137","cps           ",0.00,120.00
"NR_Cobalt             ","NR_Co-60","cps            ",0.00,100.00
"Total_CR_corr         ","NR_Total","cps           ",200.00,1200.00
"K-40                  ","AD_K-40","Bq/kg          ",0.00,1000.00
"U-238                 ","AD_U-238","Bq/kg          ",0.00,120.00
"Th-232                ","AD_Th-232","Bq/kg         ",0.00,120.00
"Cs-137                ","AD_Cs-137","Bq/kg         ",0.00,240.00
"Cobalt_CR             ","NR_Co-60","cps           ",0.00,120.00
"Nat.Terr.DL           ","DHSR_NAT","nSv/h         ",0.00,250.00
"Künst.DL              ","DHSR_ANT","nSv/h         ",0.00,250.00
"MMGC_Ratio            ","&MMGC_Ratio","%           ",4.00,6.00
"Cosmic DL             ","DHSR_COS","nSv/h         ",20.00,60.00
"Cosmic                ","CR_COS","cps            ",000.00,400.00
"Radar                 ","PH","m             ",0.00,300.00
"ODL                   ","DHSR","nSv/h         ",0.00,250
"AD_UT_K-40            ","AD_UT_K-40","Bq/kg        ",0.00,200
"AD_UT_U-238           ","AD_UT_U-238","Bq/kg       ",0.00,50
"AD_UT_Th-232          ","AD_UT_Th-232","Bq/kg      ",0.00,40
"AD_UT_Cs-137          ","AD_UT_Cs-137","Bq/kg      ",0.00,20
"Err_Co-60             ","NR_UT_Co-60","cps         ",0.00,40
"Nachweis_Cs-137       ","CR_LD_Cs-137","cps        ",0.00,100.00
"Nachweis_Co-60        ","CR_LD_Co-60","cps         ",0.00,100.00
"Cs-137 beta=0         ","AA_Cs-137","Bq/m2        ",0.00,20000.00
"AA_UT_Cs-137          ","AA_UT_Cs-137","Bq/m2      ",0.00,20
```

7.2   DefinitionFile_Det002.txt

This file defines the parameter set used for RLL detector with serial number 002 used in the civil part ARM19z of the exercise. Spectral data derived from crystal 2 was replaced by the values of crystal 3 (see section 1.1.1).

```
Definition file System
"Koordinaten"
WGS84
"Non-linearity"
4
a0  0.000000
a1  0.083333
a2  0.000000
a3  0.000000
```

```
"Recorder old RDT-Files"
8
Radar   0.00    -61.00
Baro    0.74    457.14
Cosm    0.00    1.00
Dead    5.00    0.00
Time    0.00    1.00
Temp    0.00    1.00
Pitch   0.00    76.20
Roll    0.00    90.91
"Background/Cosmic"
10
Total       62.266       5.534       0.463
K-40         6.515       0.270       0.033
U-238        2.434       0.227       0.032
Th-232      -0.013       0.294       0.029
Cs-137      10.974       0.520       0.089
Co-60        7.562       0.540       0.073
MMGC1       56.303       3.910       0.375
MMGC2        5.963       1.624       0.094
LOW          0.          0.          0.
MID          0.          0.          0.
"Stripping Coefficients"
10
1.000   0.000   0.000   0.000   0.000   0.000   0.000   0.000   0.000   0.000
0.000   1.000   0.953   0.445  -0.005  -0.002   0.000   0.000   0.000   0.000
0.000  -0.004   1.000   0.360   0.000  -0.007   0.000   0.000   0.000   0.000
0.000  -0.007   0.061   1.000  -0.001  -0.007   0.000   0.000   0.000   0.000
0.000   0.463   3.300   1.651   1.000   0.097   0.000   0.000   0.000   0.000
0.000   0.757   2.322   0.607  -0.009   1.000   0.000   0.000   0.000   0.000
0.000   0.000   0.000   0.000   0.000   0.000   1.000   0.000   0.000   0.000
0.000   0.000   0.000   0.000   0.000   0.000   0.000   1.000   0.000   0.000
0.000   0.000   0.000   0.000   0.000   0.000   0.000   0.000   1.000   0.000
0.000   0.000   0.000   0.000   0.000   0.000   0.000   0.000   0.000   1.000
"Converted Stripping Coefficients Matrix"
10
1.000   0.000   0.000   0.000   0.000   0.000   0.000   0.000   0.000   0.000
0.000   0.998  -0.947  -0.108   0.005  -0.006   0.000   0.000   0.000   0.000
0.000  -0.002   1.015  -0.367   0.000   0.004   0.000   0.000   0.000   0.000
0.000   0.001  -0.083   1.024   0.001   0.007   0.000   0.000   0.000   0.000
0.000  -0.384  -2.618  -0.460   0.996  -0.118   0.000   0.000   0.000   0.000
0.000  -0.755  -1.612   0.307   0.005   0.989   0.000   0.000   0.000   0.000
0.000   0.000   0.000   0.000   0.000   0.000   1.000   0.000   0.000   0.000
0.000   0.000   0.000   0.000   0.000   0.000   0.000   1.000   0.000   0.000
0.000   0.000   0.000   0.000   0.000   0.000   0.000   0.000   1.000   0.000
0.000   0.000   0.000   0.000   0.000   0.000   0.000   0.000   0.000   1.000
"Sigma of Converted Stripping Coefficients Matrix"
10
0.000 0.000 0.000 0.000 0.000 0.000 0.000 0.000 0.000 0.000
```

```
0.000   0.000 -0.040 -0.017  0.000 -0.016  0.000  0.000  0.000  0.000
0.000   0.000  0.000 -0.028  0.000  0.000  0.000  0.000  0.000  0.000
0.000   0.000 -0.009  0.000  0.000  0.000  0.000  0.000  0.000  0.000
0.000  -0.080 -0.103 -0.037  0.000 -0.008  0.000  0.000  0.000  0.000
0.000  -0.140 -0.068  0.013  0.000  0.000  0.000  0.000  0.000  0.000
0.000   0.000  0.000  0.000  0.000  0.000  0.000  0.000  0.000  0.000
0.000   0.000  0.000  0.000  0.000  0.000  0.000  0.000  0.000  0.000
0.000   0.000  0.000  0.000  0.000  0.000  0.000  0.000  0.000  0.000
0.000   0.000  0.000  0.000  0.000  0.000  0.000  0.000  0.000  0.000
"Attenuation Coefficients"
10
Total         0.00600     1.00000     0.0003
K-40          0.00800     1.00000     0.0008
U-238         0.00550     1.00000     0.0114
Th-232        0.00600     1.00000     0.0044
Cs-137        0.01000     1.00000     0.0100
Co-60         0.00800     1.00000     0.0080
MMGC1         0.00600     1.00000     0.0060
MMGC2         0.00650     1.00000     0.0065
LOW           0.02000     1.00000     0.01
MID           0.01500     1.00000     0.005
"3D Attenuation Coefficients"
10
Total         0.00350     2.00000
K-40          0.00420     2.00000
U-238         0.00320     2.00000
Th-232        0.00350     2.00000
Cs-137        0.00800     2.00000
Co-60         0.00800     1.00000
MMGC1         0.00600     1.00000
MMGC2         0.00650     1.00000
LOW           0.02000     1.00000
MID           0.01500     1.00000
"Conversion factors Counts to Activity"
11
Total        0         NoCalibration    "      "
K-40         7.27      AD_K-40          "Bq/kg"
U-238        2.63      AD_U-238         "Bq/kg"
Th-232       1.50      AD_Th-232        "Bq/kg"
Cs-137       2.00      AD_Cs-137        "Bq/kg"
Cs-137       34.99     AA_Cs-137        "Bq/m2"
Cs-137       7.53      AP_Cs-137        "MBq  "
Co-60        2.61      AP_Co-60         "MBq  "
Co-60        0         NoCalibration    "      "
MMGC1        0         NoCalibration    "      "
MMGC2        0         NoCalibration    "      "
"Radon"
1
0            0
```

```
"Höhenkorrektur"
4
AltMethod     1
GroundAltDGM 1
DGMType       0
PfadDHM25    C:\DATEN\Benno\Aeroradiometrie\Daten\DHM25\}
"SDI Constants"
7
Aten          0.0053
Convert       0.00087
CosmicKorr    95.5
Back          12640.0
Gain          12.0
referenz_alt 100.0
Threshold     240.0
```

7.3   DefinitionFile_Det003.txt

This file defines the parameter set used for RLL detector with serial number 003 used for the military part ARM19m of the exercise.

```
Definition file System
"Koordinaten"
WGS84
"Non-linearity"
4
a0  0.000000
a1  0.083333
a2  0.000000
a3  0.000000
"Recorder old RDT-Files"
8
Radar  0.00    -61.00
Baro   0.74    457.14
Cosm   0.00    1.00
Dead   5.00    0.00
Time   0.00    1.00
Temp   0.00    1.00
Pitch  0.00    76.20
Roll   0.00    90.91
"Background/Cosmic"
10
Total       62.266        5.534       0.463
K-40         6.515        0.270       0.033
U-238        2.434        0.227       0.032
Th-232      -0.013        0.294       0.029
Cs-137      10.974        0.520       0.089
Co-60        7.562        0.540       0.073
```

```
MMGC1        56.303        3.910        0.375
MMGC2         5.963        1.624        0.094
LOW           0.           0.           0.
MID           0.           0.           0.
"Stripping Coefficients"
10
1.000  0.000  0.000  0.000  0.000  0.000  0.000  0.000  0.000  0.000
0.000  1.000  0.933  0.364 -0.014  0.014  0.000  0.000  0.000  0.000
0.000 -0.018  1.000  0.333 -0.002 -0.010  0.000  0.000  0.000  0.000
0.000 -0.012  0.049  1.000 -0.002 -0.009  0.000  0.000  0.000  0.000
0.000  0.394  3.129  1.518  1.000  0.103  0.000  0.000  0.000  0.000
0.000  0.698  2.371  0.457 -0.012  1.000  0.000  0.000  0.000  0.000
0.000  0.000  0.000  0.000  0.000  0.000  1.000  0.000  0.000  0.000
0.000  0.000  0.000  0.000  0.000  0.000  0.000  1.000  0.000  0.000
0.000  0.000  0.000  0.000  0.000  0.000  0.000  0.000  1.000  0.000
0.000  0.000  0.000  0.000  0.000  0.000  0.000  0.000  0.000  1.000
"Converted Stripping Coefficients Matrix"
10
1.000  0.000  0.000  0.000  0.000  0.000  0.000  0.000  0.000  0.000
0.000  0.995 -0.906 -0.068  0.012 -0.024  0.000  0.000  0.000  0.000
0.000  0.009  0.989 -0.337  0.001  0.006  0.000  0.000  0.000  0.000
0.000  0.005 -0.079  1.018  0.002  0.008  0.000  0.000  0.000  0.000
0.000 -0.353 -2.442 -0.502  0.988 -0.125  0.000  0.000  0.000  0.000
0.000 -0.722 -1.708  0.376  0.000  0.997  0.000  0.000  0.000  0.000
0.000  0.000  0.000  0.000  0.000  0.000  1.000  0.000  0.000  0.000
0.000  0.000  0.000  0.000  0.000  0.000  0.000  1.000  0.000  0.000
0.000  0.000  0.000  0.000  0.000  0.000  0.000  0.000  1.000  0.000
0.000  0.000  0.000  0.000  0.000  0.000  0.000  0.000  0.000  1.000
"Sigma of Converted Stripping Coefficients Matrix"
10
0.000  0.000  0.000  0.000  0.000  0.000  0.000  0.000  0.000  0.000
0.000  0.000 -0.040 -0.017  0.000 -0.016  0.000  0.000  0.000  0.000
0.000  0.000  0.000 -0.028  0.000  0.000  0.000  0.000  0.000  0.000
0.000  0.000 -0.009  0.000  0.000  0.000  0.000  0.000  0.000  0.000
0.000 -0.080 -0.103 -0.037  0.000 -0.008  0.000  0.000  0.000  0.000
0.000 -0.140 -0.068  0.013  0.000  0.000  0.000  0.000  0.000  0.000
0.000  0.000  0.000  0.000  0.000  0.000  0.000  0.000  0.000  0.000
0.000  0.000  0.000  0.000  0.000  0.000  0.000  0.000  0.000  0.000
0.000  0.000  0.000  0.000  0.000  0.000  0.000  0.000  0.000  0.000
0.000  0.000  0.000  0.000  0.000  0.000  0.000  0.000  0.000  0.000
"Attenuation Coefficients"
10
Total         0.00600      1.00000      0.0003
K-40          0.00800      1.00000      0.0008
U-238         0.00550      1.00000      0.0114
Th-232        0.00600      1.00000      0.0044
Cs-137        0.01000      1.00000      0.0100
Co-60         0.00800      1.00000      0.0080
MMGC1         0.00600      1.00000      0.0060
```

```
MMGC2        0.00650    1.00000    0.0065
LOW          0.02000    1.00000    0.01
MID          0.01500    1.00000    0.005
"3D Attenuation Coefficients"
10
Total        0.00350    2.00000
K-40         0.00420    2.00000
U-238        0.00320    2.00000
Th-232       0.00350    2.00000
Cs-137       0.00800    2.00000
Co-60        0.00800    1.00000
MMGC1        0.00600    1.00000
MMGC2        0.00650    1.00000
LOW          0.02000    1.00000
MID          0.01500    1.00000
"Conversion factors Counts to Activity"
11
Total        0          NoCalibration    "       "
K-40         7.27       AD_K-40          "Bq/kg"
U-238        2.63       AD_U-238         "Bq/kg"
Th-232       1.50       AD_Th-232        "Bq/kg"
Cs-137       2.00       AD_Cs-137        "Bq/kg"
Cs-137       34.99      AA_Cs-137        "Bq/m2"
Cs-137       7.53       AP_Cs-137        "MBq  "
Co-60        2.61       AP_Co-60         "MBq  "
Co-60        0          NoCalibration    "       "
MMGC1        0          NoCalibration    "       "
MMGC2        0          NoCalibration    "       "
"Radon"
1
0            0
"Höhenkorrektur"
4
AltMethod    1
GroundAltDGM 1
DGMType      0
PfadDHM25    C:\DATEN\Benno\Aeroradiometrie\Daten\DHM25\
"SDI Constants"
7
Aten         0.0053
Convert      0.00087
CosmicKorr   95.5
Back         12640.0
Gain         12.0
referenz_alt 100.0
Threshold    240.0
```